WAVE POLARIZATION THROUGH THE IONOSPHERE AND LOW LATITUDE ELECTRON CONTENT

by

Ivan Jelinek Kantor

LAFE-97
July, 1969

SUBMITTED IN PARTIAL FULFILLMENT OF THE
REQUIREMENTS FOR THE DEGREE OF
MASTER OF SCIENCE

PR — Conselho Nacional de Pesquisas
Comissão Nacional de Atividades Espaciais
São José dos Campos — SP · Brazil

WAVE POLARIZATION THROUGH THE IONOSPHERE AND LOW LATITUDE ELECTRON CONTENT

by

I.J.KANTOR

Adviser

D.B.RAI

REPORT LAFE-97

July 1969

PR - Conselho Nacional de Pesquisas

Comissão Nacional de Atividades Espaciais

São José dos Campos - SP

PRESIDÊNCIA DA REPÚBLICA
CONSELHO NACIONAL DE PESQUISAS
COMISSÃO NACIONAL DE ATIVIDADES ESPACIAIS
São José dos Campos — São Paulo — Brasil

WAVE POLARIZATION THROUGH THE IONOSPHERE AND LOW LATITUDE ELECTRON CONTENT

by

Ivan J.Kantor

This report contain elements of CNAE's research program and its publication has been approved by

Fernando de Mendonça
Scientific Diretor

TABLE OF CONTENTS

WAVE POLARIZATION THROUGH THE IONOSPHERE

AND

LOW LATITUDE ELECTRON CONTENT

I.J. Kantor

Abstract

This thesis is concerned with the ionospheric electron content measured at São José dos Campos (23.22°S, 45.98°W) between 1963 and 1968. The main part of the data was reduced by means of differential Faraday method using the 40 and 41 MHz frequencies of BE-B and BE-C satellites. Here we study two distinct aspects of the same subject: the Faraday rotation and the electron content. In the second chapter we present an analysis of the polarization of waves travelling through the ionosphere. The introduction of the transverse component of the magnetic field, gives us a more general picture of the Faraday rotation, specially, near the quasi-transverse region. The analysis also provides a clue to the electron density profile determination. The third part is concerned with the measurements itselves. Variations of electron content with local time, dip angle, season and solar and magnetic activity are studied. Special attention is given to the behavior of the equatorial anomaly and the region of the Brazilian magnetic anomaly. A brief analysis of errors and reduction method is also presented.

CHAPTER 1

INTRODUCTION

1.1 - Purpose

Since 1957 many measurements of the electron content have been made but there are still some problems remaining.

Usually on the ray path of the satellite signal, the wave passes through region where the propagation satisfies the conditions of quasi-longitudinal approximation. But for stations located near the equator there is a region (QT) within the satellite path where those conditions do not hold. For equatorial stations the "QT" region is very important because its identification can eliminate the ambiguity in determining the absolute number of Faraday rotations. We shall see that in the "QT" region there is an instant at which the Faraday rotation vanishes (QT point). What happens to a wave propagation through a "QT" region is not well understood. For understanding this, in the second chapter we present a set of equations that describe, with some approximations (but including the transverse component of the magnetic field) the wave polarization in terms of the tilt angle and the axial ratio for the propagations of waves through a magnetoionic medium.

Although many measurements of electron content have been made all over the world during several years, a worldwide picture of electron content variations cannot be given; there is a lack of data for extensive geographic regions, like the south hemisphere. We analyse in the third chapter, the data obtained from 1963 to 1968 over a dip range of 0^{o} to -35^{o}. This data extends over half a solar cycle permitting us to study the behavior with solar activity. Our geographical location inside the range of dip variation of the Equatorial Anomaly is very good for its study. The strange behavior of the Equatorial Anomaly peak is presented in more detail and compared with other observations. We analyse also observations of the Brazilian Anomaly.

A slight improvement has been made in the reduction method; in the fourth chapter we also present a brief error analysis of the electron content determination.

Here we shall review only briefly the pertinent formulas on the ionosphere, magnetoionic theory and Faraday rotation leading to the results presented in the following chapters.

1.2 - Nomenclature and Symbols

B = induction of the geomagnetic field (usually in gamma units)

c = free-space velocity of electromagnetic waves

E = electric wave field with components E_x, E_y, E_z

e = electron charge or base of natural system of logarithms (2.718)

exp = exponential function

f = wave frequency

G = geometrical parameter (1.26)*

h = heigh

h_m = height of the electron density peak

h_s = satellite height

$\overline{h}$ = height of the ionospheric point

H = scale height

$i = \sqrt{-1}$

I_1 = first order electron content

I_2 = second order electron content (1.30)*

I_{2D} = second order difference electron content (4.4)*

I_{2R} = Ross second order electron content (1.27)*

j = (2.54)*

$k = \frac{\omega n}{c}$ phase constant

m = electron mass

$\overline{M}$ = (1.20)*

n = v/c phase refractive index

N = number density of electrons

N_o = maximum electron density

R = polarization of the wave-field (1.8)*

Re = real part of a complex

t = time

v = electromagnetic phase velocity

$X = \frac{N_e^2}{\epsilon_o m \omega^2}$

$Y = \frac{eB}{m\omega}$

$Y_L = Y\cos\theta$

$Y_T = Y\sin\theta$

$Z = \frac{\nu}{\omega}$

β = distribution parameter

* - Figures in parentheses denotes the equation defining the parameter.

ε = axial ratio of the polarization ellipse

ε_o = electric permitivity of free space

ζ = (2.45)*

θ = angle between the magnetic field and wave normal

λ = axial ratio angle (2.6)*

Λ= (2.41)*

ν= collision frequency

ρ= magnitude of R

τ= polarization angle (2.15)*

ϕ= phase of R

ψ= Faraday rotation (transverse magnetic field is included)

ω= $2\pi f$ angular wave-frequency

Ω= Faraday rotation (transverse magnetic field is neglected)

Units used unless advised are in the MKS system.

* - Figures in parentheses denotes the equation defining the parameter.

1.3 - Ionosphere

The ionosphere is the part of the atmosphere in which free electrons exist in sufficient quantities to affect the propagation of radio waves. The ionosphere extends from 40 or 50 km to several earth radii.

Before the propagation effects of the ionosphere can be calculated it is necessary to know how the electron number density N varies with height above the earth's surface. Here we use a simple electron density distribution given by Chapman. It uses the following assumptions:

a) An atmosphere with only one type of gas.

b) Plane stratification.

c) A parallel beam of monochromatic ionizing radiation from the sun.

d) An isothermal atmosphere.

e) The rate of electron production is proportional to the square of the electron density (loss of ions is due to a recombinations process), and the recombination coefficient is independent of height.

With these assumptions we obtain an electron density distribution

$$N = N_o \exp \frac{1}{2} \left[1 - z - \sec \chi \cdot \exp (-z)\right] \qquad (1.1)$$

where

N_o = maximum electron density

$$z = \frac{h-h_m}{H} \qquad (1.2)$$

h_m = height of the electron density peak

H = scale height

χ = zenith angle of solar ionizing radiation

This expression will be called the "Chapman law". Usually in our calculations we shall assume the following expression for the scale height, which gives a better agreement with experimental result (Potts, 1962).

$$H = 75 + 0.025\ (h - h_m) \tag{1.3}$$

all heights being expressed in km.

The average number of collisions ν which an electron makes per unit time with the air molecules depends upon the mnumber density of the molecules. Neglecting other effects, in an atmosphere which is constant in compostition and temperature.

$$\nu = \nu \exp\ (-z) \tag{1.4}$$

where ν_o is a constant.

In figure 1.1 is plotted a graph for N/N_o and ν/ν_o versus z.

Electron content I, is the number of electrons contained in a vertical column with unit base area, above the earth's surface. Usually the considered column height is the altitude of the satellite h_s used to measure I. For the satellites used (BE-B and BE-C) the electron content above the satellite height ($\simeq$ 1000 km)is small compared to the actual electron content.

So by definition we have

$$I \equiv \int_o^{\infty} Ndh \simeq \int_o^{hs} Ndh \tag{1.5}$$

We substitute (1.1) in (1.5) with constant H, and also use the substitution.

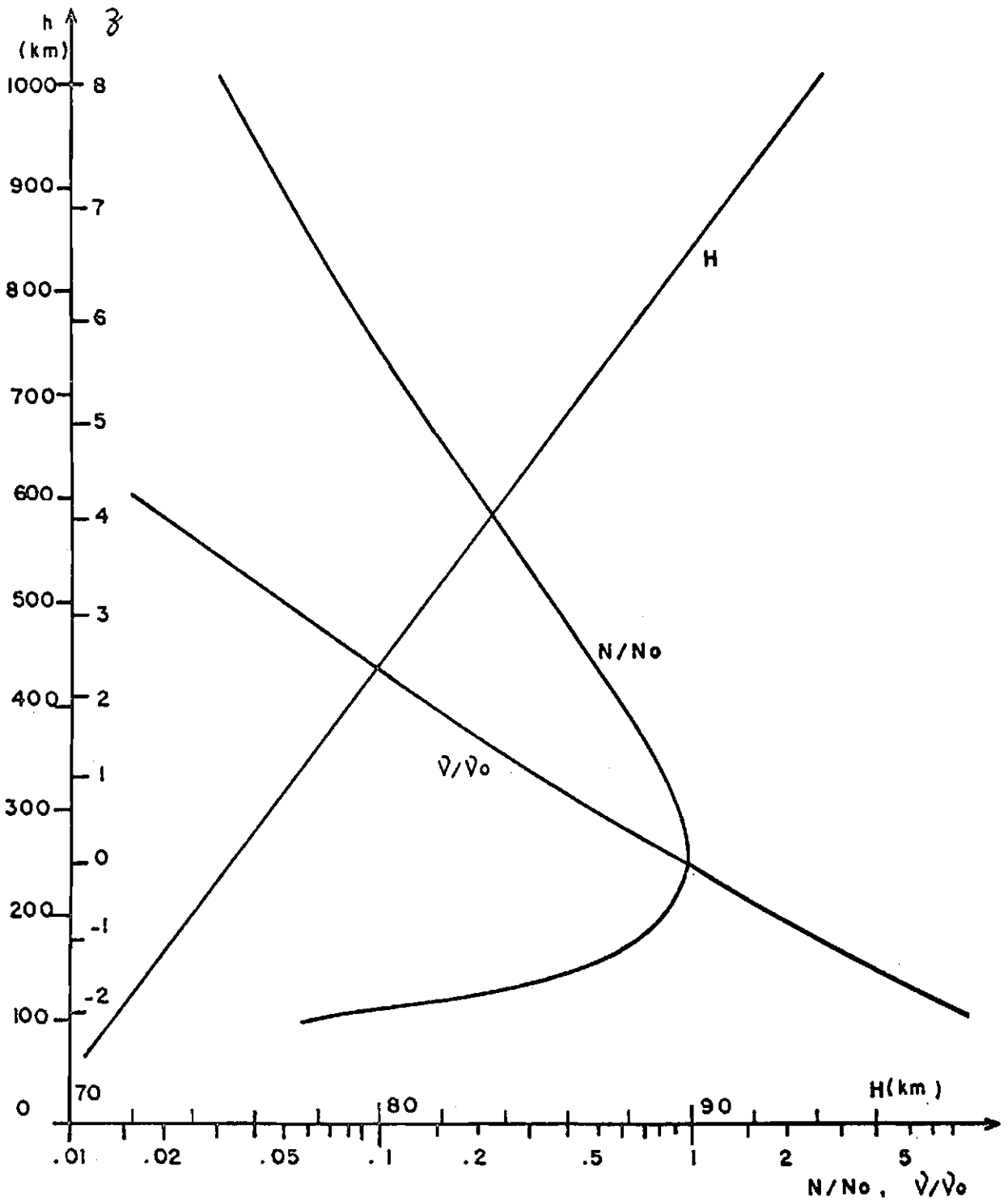

Fig.1.1 - Curve showing height variation of N/N_o, ν/ν_o and scale height H

$$\xi = \sqrt{\frac{\sec\chi}{2}} \cdot \exp(-z/2)$$

Considering that for negative height there is no contribution of N to the electron content, we obtain,

$$I = \sqrt{2\pi e \cos\chi}\ HN_o \left[1 - \mathrm{erf}(\xi_s)\right] \qquad (1.6)$$

where

$$\xi = \sqrt{\frac{\sec\chi}{2}} \cdot \exp\left(-\frac{h_s - h_m}{2H}\right)$$

erf ( ) is the error function

For $h_s \to \infty$, H (km) and N_o in electrons/m^3

$$I = \sqrt{2\pi e \cos\chi}\ HN_o = 4.14\ HN_o \cos^{1/2}\chi \ (\text{electrons/m}^2) \qquad (1.7)$$

1.4 - Magnetic Field

In calculating the electron content, it will be necessary to know the magnetic field. We use the model given by Cain et al (1964).

The potential of the internal field is written as

$$V = a \sum_{n=1} \cdot \sum_{m=0}^{n} \left(\frac{a}{r}\right)^{n+1} \left[g^{n,m} \cos(m\lambda) + h^{n,m} \sin(m\lambda)\right] P^{n,m}(\delta)$$

where

δ = colatitude

λ = longitude

a = earth radius (6378.165 km)

r = geocentric distance

g,h = Gauss coefficients

$P^{n,m}(\delta)$ = associated Legendre function (Gauss normalized)

From this potential three orthogonal components of the magnetic induction field may be derived by taking the gradient, i.e., $B = \nabla V$. In a local coordinate system, with z-axis towards the earth center and in the horizontal plane, x-axis toward north pole and y toward east, we have

$$B_x = -\frac{1}{r}\frac{\partial V}{\partial \psi} \qquad B_y = \frac{1}{r \sin \psi}\frac{\partial V}{\partial \lambda} \qquad B_z = \frac{\partial V}{\partial r}$$

The dip angle is defined by

$$\text{Dip} \equiv \tan^{-1}\left(\frac{B_z}{B_h}\right)$$

where

$B_h = \sqrt{B_x^2 + B_y^2}$ is the horizontal component of the magnetic field.

1.5 - Appleton-Hartree Equations

Here we are not going to derive Appleton-Hartree equations, but only present the assumption made and the equations that are going to be used in the following chapters. A complete derivation can be found in Ratcliffe (1962) and Budden (1961). A good review is given by Teracine (1968).

We shall define a magnetoionic medium as one in which free electrons and heavy positive ions are situated in a uniform magnetic field and are distributed with statistical uniformity, so that there is no resultant space-charge (characteristic length is greater than Debye length). There can also be neutral molecules with which the electrons can collide.

When a wave propagates through a magnetoionic medium its polarization changes but one can separate the wave into components that do not change their polarization. Those components are called characteristic waves.

The Appleton-Hartree equation gives the refractive indices ($n=v/c$) for the characteristic waves (v is the electromagnetic phase velocity) in a magnetoionic medium, as a function of the electron number density the components of the magnetic field and the collision frequency.

We choose a particular coordinate system. The z axis is taken along the wave normal, and the magnetic field lies in the yz-plane. Any other coordinate system can be transformed into this particular system by a coordinate change.

We make the following assumptions:

a) Sinusoidal progressive wave
b) Steady magnetic field $\vec{B}$
c) The force due to the electron motion in the magnetic field of the wave is negligible
d) Electron collisions are independent of electron energy
e) The thermal motions of the electrons are unimportant. (Cold plasma)
f) Steady-State solution
g) The magnetic properties of the medium are those of free space.

We define a complex quantity R, which we shall call the "polarization of the wave-field", by

$$R \equiv \frac{E_x}{E_y} \tag{1.8}$$

If R is a real quantity, the electric field of the wave is linearly polarized, if R is complex it is elliptically polarized.

We define a complex quantity Q, which we will call the "transverse-longitudinal ratio", by

$$Q \equiv \frac{Y_T^2}{2\, Y_L\, (1 - X - iZ)} \tag{1.9}$$

where X, Y_L, Y_T, Z are defined in § 1.2.

From the equation of motion for the electron we obtain the following relation (see Budden, 1961):

$$R^2 + 2iQR + 1 = 0$$

From here we obtain two solutions for the two characteristic waves, denoted by subscripts + and -, referring to ordinary and extraordinary modes, respectively.

$$R^+ R^- = 1 \tag{1.10}$$

$$R^+ + R^- = - 2iQ \tag{1.11}$$

$$R = - i \left[Q \mp \sqrt{1 + Q^2} \right] \tag{1.12}$$

The refractive index is given by the expression

$$n^2 = 1 - \frac{X}{1-iZ-iY_L R} \tag{1.13}$$

These equations are valid in a variable medium since the constitutive relations used depend only on the properties of the ionosphere at the point considered, and do not depend on how these properties vary from point to point.

1.6 - Quasi-Longitudinal and Quasi-Transverse Approximations

The complete expressions for the complex refractive index (1.13)and the polarization (1.12) are quite complicated. There are some important cases when we can make some approximations, one of which applies when waves are propagating sufficiently nearly along the direction of the imposed field (quasi-longitudinal, QL) and the other when they are propagating sufficiently perpendicular to it (quasi-transverse, QT). The

conditions for which they hold are

$$|Q^2| << 1 \quad \ldots\ldots \quad [QL]$$

$$|Q^2| >> 1 \quad \ldots\ldots \quad [QT]$$

The expressions for R and n become

QL:

$$R_{QL} \simeq \pm i \quad \text{(circularly polarized)} \tag{1.14}$$

$$n^2_{QL} \simeq 1 - \frac{X}{1 - iZ \pm Y_L} \tag{1.15}$$

QT:

$$\left.\begin{aligned} R^+_{QT} &\simeq 0 \\ R^-_{QT} &\simeq \infty \end{aligned}\right\} \text{(linearly polarized)}$$

When the collision term is negligible Q is a real quantity ar we shall represent it by the following symbols:

$$q_{TL} \equiv \frac{1}{q_{LT}} \equiv \frac{Y_T^2}{2Y_L(1-X)} \tag{1.16}$$

1.7 - Faraday Effect

1.7.1 - First Order Theory

The Faraday effect on electromagnetic waves in a magnetoionic medium consists in the change of the plane of polarization of an originaly linearly polarized wave, propagating through the medium. From the Faraday rotation the electron content can be calculated.

Let us explain how this occurs, making some approximations.

For high-frequency waves, frequently we can apply the QL approximations.

In our case for BE-B and BE-C f = 40 MHz, the maximum angle θ (angle between the ray path and the magnetic field component in the plane of incidence of the wave) for which the QL-approximations holds is $\theta \simeq 84^{o}$, from expression 1.16, using ghe typical values of Fig.2.8, for X = 0.05 and Y = 0.02.

Normally during a BE-B satellite pass the QL-approximation does not hold only during 40 seconds.

In the QL-approximation the radio wave can be decomposed into two circularly polarized characteristic waves (§ 1.6) with the following refractive indices.

$$n^2 \simeq 1 - \frac{X}{1 \pm Y_L} \qquad (1.17)$$

where the collision term is neglected.

Relation 1.17 shows that the two modes propagate with different phase velocities. We assume an initially linearly polarized electromagnetic wave, represented in a complex plane normal to the ray path, and separated in the two characteristic waves

$$E(o) = E_o \left[\text{expi}\ (\Omega_o + \omega t) + \text{expi}(\Omega_o - \omega t)\right]$$

where Ω_o is the initial tilt angle of the polarization plane and each term of the second member represents one of the characteristic waves. After the wave propagates a distance dz we have

$$E(dz) = E_o \left[\text{expi}(\Omega_o + \omega t - k^{+} dz) + \text{expi}(\Omega_o - \omega t + k^{-} dz)\right]$$

The polarization conserves its linearity and the tilt angle will be given by

$$\Omega_o + \omega t - k^+ dz = \Omega_o - \omega t + k^- dz = \Omega$$

Hence

$$d\Omega = \Omega - \Omega_o = \frac{1}{2} (k^- - k^+)\, dz$$

So

$$d\Omega = \frac{\omega}{c} (n^- - n^+)\, dz \qquad (1.18)$$

Developing (1.17) in a bynomial series and assuming X and Y_L small quantities

$$n^- - n^+ \simeq XY_L$$

Integrating (1.18) along a straight ray path, substituting the expression given in §1.2 and supposing that there are no horizontal gradients in the electron density N we have

$$\Omega = \frac{A}{f^2} \int_o^{h_s} NM\,dh \qquad (1.19)$$

where

$$A = \frac{e^3}{8\pi^2 \varepsilon_o m^2 c} = 2.36 \times 10^4 \text{ (MKS units)}$$

$M = B \cdot \cos\theta \cdot \sec\chi$

θ is the angle between the ray path and the magnetic field component in the plane of incidence of the wave

χ the zenith angle of the ray path at height h.

Ω is given in radians

h_s is the satellite height

Defining

$$\bar{M} = \frac{\int_o^{h_s} M.Ndh}{\int_o^{h_s} Ndg} \qquad (1.20)$$

we obtain

$$\Omega = A\bar{M}\, I_1/f^2 \qquad (1.21)$$

where I_1 is the electron content defined in (1.5), and will be called "first order electron content".

For a down-coming wave the value of M varies almost linearly; and taking a linear variation for M with height

$$M = M_o + M_1 \cdot h$$

substituting in (1.20)

$$M_o + M_1 \cdot \bar{h} = \frac{\int_o^{h_s} (M_o + M_1 . h)\, Ndh}{\int_o^{h_s} Ndh}$$

the solution for $\bar{h}$ gives

$$\bar{h} = \frac{\int_o^{h_s} hNdh}{\int_o^{h_s} Ndh}$$

which represents the centroid of the N x h profile.

The point where the ray path crosses this height is called "ionospheric point", and the electron content will be associated to the coordinates of this point. Its projection on to the earth is called "sub-ionospheric point". Using expression 1.6 we can compute $\bar{h}$ by taking

$$\int_0^{\bar{h}} Ndh = \int_{\bar{h}}^{\infty} Ndh$$

whence, for vertical incidence of solar radiation, we get

$$\bar{h} - h_m = 2H \ln (\sqrt{2} \cdot \mathrm{erf}^{-1} 5) = 0.986H$$

In our case we do not have ionogram data, so we consider $h_m \simeq 300$ km and $H \simeq 100$ km and obtain $\bar{h} \simeq 350$ km, which is used in all our electron content calculations. So a good approximation is reached assuming $\bar{M}$ as the value of M taken at the height $\bar{h}$. A variation of 50 km about the assumed value of 50 km about the assumed value of 350 km results in about 5% deviation on the electron content. (O.G. Almeida and H.Waldman, 1967).

From relation (1.21) finally we have the expression of the electron, which gives for f = 40 MHz

$$I_1 = \frac{f^2}{A} \cdot \frac{\Omega}{\bar{M}} = 2.1268 \times 10^{20} \frac{\Omega}{\bar{M}} \qquad (1.22)$$

where Ω is given in half turns of the tilt angle or cycles in a recorded signal (see Fig.3.12) and $\bar{M}$ is given in gammas.

Interpreting physically the relations obtained we see that:

The total electric field is linearly polarized and its plane of polarization rotates as given by (1.19) because the two circularly polarized characteristic waves propagate with different phase velocities (1.17). This rotation Ω is proportional to the electron content (1.21) and therefore it can be computed by knowing the Faraday rotation angle (1.22). Ω is inversely proportional to the signal frequency, so for very high frequencies Ω will be very small. In regions where the longitudinal component of the magnetic field is very small, the value of $\bar{M}$ will also be small and therefore Ω will have a small value. When the ionospheric point passes through

a region where the magnetic field lies in a plane normal to the ray path; $\overline{M} = 0$ and $\Omega = 0$. For deduction of (1.21) the QL approximations are not valid; and in chapter 2 we study the behavior of Ω near this region and we see that there is little Faraday rotation. The point where this happens is named the "QT region" and its identification in the satellite recorded signal leads us to determine the absolute number of Faraday rotations.

1.7.2 - Second Order Theory

In deducing (1.22) we made several approximations. In order to improve the results we shall introduce some second-order effects.

We are going to use the relation obtained by Ross (1965) that includes the following second-order effects:

a) The non-uniform distribution of ionization that causes the various rays to be refracted and follow different paths between the source and the receiver

b) The non-linearity of the refractive index with electron density and magnetic field intensity

c) The anisotropy of the medium which causes the wavenormal and ray for a particular mode of propagation to be non-coincident in direction.

However, it also makes use of some simplifications:

a) The spherically stratified ionosphere model is replaced by a plane stratified model in which the originally spherical ionization contours are replaced by a set of parallel plane contours tangent to the former at the point where the straight line path intersects the ionospheric point.

b) The non-uniform magnetic field is replaced by a uniform field having the magnitude and direction of the original field at the ionospheric point

c) The methods of ray optics are used.

d) The refractive index is given by the quasi-longitudinal form of the Appleton Hartree equation.

Taking all these into consideration Ross (1965) obtained the polarization rotation angle Ω_m as determined by the second-order theory, in terms of the rotation angle Ω_1 given by first-order theory (1.21) as

$$\Omega_m = \Omega_1 \left[1 + \frac{\overline{X}}{2} \left[\beta + (\beta - 1)\, G\right]\right] \tag{1.23}$$

where

$\overline{X}$ is the height average of X over the range of integration.

β is the distribution parameter

G is the geometrical parameter

The distribution parameter β measures the non-uniformity in which the ionization is distributed over the height of integration. It is defined by

$$\beta = \frac{h_s \int_0^{h_s} X^2 dh}{\left[\int_0^{h_s} S dh\right]^2} \tag{1.24}$$

Using expression 1.1 for the electron density distribution in (1.24) and integrating we get

$$\beta = \frac{h_s}{2\pi H} \tag{1.25}$$

for h_s = 1000 km and H = 60 km we get β = 2.64.

For a uniform slab layer of thickness Δh we obtain $\beta = h_s/\Delta h$.

If we relate β to the slab thickness τ then for the electron density distribution given by (1.1)

$$\tau = \frac{\int_0^{h_s} N dh}{N_o} = H\sqrt{2\pi e} = 4.13H$$

this substituted in (1.25) gives

$$\beta = \frac{h_s}{\tau} \sqrt{\frac{e}{2\pi}} = \frac{h_s}{1.54\tau}$$

So finding the slab thickness we would have the value for β.

The geometrical parameter G is defined by

$$G = \tan \chi \cdot (\tan \chi - \frac{B_1}{B_L}) \tag{1.26}$$

where

χ is the zenith angle of the ray path

B_1 is the transverse component of the magnetic field $\vec{B}$ in the plane of incidence of the wave, and measured positively upwards.

B_L is the component of $\vec{B}$ along the straight line path, measured positively upwards.

Figure 1.2 shows the geometry of the involved quantities.

Map of G for geographical region near S.J.Campos can be found in Mendonça et al (1965).

Multiplying both sides of (1.23) by $f^2/A\overline{M}$ we have

$$I_1 = I_2 \quad 1 + \frac{\overline{X}}{2} \left[\beta + (\beta - 1)\, G\right] \tag{1.27}$$

$$\overline{X} = \frac{80.5}{f^2 h_s} \quad I_2$$

This is a quadratic equation for I_2 and is further discussed in §4.2. The electron contents calculated from (1.27) have a typical improvement in accuracy of an order of magnitude over the first order (1.22).

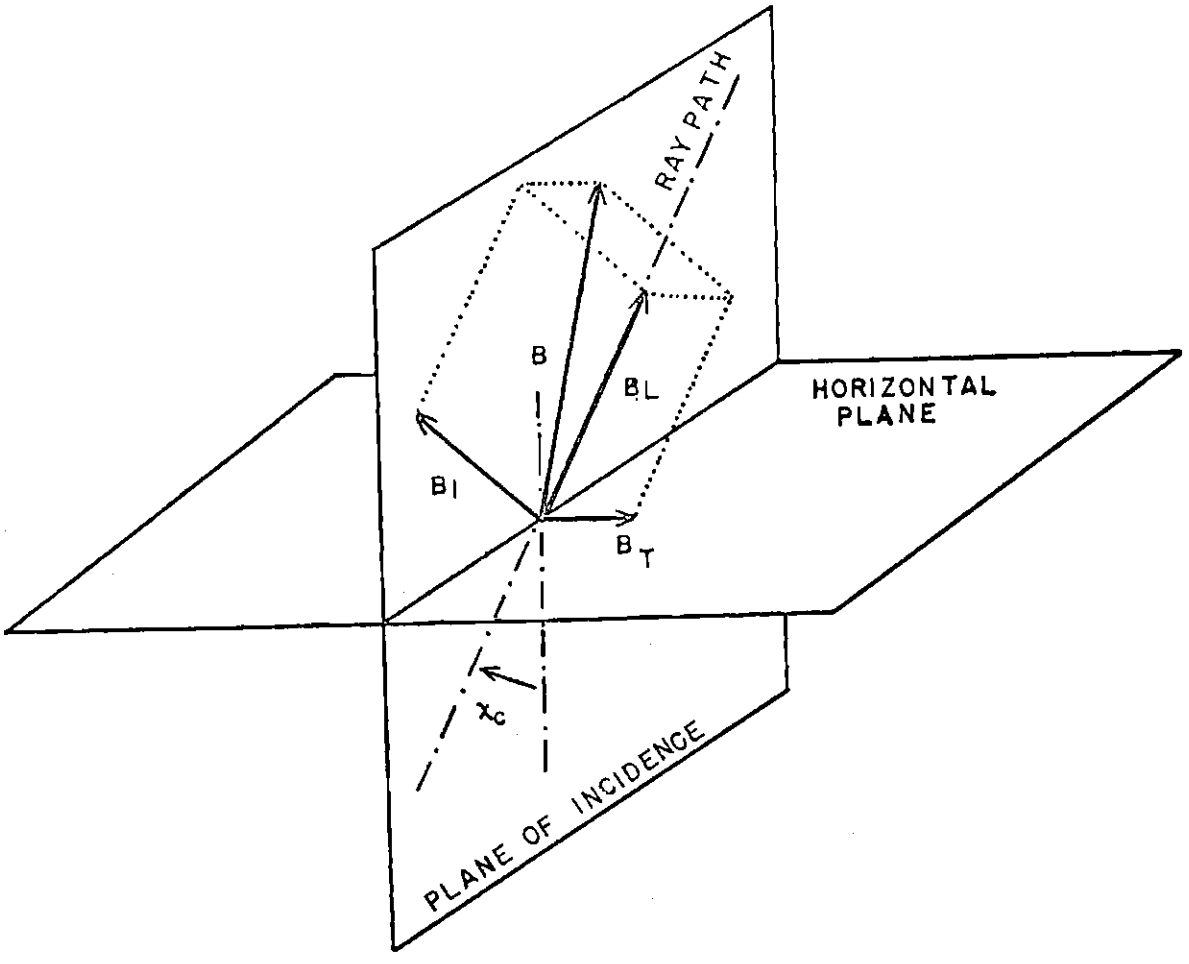

Fig.1.2 - Geometry for the calculation of G

1.7.3 - Closely-Spaced Frequencies Electron Content Determination

Using closely-spaced frequencies the second order correction term of (1.27) can be determined. (Mendonça et al, 1965).

The frequency dependence of the parameters in (1.23) are

$$\Omega = \Omega_o/f^2 \propto f^{-2}$$

$$\overline{X} = \overline{X}_o/f^2 \propto f^2$$

so we can write expression (1.23) as

$$\Omega_m = \frac{\Omega_{o1}}{f^2} \left[1 + \frac{\overline{X}_o}{2f^2} C \right] \tag{1.28}$$

where $C = \beta + (\beta - 1) G$ which is independent of the frequency.

Differentiating (1.28) we have

$$d\Omega_m = - 2\Omega_1 \frac{df}{f} (1 + \overline{X} C)$$

From (1.28) it turns out that

$$\overline{X}C = 2 \frac{\Omega_m - \Omega_1}{\Omega_1} \tag{1.29}$$

therefore

$$d\Omega_m = -2 \frac{df}{f} (2\Omega_m - \Omega_1)$$

and

$$\Omega_1 = \Omega_m \left(2 + \frac{f d\Omega_m}{2\Omega_m df}\right)$$

If the frequencies are closely spaced (in our case 40 and 41 MHz) the differentials can be replaced by differences Δ, and multiplying both sides by $f^2/A.\overline{M}$ we have

$$I_2 = I_1 \left(2 + \frac{f\Delta\Omega_m}{2\Omega_m \Delta f}\right) \tag{1.30}$$

where I_2 is the second order electron content, I_1 the first order electron content (1.22), Ω_m is the measured Faraday rotation and $\Delta\Omega_m$ the difference between the measured Faraday rotations in the two frequencies.

For the received frequencies (40 and 41 MHz) we have

$$I_2 = I_1 \left(2 + 20 \frac{\Delta\Omega_m}{\Omega_m}\right) \tag{1.31}$$

Knowing $\bar{M}$ by the satellite ephemerides and a magnetic field model §1.4, and the measured Faraday rotation by (1.22) we obtain I_1. Measuring the difference of Faraday rotations between the two frequencies by means of the coincidence of Faraday nulls in a recorded signal the second order electron content I_2 can be calculated by (1.31).

Additional comments will be made in chapter 4.

CHAPTER 2

POLARIZATION OF WAVES THROUGH THE IONOSPHERE

2.1 - Introduction

Here we are going to deduce a set of equations that gives the tilt-angle and axial ratio of the polarization ellipse for a wave travelling through a magnetoionic medium.

Special attention is given to the propagation through a quasi-transverse region, where we are looking for a particular phenomenon that cannot be explained by the equations describing the Faraday effect (§1.7) when the transverse component of the magnetic field is not considered. This analysis leads us to a method for determining the electron density profile near the QT point.

2.2 - Polarization

2.2.1 - Tilt-Angle and Axial Ratio

The polarization of a wave can be described by the complex R defined in (1.8).

$$R = \rho \cdot \exp i\phi = \frac{E_x}{E_y} \qquad (2.1)$$

In this section we are going to find the inclination of the polarization ellipse with respect to the coordinate axis (tilt-angle, ψ) and the ratio of the minor axis and major axis (axial ratio, ε), in terms of the complex R. This ellipse is given by the locus of E = ReEx + i ReEy as a function of time (Fig.2.1).

We consider the same coordinate system as in § 1.5 and associate a complex plane with the xy-plane. Suppose a sinusoidal electromagnetic wave of the type

$$\left.\begin{aligned} E_x &= E_{xo} \exp i(\phi_x + \omega t) \\ E_y &= E_{yo} \exp i(\phi_y + \omega t) \end{aligned}\right\} \qquad (2.2)$$

propagating in the medium.

Any plane monochromatic wave can be decomposed into two circular components rotating in opposite directions

$$E_a = E_{ao} \exp i (\chi_a + \omega t) \qquad (2.3)$$

$$E_b = E_{bo} \exp i (\chi_b - \omega t) \qquad (2.4)$$

where E_{ao}, E_{bo} are real positive quantities. The total field in the complex plane is described by

$$E = E_a + E_b \qquad (2.5)$$

The major axis and the minor axis are respectively given by

$$a = E_{ao} + E_{bo}$$

$$b = E_{bo} - E_{ao}$$

the axial ratio is given by $\varepsilon = b/a$. We define an "axial ratio angle" λ (Fig. 2.2) by

$$\tanh \lambda = \varepsilon = \frac{b}{a} = \frac{E_{bo} - E_{ao}}{E_{ao} + E_{bo}} \qquad (2.6)$$

when $\lambda > 0$ it is right hand polarized

$\lambda < 0$ it is left hand polarized

The tilt angle ψ is given when E_a and E_b are in phase. It should be noted that we take for convenience the tilt angle measured clockwise from y axis (Fig. 2.1).

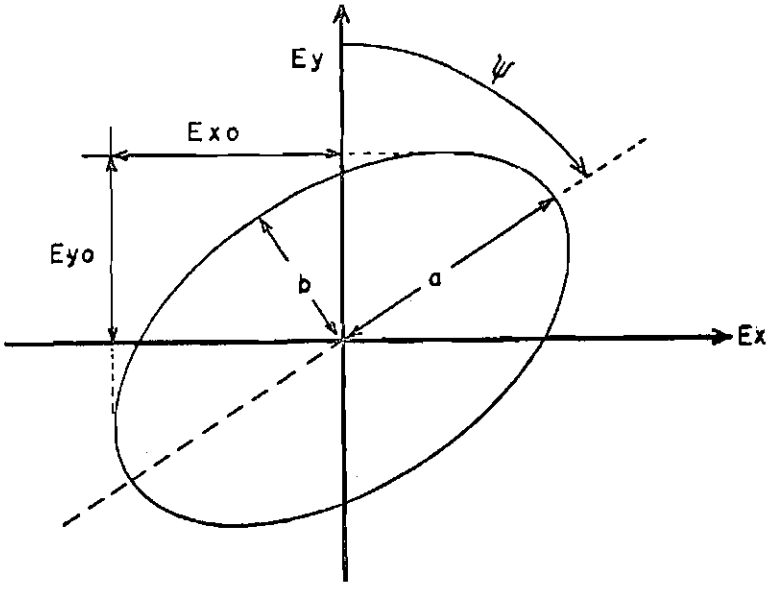

Fig.2.1 - Polarization ellipse showing coordinate system and axis

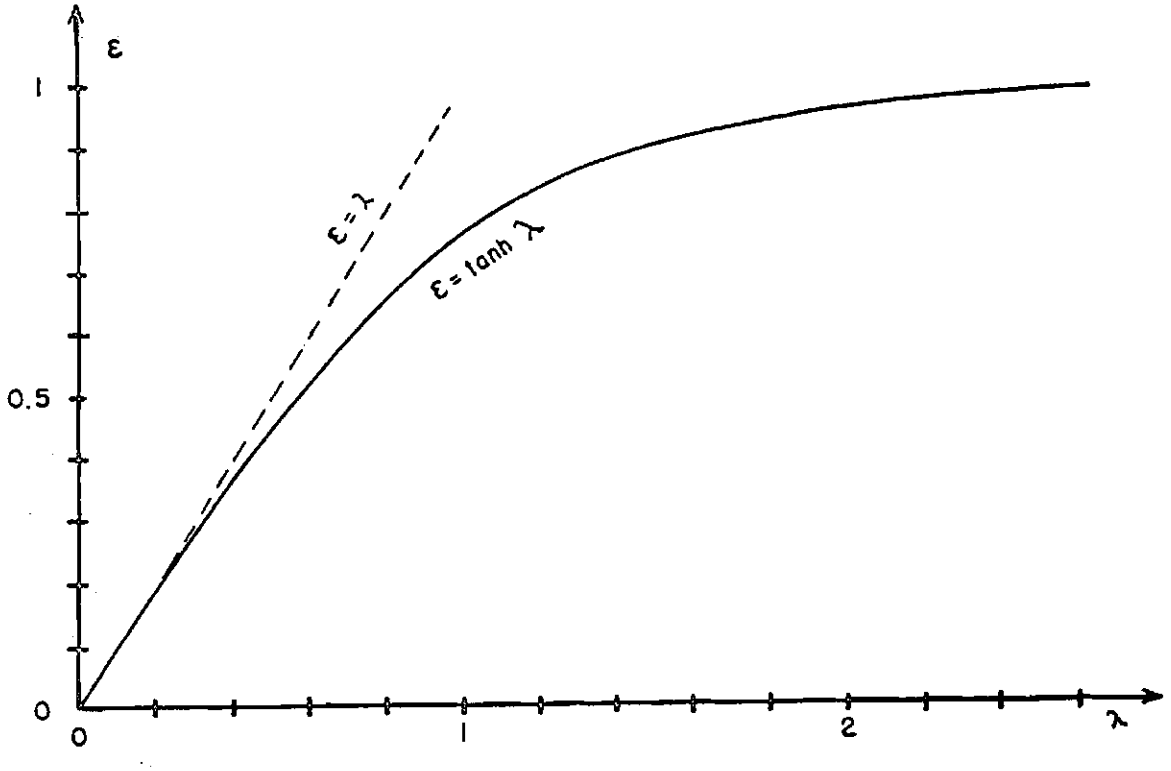

Fig.2.2 - Relation between axial ratio ε and λ. ($\tanh(-\lambda) = -\varepsilon$)

$$\pi/2 - \psi = \chi_a + \omega t = \chi_b - \omega t$$

Hence

$$\psi = \frac{1}{2} \left[\pi - (\chi_a + \chi_b) \right] \tag{2.7}$$

Now we shall relate these parameters ψ, λ with the polarization R. From (2.1) and (2.2) it follows that

$$R = \frac{E_x}{E_y} = \left(\frac{E_{xo}}{E_{yo}}\right) \exp i(\phi_x - \phi_y) \tag{2.8}$$

The polarization ellipse is described by

$$E = E_a + E_b = \mathrm{Re}E_x + i\mathrm{Re}E_y \tag{2.9}$$

where

$$\mathrm{Re}E_x = \frac{E_x + E_x^*}{2} \qquad \mathrm{Re}E_y = \frac{E_y + E_y^*}{2}$$

We have the linear relations between E_a, E_b and E_x, E_y

$$\left.\begin{aligned} E_a &= a_{11} E_x + a_{12} E_y \\ E_b &= a_{21} E_x^* + a_{22} E_y^* \end{aligned}\right\} \tag{2.10}$$

The conjugate (*) is taken because the relation must be independent of time.

The relation must be independent of the value of E_x and E_y, substituting equation 2.10 in (2.9), and taking each part separately, it follows that

$$E_x + E_x^* = 2 (a_{11} E_x + a_{21} E_x^*)$$

$$i (E_y + iE_y^*) = 2 (a_{12}E_y + a_{22}E_y^*)$$

Separating the expression into its real and imaginary parts, the equations must be satisfied by arbitrary E_x and E_y. The result gives

$$\left.\begin{aligned} E_a &= \frac{1}{2}(E_x + iE_y) = \frac{1}{2}E_x(1 + iR) \\ E_b &= \frac{1}{2}(E_x^* + iE_y^*) = \frac{1}{2}E_x^*(1 + iR^*) \end{aligned}\right\} \tag{2.11}$$

Taking the inverse relation we get

$$\left.\begin{aligned} E_x &= E_a + E_b^* \\ E_y &= -i(E_a - E_b^*) \end{aligned}\right\} \tag{2.12}$$

Substituition of (2.12) into (2.1) gives

$$R = \frac{E_x}{E_y} = \frac{E_a + E_b^*}{E_a - E_b^*} = i\,\frac{\left(\frac{E_{ao}}{E_{bo}}\right)\exp i(\chi_a + \chi_b) + 1}{\left(\frac{E_{ao}}{E_{bo}}\right)\exp i(\chi_a - \chi_b) - 1} \tag{2.13}$$

From (2.6) and (2.7) we obtain

$$\chi_a + \chi_b = \pi - 2\psi$$

$$(E_{ao}/E_{bo}) = \exp(2\lambda)$$

which substituted in (2.13), after some rearrangement becomes

$$R = \tan(\psi + i\lambda) \tag{2.14}$$

It is convenient to write

$$T \equiv \psi + i\lambda \quad (\text{"polarization angle"}) \tag{2.15}$$

so that

$$\tan T = R \tag{2.16}$$

2.2.2 - Properties of the Polarization angle

In Fig. 2.3 we display a polarization chart showing the lines of constant ρ and ϕ (2.1) in a T plane.

It can be shown that if than $T = R$

the following relations hold

$$\tan T^* = R^*$$

$$\tan(-T) = R \exp i$$

The sense of rotation of the ellipse can be found from (2.2)

right hand $\phi(\text{mod } \pi) > 0$ or $\lambda > 0$

left hand $\phi(\text{mod } \pi) < 0$ or $\lambda < 0$

To express ρ, ϕ in the terms of ψ, λ we separate (2.14) into real and imaginary parts and solving for ψ and λ we get

$$\tan(\psi + i\lambda) = \frac{\tan \psi + i\varepsilon}{1 - i\varepsilon \tan \psi} \tag{2.17}$$

$$\left.\begin{aligned} \tan 2\psi &= \frac{2\rho \cos \phi}{1 - \rho^2} \\ \tanh 2\lambda &= \frac{2\rho \sin \phi}{1 + \rho^2} \end{aligned}\right\} \tag{2.18}$$

From where the axial ratio ε can be found as

$$\varepsilon = \frac{1}{\tanh 2\lambda} \left[1 - \sqrt{1 - \tanh^2 2\lambda}\right] \tag{2.19}$$

2.2.3 - Approximations and Formulas

Within some limits we can use ε in place of λ , the error is given by $\approx 33\ \varepsilon^2$ (%)

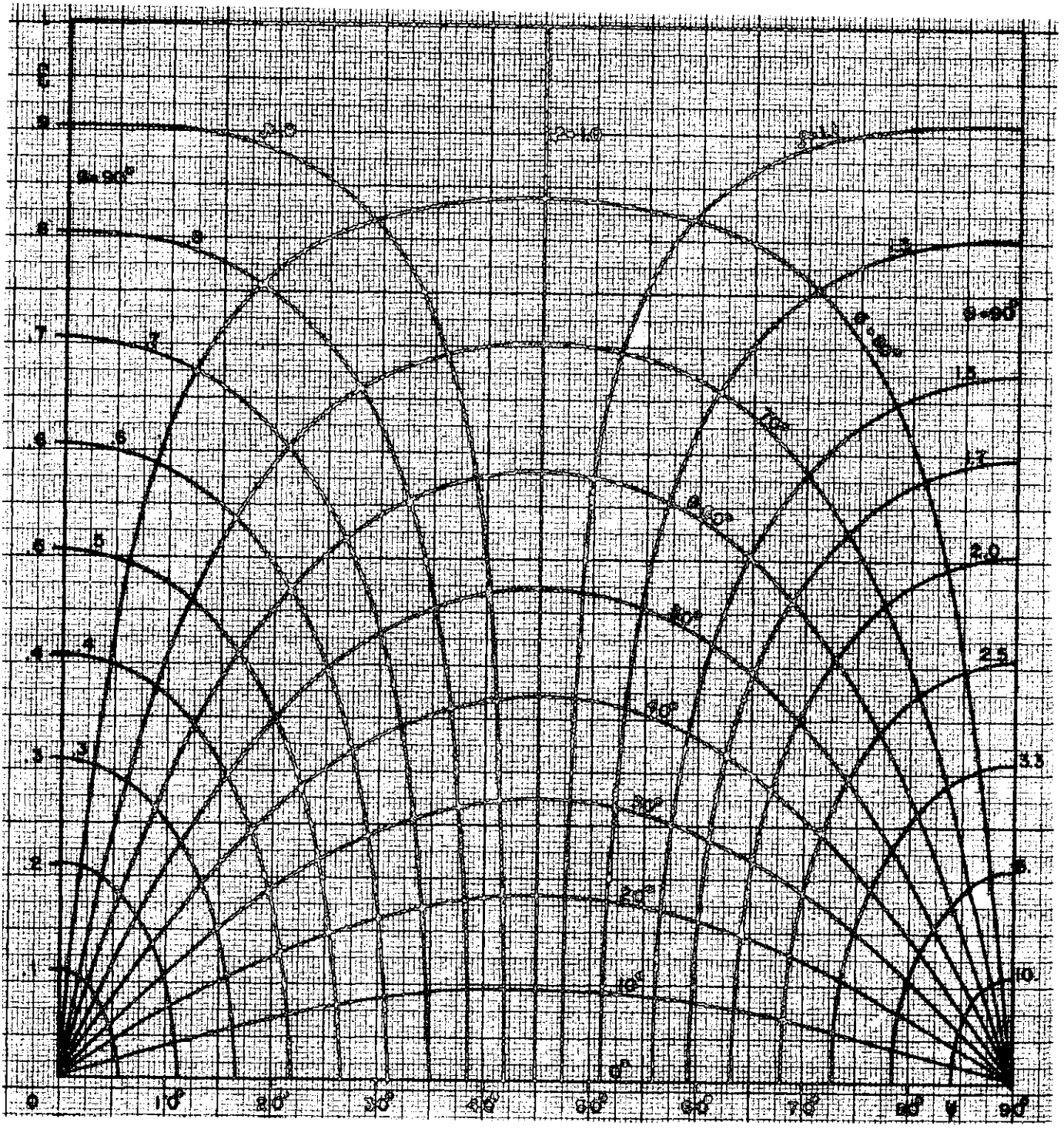

Fig 2.3 Lines of constant ρ and ϕ ($R=\rho e^{i\phi}$) in the complex plane $\Upsilon=\psi+i\varepsilon$. For ϕ outside the first quadrant we can use the following relations $R^{*}=\tan \Upsilon^{*}$ and $Re^{i\Pi}=\tan(-\Upsilon)$ when $R=\tan\Upsilon$.

for $\varepsilon < 0,35$ error < 5%

$\varepsilon < 0,51$ error < 10%

The following expressions relating λ and ε will be used in the text

$$Sh2\lambda = \frac{2\varepsilon}{1 - \varepsilon^2} \tag{2.20}$$

$$Ch2\lambda = \frac{1 + \varepsilon^2}{1 - \varepsilon^2} \tag{2.21}$$

$$\tanh 2\lambda = \frac{2\varepsilon}{1 + \varepsilon^2} \tag{2.22}$$

$$d\lambda = \frac{d\varepsilon}{1 - \varepsilon^2} \tag{2.23}$$

2.3 - Polarization Variation of Waves in a Magneto-Ionic Medium

2.3.1 - Homogeneous Magnetoionic Slab

Here we find the expression for the change of polarization when a wave passes through a slab of magnetoionic medium.

Let a plane radio wave be normally incident on a homogeneous magnetoionic slab (Fig.2.4) with thickness Δz. The electric field of the wave can be decomposed into its ordinary and extraordinary modes.

Using matrix notation

$$\vec{E} = \begin{bmatrix} Ex \\ Ey \end{bmatrix} \quad \text{and} \quad \vec{E}^{\pm} = \begin{bmatrix} E^{+} \\ E^{-} \end{bmatrix}$$

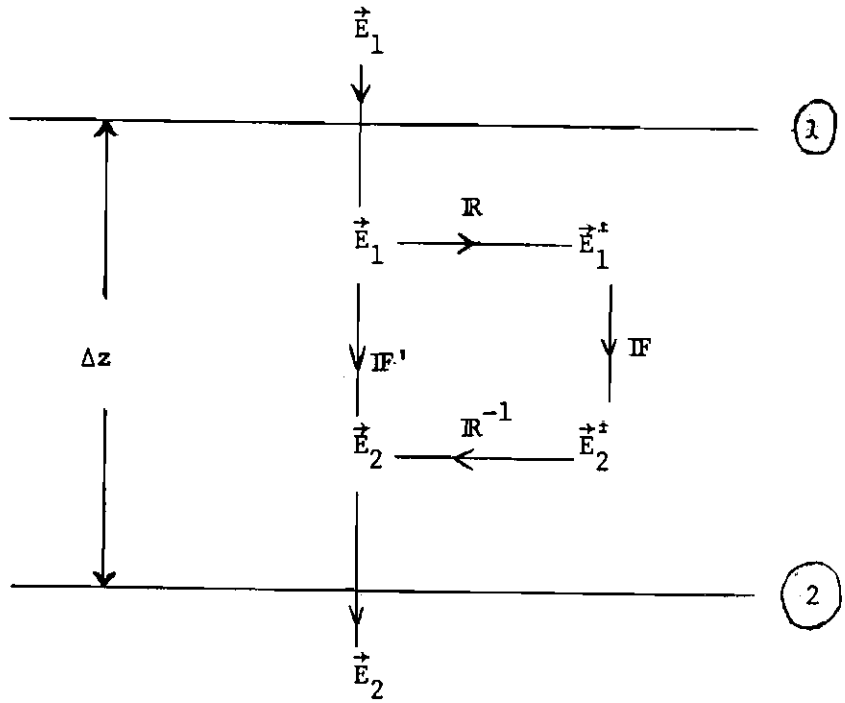

Fig.2.4 - Scheme of wave component transformations

by definition (1.8) we have

$$R^{+} \equiv \frac{Ex^{+}}{Ey^{+}} \qquad\qquad R^{-} \equiv \frac{Ex^{-}}{Ey^{-}}$$

So

$$\begin{cases} Ex = Ex^{+} + Ex^{-} = R^{+}\, Ey^{+} + R^{-} Ey^{-} \\ Ey = Ey^{+} + Ey^{-} \end{cases}$$

whence

$$\vec{E} = \mathbb{R}\, \vec{E}^{\pm} \qquad (2.24)$$

where

$$\mathbb{R} = \begin{bmatrix} R^{+} & R^{-} \\ 1 & 1 \end{bmatrix}$$

Each characteristic wave will change its phase at the end of the slab, as follows:

$$E_2 = \mathbb{F} \; E_1 \tag{2.25}$$

where

$$\mathbb{F} = \begin{bmatrix} e^{-ik^{+}\Delta z} & 0 \\ 0 & e^{-ik^{-}\Delta z} \end{bmatrix} \tag{2.26}$$

$$k = \frac{\omega n}{c}$$

We need a relation between $\vec{E}_2$ and $\vec{E}_1$

$$\vec{E}_2 = \mathbb{F}' \; \vec{E}_1 \tag{2.28}$$

Using (2.24) and (2.25), gives

$$\mathbb{F}' = \mathbb{R} \; \mathbb{F} \; \mathbb{R}^{-1} \tag{2.29}$$

The expression of the total wave polarization is given by $R = Ex/Ey$ and from (2.28) we can express the total wave polarization in each side of the slab in terms of the matrix coefficients of $\mathbb{F}'$

$$R_2 = \frac{F'_{11} R_1 + F'_{12}}{R'_{21} R_1 + F'_{22}} \tag{2.30}$$

Defining $\Delta k \equiv k^{+} - k^{-}$ (2.31)

and rewriting (2.29) explicitely

$$\mathbb{F}' = \frac{e^{-ik^{-}\Delta z}}{R^{+} - R^{-}} \begin{bmatrix} (R^{+} e^{-i\Delta k\Delta z} - R^{-}) & (1 - e^{-i\Delta k\Delta z}) \\ (e^{-i\Delta k\Delta z} - 1) & (R^{+} - R^{-} e^{-i\Delta k\Delta z}) \end{bmatrix}$$

Substituting the above expression in (2.30) we obtain

$$R_2 = \frac{\left[R_1 R^{+} - 1\right] e^{-i\Delta k\Delta z} - R^{-} R_1 + 1}{\left[R_1 + R^{-}\right] e^{-i\Delta k\Delta z} - R_1 + R^{+}}$$

Adding and subtracting R_1, making use of (1.10), after some rearrangement, it becomes

$$\Delta R \equiv R_2 - R_1 = \frac{(R_1 - R^{+})(R_1 - R^{-})(1 - e^{-i\Delta k\Delta z})}{(R_1 - R^{-})\, e^{-i\Delta k\Delta z} - (R_1 - R^{+})} \qquad (2.32)$$

From the above expression, it can be seen that when the polarization of the wave is the same as of one of the characteristic waves, there is no change of polarization. ΔR depends only in the slab thickness, difference of refractive index and the differences between the wave polarization and the "characteristic polarization".

2.3.2 - Slowly Varying Medium

Let us consider a slowly varying medium, where dn/dz and d^2n/dz^2 are sufficiently small, but n is not too small; in this case the reflections can be neglected (Budden, 1961). The electron density and collision frequency in the ionosphere vary continuously with the height, but we may imagine that the ionosphere is replaced by a number of thin discrete strata, in each of which the medium is homogeneous. By making these strata thin enough and numerous, we may approximate the actual ionosphere as closely as desired.

With an infinitesimal thickness dz, the second order term in equation 2.32 can be neglected and this equation reduces to

$$\frac{dR}{dz} = i \left[1 + R^2 - (R^+ + R^-) \cdot R \right] \frac{\Delta k}{R^+ - R^-} \qquad (2.33)$$

After substituition of expression (A.3) from appendix A, it becomes

$$\frac{dR}{dz} = \left[(1 + R^2)\, Y_L + \frac{i\, Y_T^2\, R}{(i-X-iZ)} \right] \frac{X}{2(1-X-iZ)} \cdot \frac{\omega}{c} \qquad (2.34)$$

Expressing the above equation in terms of T and using (2.16) we get

$$\frac{dT}{dz} = \left[Y_L + \frac{Y_T^2}{2(1-X-iZ)} \right] \mathrm{Sh}\ 2iT\ \frac{X}{2(1-X-iZ)}\ \frac{\omega}{c} \qquad (2.35)$$

It should be remarked that the advantage in using (2.35) rather than (2.34) are:

a) We are more interested in the variation of the tilt angle and axial ratio than in the polarization R.

b) Suppose a plane-polarized wave propagating through a magnetoionic medium where the transverse component of the magnetic field is negligible. From §1.7 it is seen that the plane of polarization will change continuously and the polarization will remain linear. In this case the polarization vector is given by $R = \tan\psi(z)$. When $\psi(\mathrm{mod}\ 2\pi) = \pm \pi/2$, R becomes infinity, presenting difficulties in the numerical solutions of the differential equation (2.34). This does not happen with (2.35).

The conditions for (2.35) to be valid in the ionosphere are:

a) Slowly varying medium

b) Plane stratification of the ionosphere

c) Vertical incidence of plane waves

d) No reflection occurs

d) C, Y_L, Y_T, Z << 1

For a plane wave incident obliquely on the ionosphere in this chapter, we neglect the curvature of the ray path and the splitting between oridinary and extraordinary modes. These approximations are valid in the range of validity of (2.35). We also make the transformation

$$dz = \sec \chi \cdot dh \tag{2.36}$$

where χ is the zenith angle of the ray path at the heigh $\bar{h}$.

It is convenient to write

$$\left.\begin{aligned} x &\equiv \frac{\omega}{2c} \frac{X}{(1 - X)} \\ y_L &\equiv Y_L \\ y_T &\equiv \frac{Y_T^2}{2(1-X)} \end{aligned}\right\} \tag{2.37}$$

From (1.16) $q_{TL} = \dfrac{1}{q_{LT}} = \dfrac{y_T}{y_L}$

So that when Z is negligible, (2.34) and (2.35) becomes

$$dR = \left[(1 + R^2)\, y_L + 2iy_T R \right] x\,dz \tag{2.38}$$

and similarly

$$d\tau = (y_L + y_T \cdot \mathrm{Sh}\, 2i\tau)\, x\,dz \tag{2.39}$$

2.3.3 - Some General Properties of Polarization Equation

a) Equation (2.35) can be written as

$$\dot{T} = f_L(z) + f_T(z) \cdot Sh2iT$$

the dot (.) represents derivate with respect to z.

Changing the variable $v = \exp(2iT)$, the differential equation becomes

$$\dot{v} = i f_T v^2 + 2 i f_L v - i f_T$$

So the differential equation (2.35) is of Riccati type.

By the transformations $v = i\dot{s}/f_T$ we transform this non-linear first order equation into the linear second-order equation

$$\ddot{s} - (2if_L + \dot{f}_T/f_T)\,\dot{s} + f_T^2\, s = 0$$

b) All the deduced equations are functions of path length and electron density. Neglecting second order dependence of y_T with the electron density we show that it is possible to obtain a relation without height and electron density, in terms of Λ and Ω (actual Faraday rotation for longitudinal field, see § 1.7 or § 2.4.1.1).

For the case of no collisions (Z=0), using

$$\Omega(z) = \int_0^z xy_L dz$$

we can find an inverse relation; introducing this expression in (2.39) we obtain

$$dT = \left[1 + q_{TL}(\Omega)\ Sh\ 2iT\right] d\Omega \qquad (2.40)$$

$$\Lambda(z) \equiv \int_0^z xy_T \, dz \tag{2.41}$$

we get

$$d\Gamma = \left[q_{LT} (\Lambda) + \mathrm{Sh}\ 2i\Gamma \right] d\Lambda \tag{2.42}$$

These equations are interesting for the understanding of the general behavior of T. The only problem with (2.40) is that near QT region the "transverse-longitudinal ratio" q_{TL} becomes infinite.

2.4 - Particular Solutions of Polarization Equation

2.4.1 - Collisions Neglected

Neglecting the collisions (Z=0), using (2.15) in (2.39) and separating the real and imaginary part, we get

$$d\psi = (y_L - y_T \cos 2\psi . \mathrm{Sh}2\lambda) x dz$$

$$d\lambda = xy_T \sin 2\psi \, . \, \mathrm{Ch}2\lambda \, . \, dz \tag{2.44}$$

Integrating (2.44) and taking

$$\zeta(z) \equiv \int_0^z xy_T \sin 2\psi \, dz \tag{2.45}$$

$$\zeta_o = \frac{1}{2} \tan^{-1} \left[\mathrm{Sh}\ 2\lambda\ (o) \right]$$

we obtain $\mathrm{Sh}2\lambda = \tan 2(\zeta - \zeta_o)$ (2.46)

It can be proved that the axial ratio is given by

$$|\varepsilon| = \sqrt{\frac{1 - |\cos 2(\zeta - \zeta_o)|}{1 + |\cos 2(\zeta - \zeta_o)|}} = \min \left[\tan (\zeta - \zeta_o), \operatorname{cotan} (\zeta - \zeta_o) \right] \tag{2.47}$$

the sign of ε is the same as $\tan 2(\zeta-\zeta_o)$ or $2(\zeta-\zeta_o)$ (modπ). Figure 2.5 shows the relation between $(\zeta-\zeta_o)$ and ε.

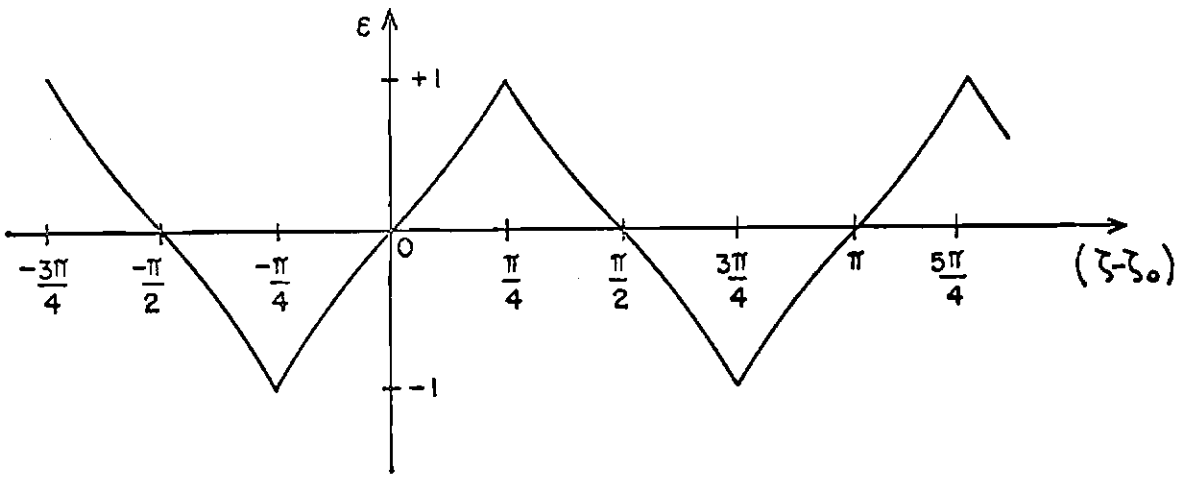

Fig.2.5 - Relation between ε and $(\zeta-\zeta_o)$

The expressions (2.43), (2.45)and (2.47) were used to simulate the polarization of a wave transmitted by a satellite when propagatin through the ionosphere. In appendix B we give details of the simulation progra

Parameters ψ and λ have maximum values that can be obtained by (2.43) and (2.44).

The maximum for λ is given by

$$\frac{d\lambda}{dz} = xy_T \sin 2\psi \cdot \mathrm{Ch}2\lambda = 0$$

when X, $Y_T \neq 0$, we have a maximum only when

$$\sin 2\psi = 0 \rightarrow |\psi| = n\frac{\pi}{2} \quad \text{with } n = 0, 1, 2 \ldots \qquad (2.48)$$

The maximum for ψ is given by

$$\frac{d\psi}{dz} = x\,(y_L - y_T \cos 2\psi\ Sh2\lambda) = 0$$

If $X \neq 0$, in the longitudinal propagation we have a maximum when $Y_L = 0$ and in transverse propagation when $Y_T = 0$ or $\varepsilon = 0$ or $\psi = (2n+1)\,\pi/2$. In general

$$q_{LT} = \cos 2\psi\ Sh2\lambda = \frac{2\varepsilon}{1-\varepsilon^2}\ \cos 2\psi$$

2.4.1.1 - Longitudinal Propagation

When $Y_T = 0$, (2.39) reduces to

$$dT = xy_L\,dz$$

$$\left.\begin{aligned} &\text{after integration } \psi(z)-\psi_o = \int_o^z xy_L dz \equiv \Omega(z) - \Omega_o \\ &\varepsilon(z) = \varepsilon_o \end{aligned}\right\} \qquad (2.49)$$

where ψ_o (or Ω_o) and ε_o are initial values. It is seen that for the longitudi case the axial ratio does not change.

2.4.1.2 - Transverse Propagation

When $Y_L = 0$, (2.38) reduces to

$$dR = 2\,iy_T\,xR\,dz$$

after integration

$$\left.\begin{aligned} &R = R_o \exp\left(2i \int_o^z xy_T\,dz\right) \\ &\text{or} \quad \tan T = \tan T_o \,.\, \exp(2i\Lambda) \end{aligned}\right\} \qquad (2.50)$$

from (2.1) it can be seen that only the phase of the polarization vector changes

$$\left.\begin{aligned} \rho &= \rho_o \\ \phi &= \phi_o + 2\int_o^z xy_T\, dz = \phi_o + 2\Lambda \end{aligned}\right\} \tag{2.51}$$

where Λ is defined by (2.41).

From (2.18) and (2.19) we see that the tilt angle and axial ratio oscillate between the limits given by:

when

$$\rho \leq 1 \qquad |\psi - n\pi| \leq (\tan^{-1}\rho) \pmod{2\pi}$$

$$\rho \geq 1 \qquad |\psi - (2n-1)\tfrac{\pi}{2}| \leq (\tan^{-1}(1/\rho)) \pmod{2\pi}$$

where n is an integer

and

$$|\varepsilon| \leq \min(\rho, 1/\rho)$$

From Fig.2.6 ($q_{LT} = 0$) we can observe this behavior of the polarization. Dividing (2.43) by (2.44) when $y_L = 0$, and integrating, we get the equation relating ψ and ε.

$$\frac{\cos 2\psi}{Ch2\lambda} = \left(\frac{1-\varepsilon^2}{1+\varepsilon^2}\right) \quad \cos 2\psi = \text{constant}$$

So, in pure transverse propagation the plane of polarization never rotates more than $\pi/2$, but only oscillates with amplitude less than $\pi/4$ from the x or y axis.

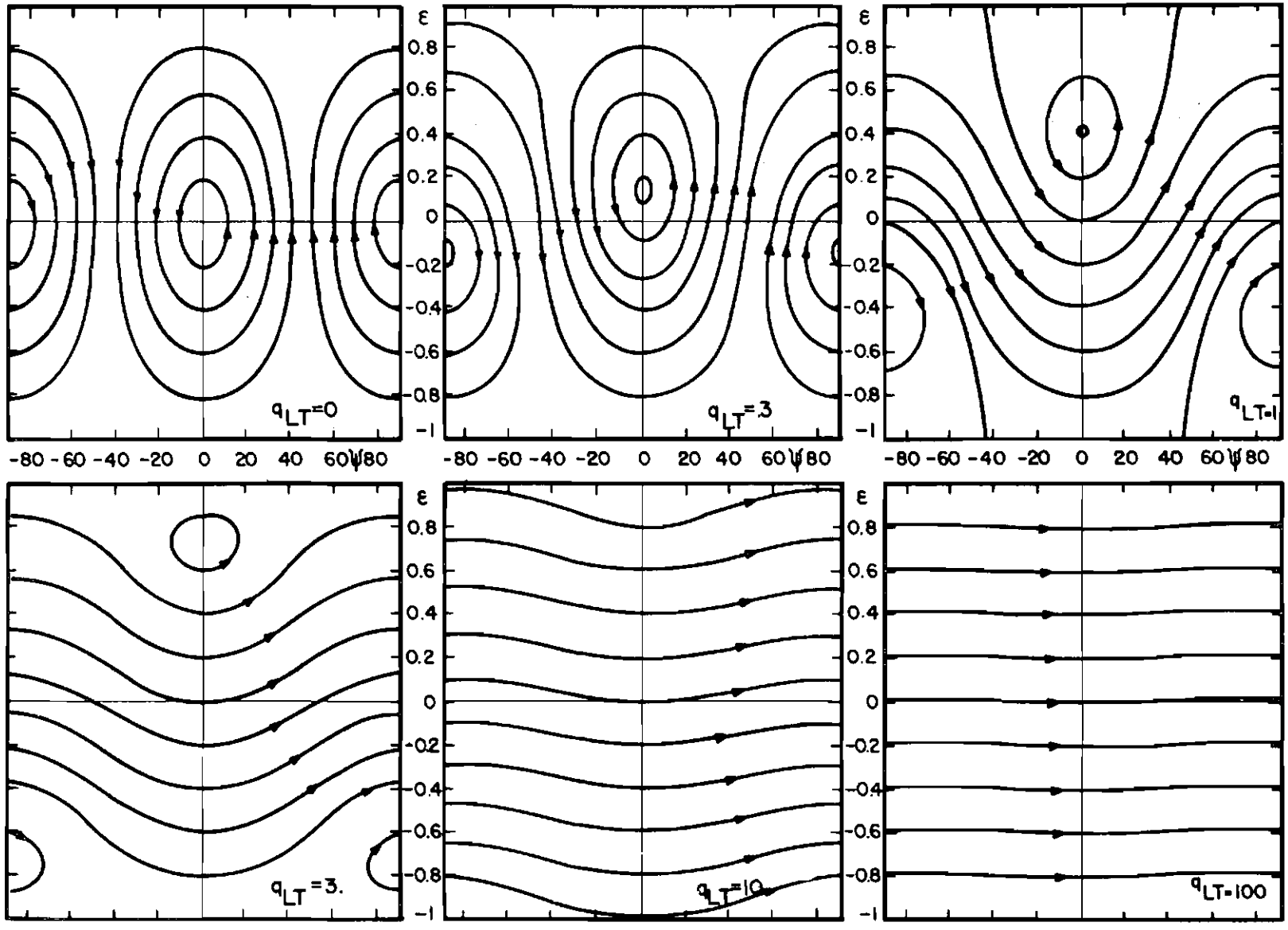

FIG. 2.6 BEHAVIOR OF THE POLARIZATION IN THE COMPLEX PLANE (ψ, ε) FOR CONSTANT q_{LT}

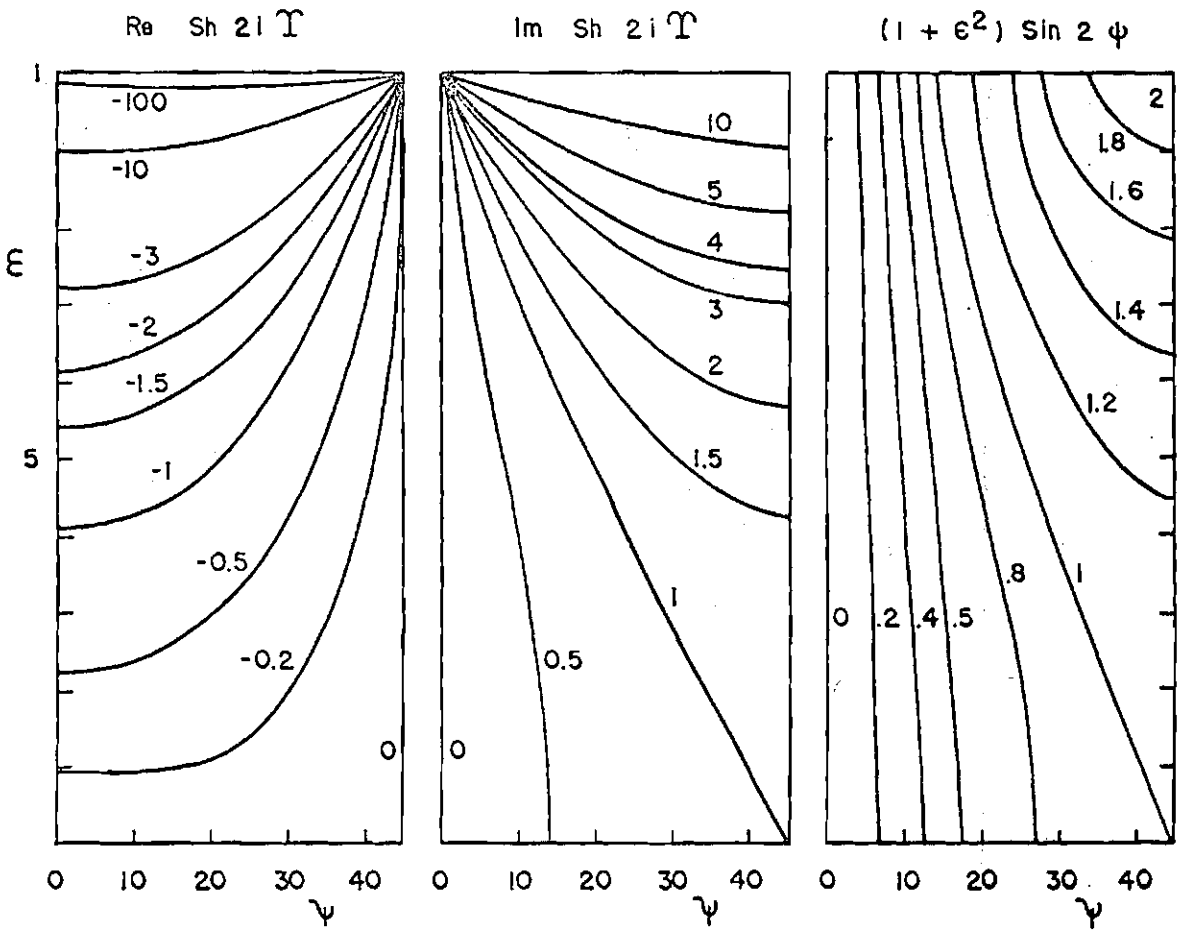

Fig. 2.7 - a,b) Real and imaginary parts of Sh2iT as a function of ψ and ε

c) Curves of constant values of $(1 + \varepsilon^2) \sin 2\psi$ as a function of ψ and ε. (See §2.5.4).

2.4.1.3 - The "Quasi-Longitudinal" Approximation

When $q_{TL} \leq \pi/4 \simeq 0.8$ and $|\varepsilon| \leq 0.414$

the second term of (2.43) is negligible

$$y_L >> y_T \cos 2\psi \cdot Sh2\lambda$$

thus from (2.49) $\psi \simeq \Omega$.

a) Making use of the above relations in (2.46) and taking a medium value of q_{TL} over the integration interval we obtain

$$Sh2\lambda \simeq \tan \left[\overline{q_{TL}} \, (\cos 2\Omega + \zeta_o) \right] \tag{2.52}$$

Using (2.47) we get

$$\varepsilon \simeq \tan \left[\frac{\overline{q_{TL}}}{2} \, (\cos 2\Omega + \zeta_o) \right] \simeq \frac{\overline{q_{TL}}}{2} \, (\cos 2\Omega + \zeta_o) \tag{2.53}$$

The second order variations of ψ is obtained by substituting (2.52) into (2.43), using the initial approximations; after the integration we get

$$\psi \simeq \Omega \left(1 - \frac{\overline{q_{LT}}^2}{2}\right) + \frac{\overline{q_{LT}}^2}{8} \sin 4\Omega$$

These oscillations are clearly visible in Figs. 2.6 and 2.11. The Faraday recordings (Fig.2.12) also show this feature in the oscillation of the minimum of Faraday nulls. But here we have a sampling of the axial ratio and the oscillations are more due to an aliasing effect.

b) Again making use of the same relations we can get a better idea of the axial ratio. Taking

$$j\ (h) \equiv \int_{h}^{h_s} x\,dz \qquad (2.54)$$

we have

$$\psi = \int_{h}^{h_s} x y_L\,dz = \bar{y}_L \cdot j$$

The mean value $\bar{y}_L$ can be assumed to vary more or less linearly with j, and j_o being the value for $\bar{y}_L = 0$, we have

$$\bar{y}_L = y_1\ (j - j_o)$$

where y_1 is the vertical gradient of the mean value $\bar{y}_L$ which is nearly constant over the latitude range of the record of a single satellite pass. After substituition of these relations in (2.45)with the assumption that y_T does not vary too much with height

$$\zeta - \zeta_o = \bar{y}_T \int_{h}^{h_s} \sin 2\ y_1\ (j - j_o)\ j\ dj$$

After integration we obtain

$$\zeta-\zeta_o = \frac{\bar{y}_T}{2}\sqrt{\frac{\pi}{y_1}}\left\{ \cos\left(\frac{y_1 j_o^2}{2}\right) S\left[\sqrt{\frac{y_1}{\pi}}\,(2j-j_o)\right] - \sin\left(\frac{y_1 j_o^2}{2}\right) C\left[\sqrt{\frac{y_1}{\pi}}\,(2j-j_o)\right] \right\}_o^{j(o)} \qquad (2.55)$$

where S and C are Fresnel integrals.

If $\left|\sqrt{\frac{y_1}{\pi}}\,(2j-j_o)\right| \gg 1$ for $j = 0,\ j(o)$

we have that $S(s) \triangleq C(x) \approx \frac{1}{2}$ sign (x) and when there is a QT region on the path of the wave we obtain

$$\zeta - \zeta_o \simeq \bar{y}_T \quad \frac{2\pi}{y_1} \sin \left(\frac{\pi}{4} - \frac{y_1 j_o^2}{2}\right) \tag{2.56}$$

The general picture of the Fresnel integrals is a step function with oscillations on each side, whose amplitude decreases as we go away from the step. This coincides with the form of the curve showing the axial ratio for a down coming wave. (Fig.2.11).

2.4.1.4 - Constant Longitudinal-transverse Ratio

If we take y_L and y_T as constants, by substituition of (2.54) in (2.39) we get

$$\tan^{-1} \left[e^{-i\gamma} \tan \left(\frac{\pi}{4} - T\right) \right]_{T_o}^{T} = - yj$$

where

$$\tan\gamma = y_T/y_L$$

$$y^2 = y_T^2 + y_L^2$$

So

$$\tan \left(T - \frac{\pi}{4}\right) = e^{i\gamma} \cdot \tan (yj - j_o) \tag{2.57}$$

where j_o represents an initial value, that can be given by

$$\tan j_o = e^{-i\gamma} \quad \text{when for} \quad j = 0 \quad \text{we have} \quad T = 0$$

2.4.2 - Effect of Collisions

Here we consider $Z \ll 1$. The use of binomial series gives

$$\frac{1}{1 - X - iZ} \simeq \frac{1}{(1 - X)} \left(1 + i \frac{Z}{1-X} + \ldots \right) \qquad (2.58)$$

2.4.2.1 - Longitudinal Propagation

Introducing (2.58) in (2.35) for $Y_T = 0$, we have

$$\begin{cases} \psi_c = \int_0^z xy_L dz = \psi \\ \lambda_c = \int_0^z \frac{Z}{1 - X} xy_L dz \simeq \overline{\left[\frac{Z}{1 - X} \right]} \psi + \lambda_o \end{cases}$$

where $\overline{[Z/(1-X)]}$ is the mean value over the range of integration.

For longitudinal propagation the first order effect of collisions is to change the axial ratio, due to the unequal damping of the ordinary and extraordinary modes. If initially the wave is linearly polarized, it will become elliptically polarized. Taking a model ionosphere (Fig.2.8) it can be seen that $Z << X, Y_L, Y_T < 1$ for high frequencies and therefore, for normal values of ψ, the effect of the collisions on the polarization of the received wave will be very small. For lower frequencies the expression for the axial ratio could provide a means to determine the mean collision frequency, by measuring the axial ratio of the incoming satellite wave. It can be seen that $\lambda_c \propto f^{-3}$, so at a lower frequency we have a greater axial ratio. This method was proposed by Papagiannis (1966). His study shows that for f = 12 MHz we would have a representative value of 0.077 for the axial ratio, but during sudden ionospheric disturbances (S.I.D.) it would increase to 0.29.

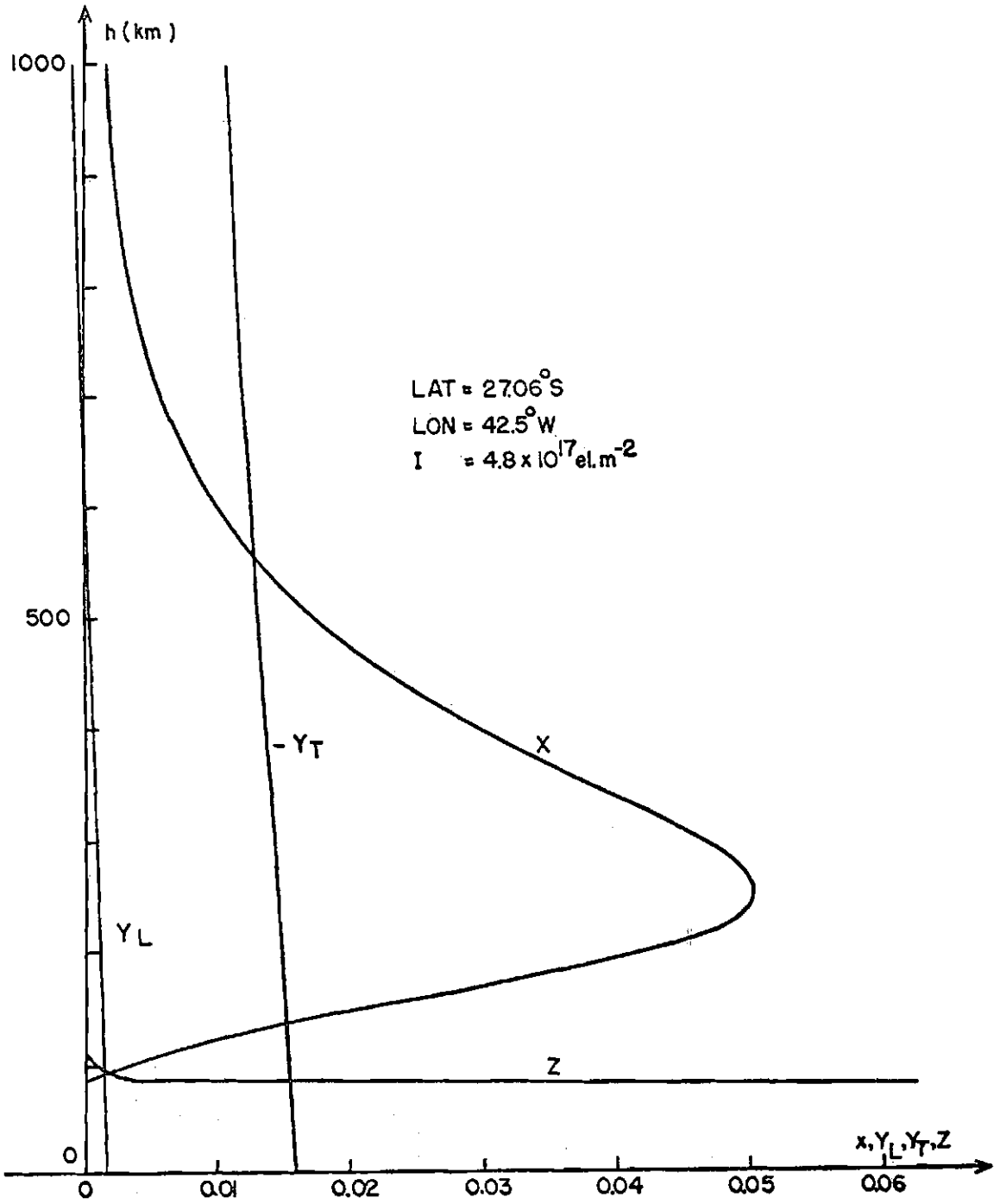

Fig.2.8 - Curves showing the height variations of X, Y_L, Y_T, Z for a particular satellite position near S.J.dos Campos.

2.4.2.2 - Transverse Propagation

Introducing (2.58) in (2.34) for $Y_L = 0$, and neglecting Z^2 we have

$$dR = 2ixy_T \left(1 + \frac{2iZ}{1-X}\right) Rdz$$

Integrating and comparing with the solution without collisions (§ 2.4.1.2)

$$\begin{cases} \rho_c = \rho \ esp \ (-4 \int_o \frac{Z}{1-X} \ xy_T dz) \\ \phi_c = \phi \end{cases}$$

The general effect in this case is to increase or decrease, depending upon the sign of y_T, the amplitude of the oscillations of the axial ratio and the tilt angle.

2.5 - Simulation of a Satellite Pass Near the Quasi-Transverse Region and Comparison with a Real Signal

Using the equations 2.43, 2.45 and 2.46 we shall solve the differential equation by numerical method. In this simulation we considered a polar orbit satellite transmitting linearly polarized signal. The equations used were deduced for vertical incidence; to consider an obliquely incident wave we use (2.36), which for a not very large zenith angle will not give much error, and the conclusions obtained will not be much different from those that we would get, deducing the equations for oblique incidence.

In appendix B we present the computer program we used and its details.

To have a general idea of the values of the ionospheric parameters in Fig.2.8, we present the variation of X, Y_L, Y_T and Z with height for a particular satellite position.

The position of the satellite (in time) is relative to the position of a QT point observed in a particular satellite data, it does not mean that the QT point will be located exactly on zero time.

Simulation is made only for time near the QT point.

2.5.1 - Behavior of the Polarization with Height and Time

We separate the behavior in the two parameters ψ and ε the tilt angle and axial ratio respectively.

In Fig.2.9 we show the height variation of ψ with time. The dashed line represents the points where we have a transverse magnetic field. On this line the tilt angle ψ has a maximum except for a few seconds after the QT point. The plane of polarization rotates one way reaching a maximum near the QT region, then begins to rotate in the opposite sense. (See also Fig.2.11), following closely the tilt angle that would be obtained with QL-approximations Ω. During some seconds after $\psi = 0$ the above behavior does not occur.

In Fig.2.10 we present a composite plot of the axial ratio with time and height and in Fig.2.11 the behavior of ψ and ε with height for a single satellite position. The dashed line also represent the transversal points. The axial ratio oscillates when comming to the ground and with time the oscillation phase moves upwards or downwards according to (2.48) showing a complicated pattern (see Fig.2.10). In Fig.2.11 the time is fixed; within the region where the ratio $|q_{TL}| < 1/3$ there is a large change in ε (in this region ψ does not change very much) and outside this region the axial ratio oscillates. The maxima of the oscillations behave as predicted by (2.48) and their amplitudes follow the values given by the approximation (2.53). (See the inset of 2.11).

2.5.2 - Received Signal

The polarization received by the receiver can be seen in Figs. 2.16, 2.17 and 2.18 for various electron contents and frequencies.

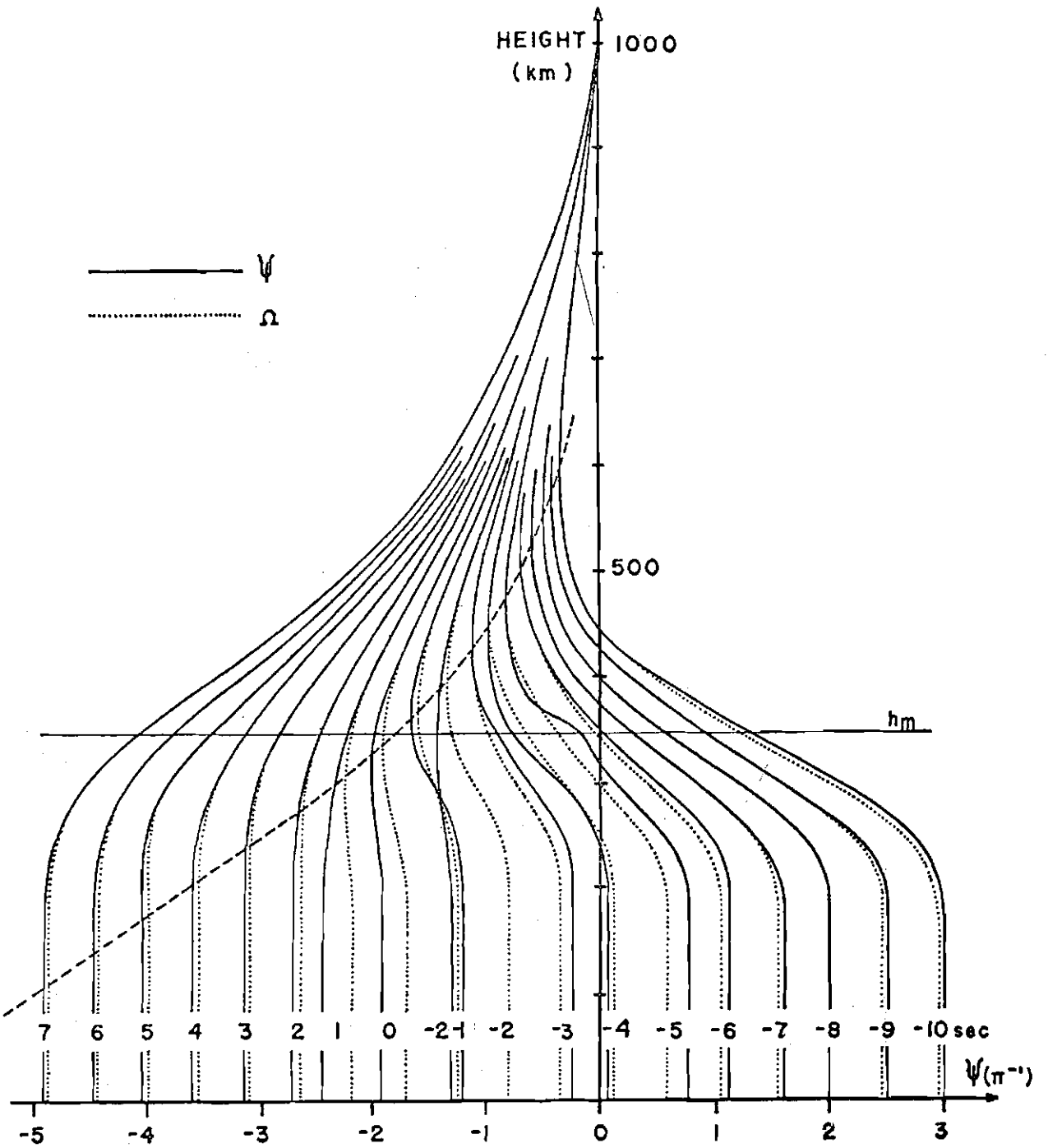

Fig.2.9 - Height variation of ψ and Ω for various time positions of the satellite. The dashed line represents the points of transverse magnetic field.

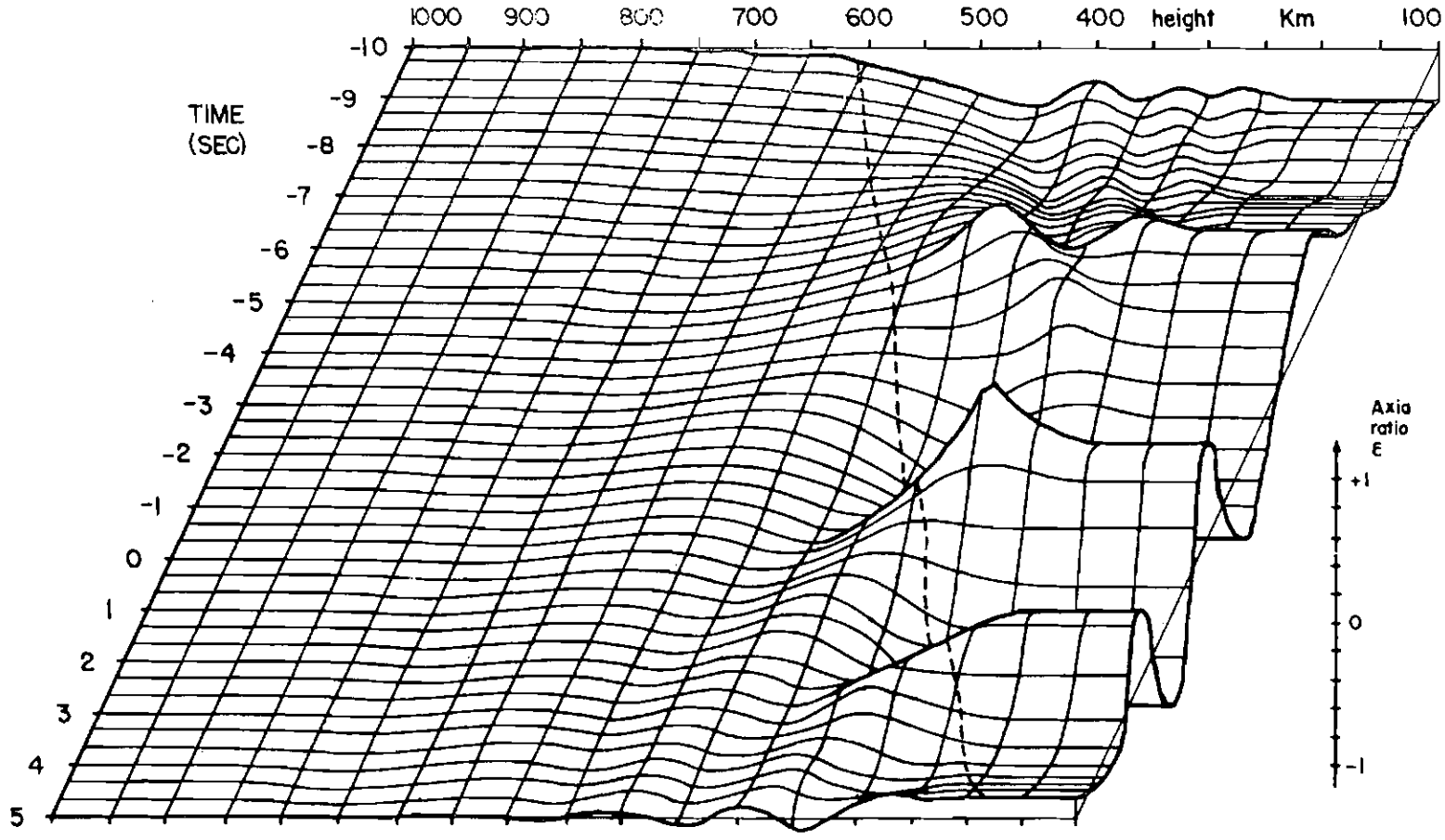

FIG.2.10 COMPOSITE PLOT OF HEIGHT-TIME VARIATION OF THE AXIAL RATIO. THE DASHES REPRESENT THE QUASI-TRANSVERSAL POINTS.

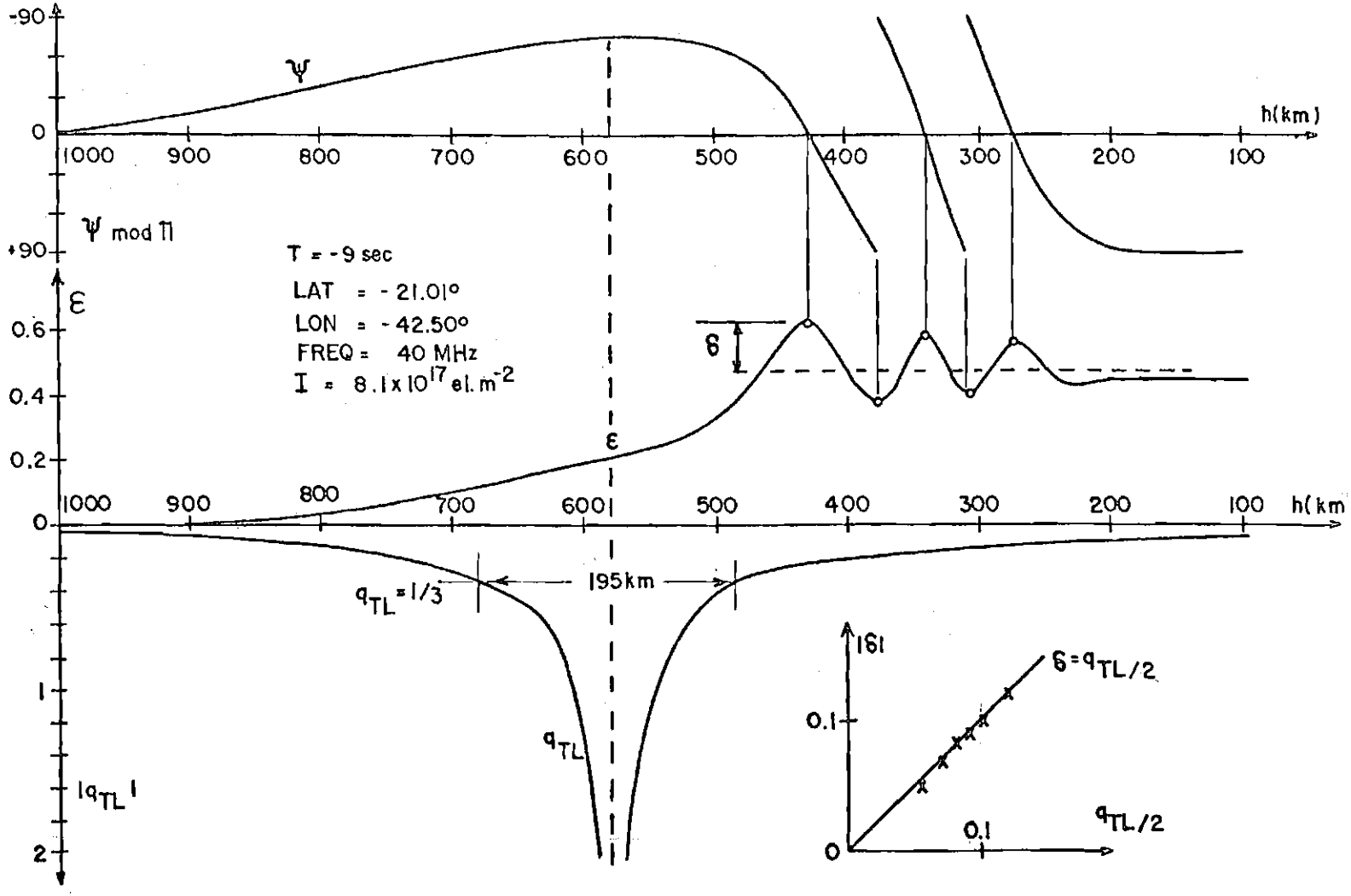

Fig.2.11 - Curve showing ψ and ε for a downcominb wave, the botton curve gives the ratio q_{TL} for each height. The inset gives the difference δ as a function of $q_{TL}/2$

The received tilt angle rotates always in the same sense passing through a null point. The axial ratio starts with near zero value when the transverse point is at the satellite height, then it begins to oscillate with increasing amplitude and decreasing period untill the transverse point passes by the height of the peak electron density. From then on the amplitude decreases to zero and the period is constant. In the simulation this takes about 30 seconds which is less than the time during which there is a transverse point within the ray path (40 sec).

Simulating how the system would record the received signal (see Appendix B) we present in Fig.2.12 two examples of simulated signals for two different electron contents compared with a copy of a recorded signal obtained in S.J.dos Campos for the same frequency. Observe that the distorted Faraday null that appears in the QT regions can be seen also in the simulation. The ellipticity of the polarization prevents the signal to come to zero. In the example for $I = 8.1 \times 10^{17}$ el/m^2 the format of the signal is more involved but near the point where $\Omega = 0$ the signal also presents the ellipticity effects.

The angle between the antenna and the emitted plane of polarization gives the displacement of the observed QT point in the recorded signal and the point where $\Omega = 0$. In order to coincide the observed QT point and a null in the absolute Faraday rotation, the antenna must be placed perpendicular to the initial plane of polarization.

In Table 2.1 we present the time displacement given by the difference between the minimum in the QT Faraday null and the time when $\Omega=0$ in the simulation for 40 MHz.

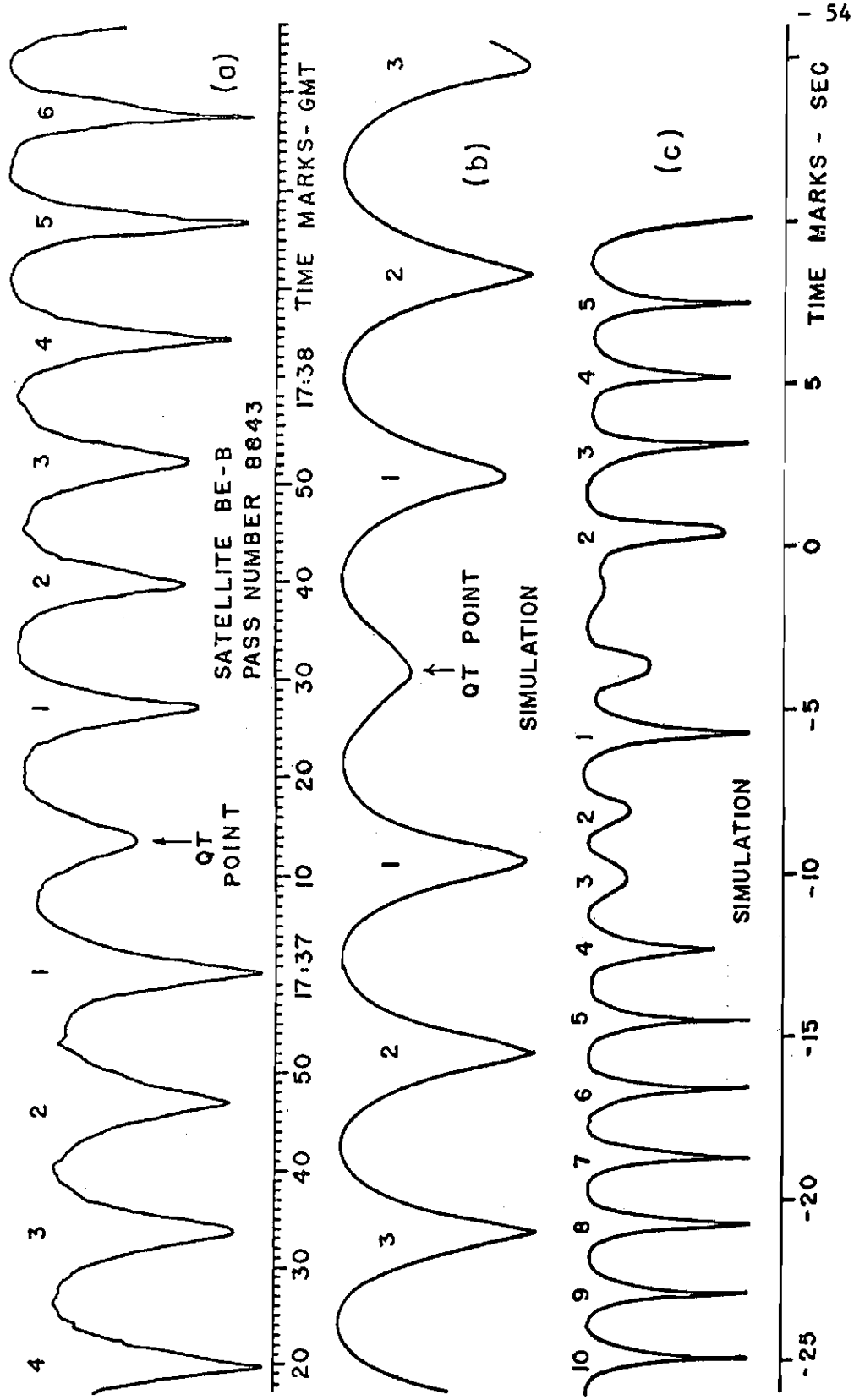

Fig.2.12 - a) Copy of a recorded signal obtained in S.J.dos Campos.
b) Simulated signal for $I = 3.2 \times 10^{17}$ el/m^2
c) Simulated signal for $I = 8.1 \times 10^{17}$ el/m^2
(Time for simulation is arbitrary).
The digits represent number of half turns of the tilt angle.

Electron content in units of x 10^{17} el/m^2	Δ time (sec)
1.6	-.15
3.2	0
4.8	.05
6.4	-0.1

From Table 2.1 can be seen that this difference is quite negligible.

2.5.3 - Tilt-Angle Discontinuity

For the downcomming wave a discontinuity can be observed in the simulation in ψ. (See Figs. 2.14 and 2.16). When the polarization becomes nearly circular in a short height variation the tilt angle changes very rapidly.

In a qualitative way, when an elliptically polarized wave becomes circularly polarized and then again elliptically polarized, and the tendency,to change the ellipticity is always in the same "direction", the tilt angle would give a jump of $\pm \pi/2$. Figure 2.13 shows a form changing ellipse making a jump of $\pm \pi/2$.

Decomposing the wave into two circularly polarized waves rotating in opposite directions (2.3 and 2.4), the total energy remaining constant we have

$$E_{ao}^2 + E_{bo}^2 = \text{constant}$$

So in Fig. 2.13 the vector $\vec{E}_b$ changed the sign of the amplitude.

In equation 2.43 to $d\psi/dz$ can have a discontinuity, only when $\varepsilon \simeq \pm 1$ and Sh2λ will have large values making the longitudinal term negligible. In this case the transverse conditions should be applied with caution. In Fig.2.6 ($q_{LT} = 0$) for $|\varepsilon| > 0.9$ there can be a jump of

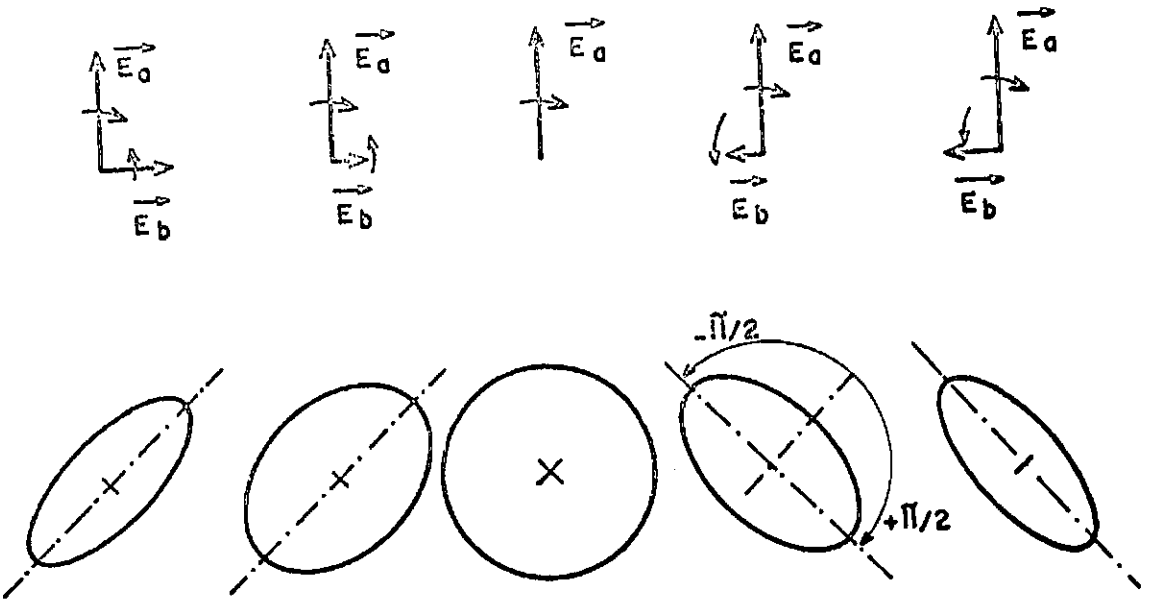

Fig.2.13 - Polarization changing ellipse making a jump of $\pm \pi/2$.

$$|\Delta\psi| \leq \pi/2 \qquad \text{but} \qquad \simeq \pi/2$$

and the only possible initial value for ψ is

$$\psi \simeq \frac{\pi}{4} (2n + 1) \qquad n \text{ is an integer}$$

the jump direction can be given by analysing the signal of $d\psi/dz$ in (2.43), which gives

$$\text{sign } (\Delta\psi) = \text{sign } (-\varepsilon y_T \cdot \cos 2\psi)$$

When the above conditions are fulfilled there will occur a jump in the received signal. Figure 2.14 shows the variation of ψ and ε for satellite positions near a discontinuity.

The number of discontinuities increases when the electron content is higher, as shown in Fig.2.16.

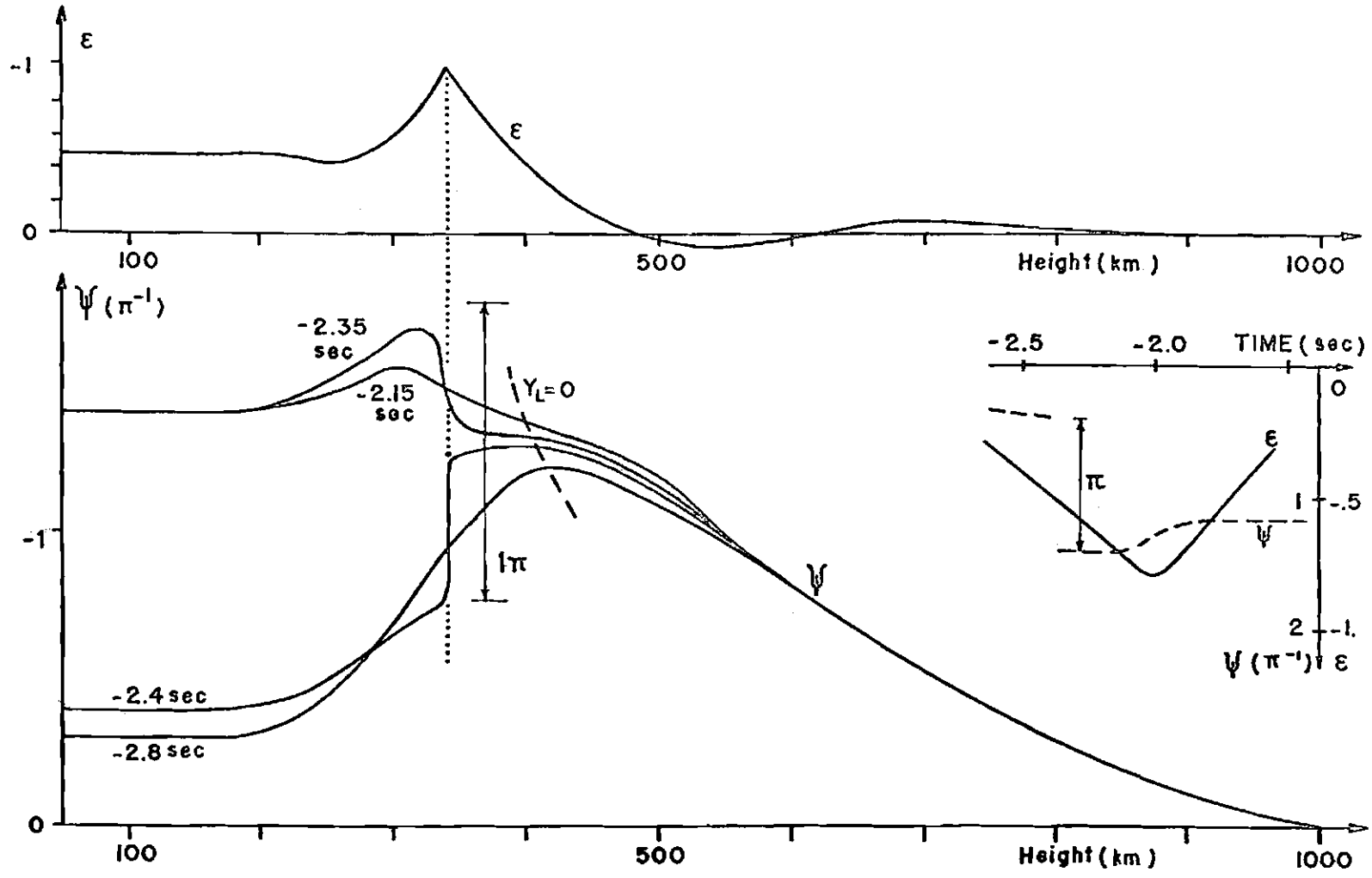

Fig.2.14 - Variation of ψ and ε for satellite positions near a discontinuity. The inset shows the received ψ and ε.

It should be noticed that a half turn discontinuity in the tilt angle cannot be observed using a dipole antenna. In Table 2.2 we present the discontinuities obtained for the simulation with I = 8.1 x 10^{17} electrons/m^2.

Table 2.2 - Discontinuities in ψ for a simulation with I 2 8.1 x 10^{17} el/m^2

time (sec)	Initial ψ	ψ after jump	$\Delta\psi$
	ψ in half turns		
- 2.4	$-1\frac{1}{4}$	$-\frac{3}{4}$	$+\frac{1}{2}$
		$-1\frac{3}{4}$	$-\frac{1}{2}$
- 0.5	$-1\frac{3}{4}$	$-1\frac{1}{4}$	$+\frac{1}{2}$
		$-2\frac{1}{4}$	$-\frac{1}{2}$
+ 0.9	$-2\frac{1}{4}$	$-1\frac{3}{4}$	$+\frac{1}{2}$

2.5.4 - Differences between the Simulated Polarization and the QL-approximatio

In Fig.2.15 for a particular satellite pass we first present the received difference between the simulated tilt angle ψ and the tilt angle that would be calculated by the QL-approximations Ω given by (2.49). In Fig. 2.9 we present this difference for various heights and satellite positions. The difference is greater when the transversal point is lower than the peak of the electron density. In our simulations it is less than a half turn.

We also present curves showing the axial ratio computed with (2.45) ε_ψ and using the same expression but with Ω instead of ψ.

$$\zeta(z) = \int_0^z xy_T \sin 2\Omega \, dz$$

This gives, using (2.46) and (2.47), an approximated axial ratio ε_Ω, that is easier to calculate. The formats of both curves are similar; in general ε_Ω has greater absolute value than ε_ψ.

For a constant longitudinal-transverse ratio (q_{LT}) Fig.2.6 presents the behavior of (ψ,ε). When $q_{LT} > 1$ we have a quite linear variation of ψ and an oscillation of ε with peak to peak amplitude of approximately $1/q_{LT}$ for $|\varepsilon| < 0.5$. When $q_{LT} < 1$, depending on the initial (ψ,ε) they will oscillate or behave as with $q_{LT} > 1$ but with greater amplitude of oscillation. The values of Sh2iT are given in Fig.2.7. In equation 2.42 only the real part of Sh2iT is modified by the longitudinal-transverse ratio q_{LT}. In Fig.2.7a we see that the larger influence on the real part of dT, which is the different tilt angle, is observed for higher values of $|\varepsilon|$.

Introducing (2.21) and (2.23) in (2.44) we obtain the differenti tilt angle

$$\frac{d\varepsilon}{xy_T \, dz} = (1 + \varepsilon^2) \sin 2\psi$$

which is given in Fig.2.7c. It can be seen that the larger derivative of ε with height is obtained when $\psi \pmod{\pi/2}$ is close to $\pm 45^o$.

2.5.5 - Electron Content Variation

The polarizations received in the ground station have different aspects for high and low electron content values.

In Fig.2.16 we present the tilt angle ψ as a function of time for different values of electron content. It can be seen that for low values (≤ 3.2) the variation is almost linear and for high values (> 6.4) some

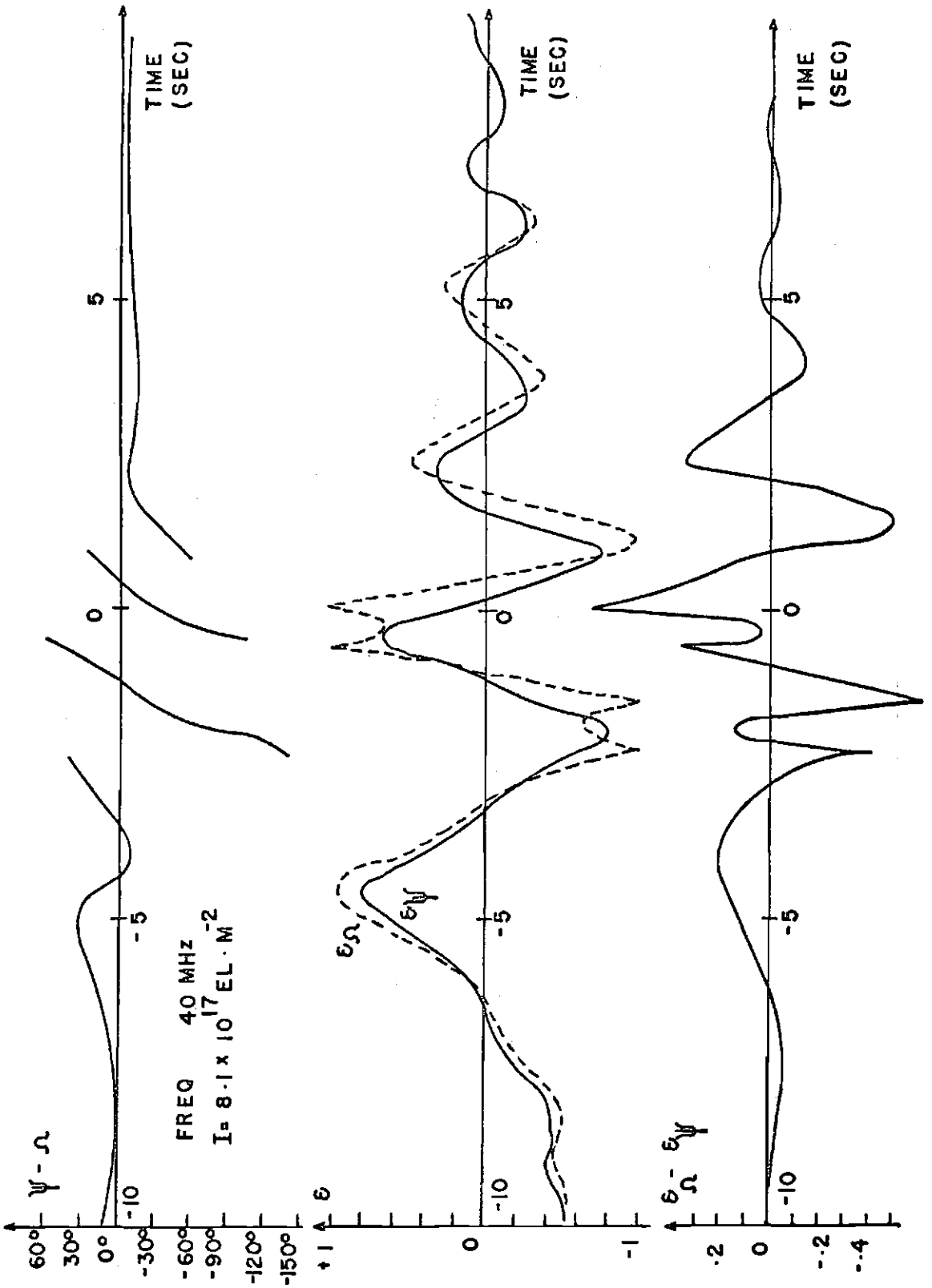

Fig.2.15 - Curves showing comparison between ψ and Ω, ε_ψ and ε_Ω. See text in §2.5.4.

discontinuities appear (§ 2.5.3). The effect of these discontinuities in the received signal in a dipole antenna is to lower the Faraday rotation rate. It can also be seen that $\psi = 0$ occurs during a time interval of less than a half second for all the simulated electron content values.

In Fig.2.17 we present the time variation of the axial ratio received in the ground station for different value of electron content. It can be seen that the period of the oscillations are greater for lower values of electron content and the amplitudes are greater for higher values. This behavior is in accord with the expression 2.65 obtained with the simplificatio made in §2.6. The relative time-occurrence of the peaks of ε is different for different electron content values which explains the different formats obtained near the QT point in the satellite signal recordings (Fig.2.12).

2.5.6 - Frequency Dependence

When the propagating wave passes through a region where QL approximations are valid $\psi \propto f^{-2}$ and the amplitude of ε oscillations is approximately

$$\varepsilon \propto q_{LT} \propto f^{-1}$$

because of the proportionality of the parameters $xy_L \propto f^{-2}$ and $xy_T \propto f^{-3}$. (See § 2.4.1.3). This behavior can be seen in Fig.2.18.

When the propagating wave passes through a region where the transverse magnetic field is predominant the phase of the polarization vector R (see § 2.4.1.2) $\phi \propto f^{-3}$, but there is no proportionality between ψ and λ with f.

In Fig.2.19 we present the variation of $\psi_{40}/\Delta\psi$ where ψ_{40} is the tilt angle received on 40 MHz and, $\Delta\psi$ the difference of tilt angles for 40 and 41 MHz. It can be seen that away from the QT point this ratio

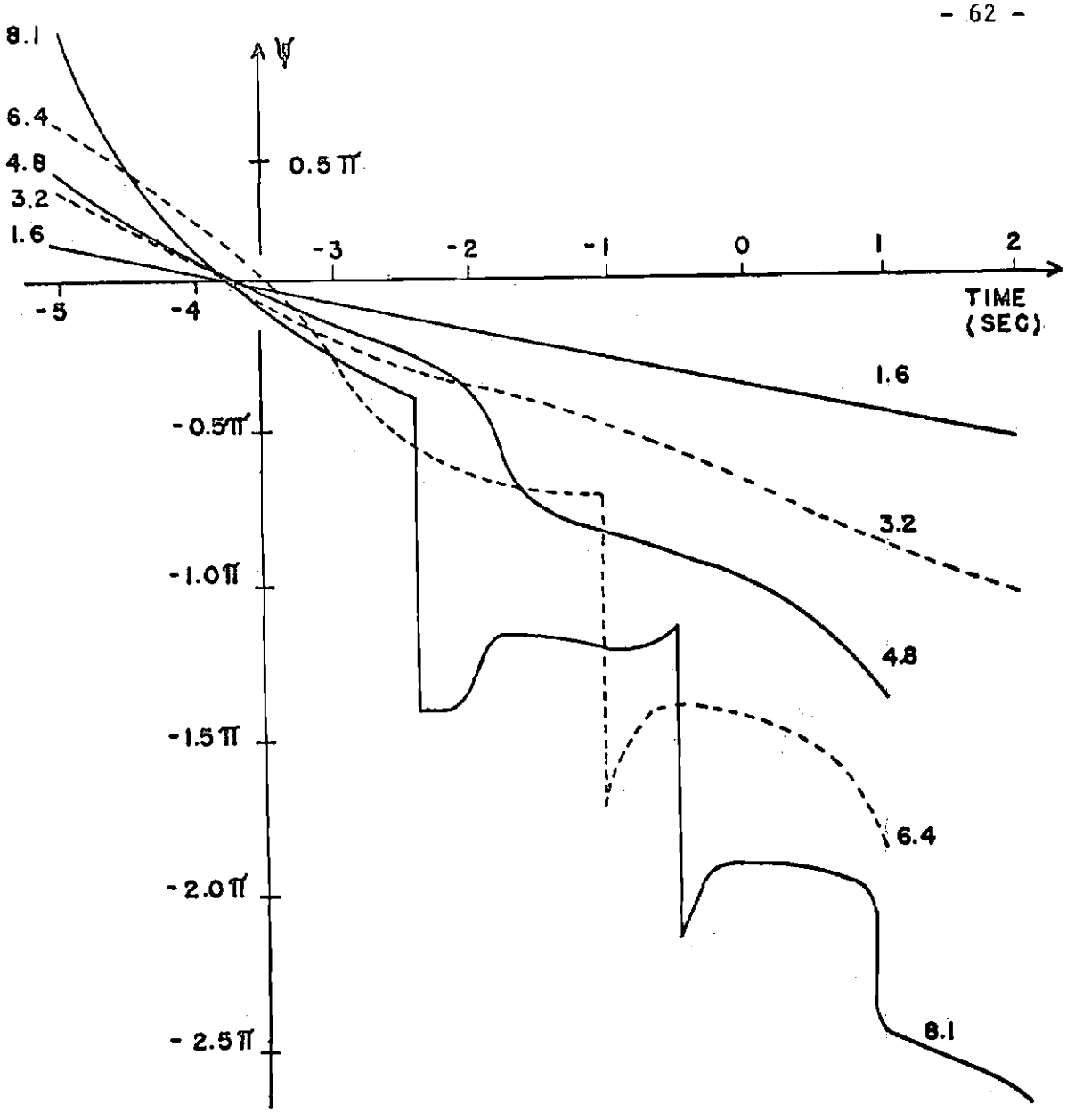

Fig.2.16 - Tilt angle ψ as a function of time for different values of electron content. (In units of 10^{17} electrons/m^2)

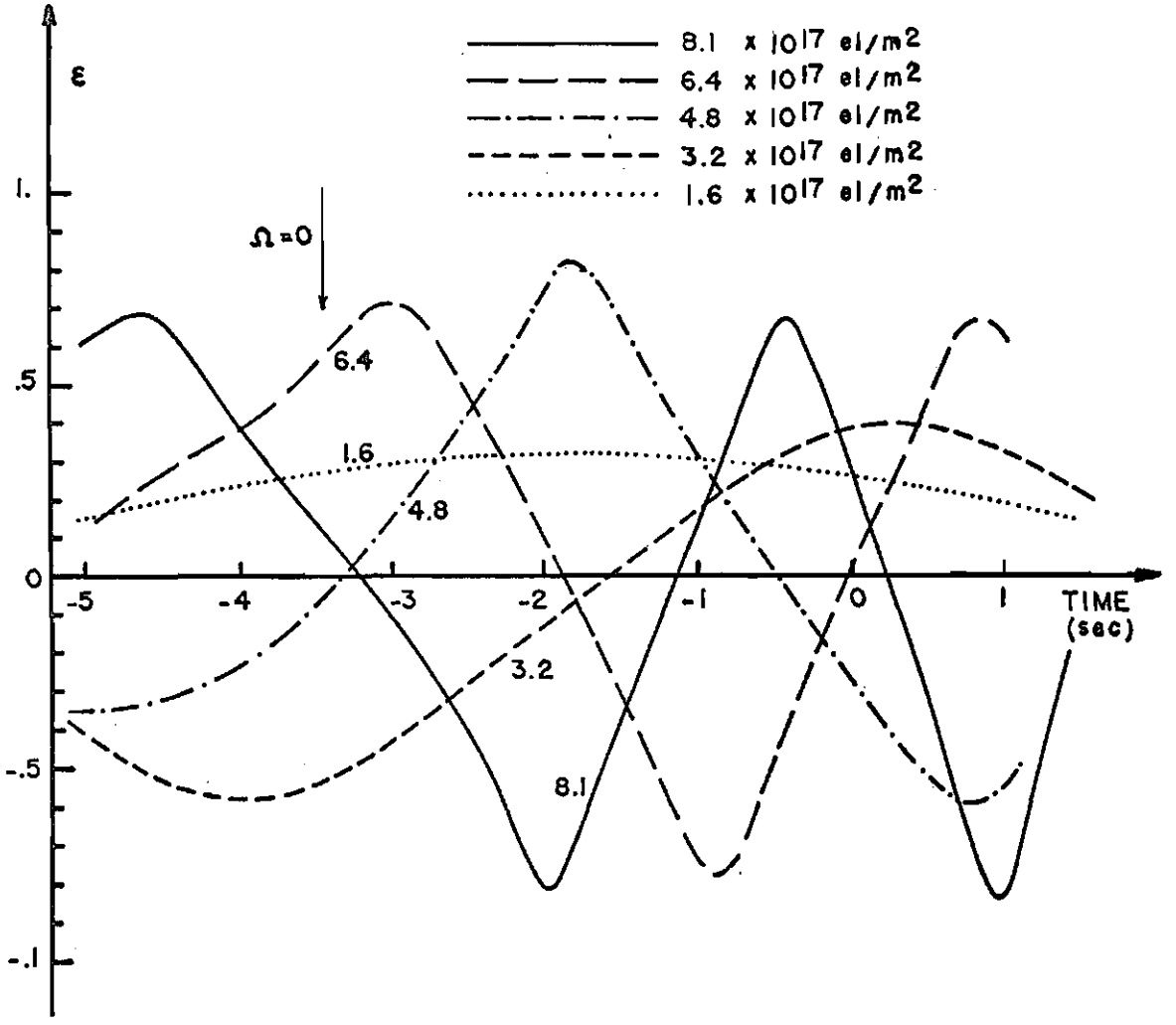

Fig.2.17 - Axial ratio ε as a function of time for different values of electron content.

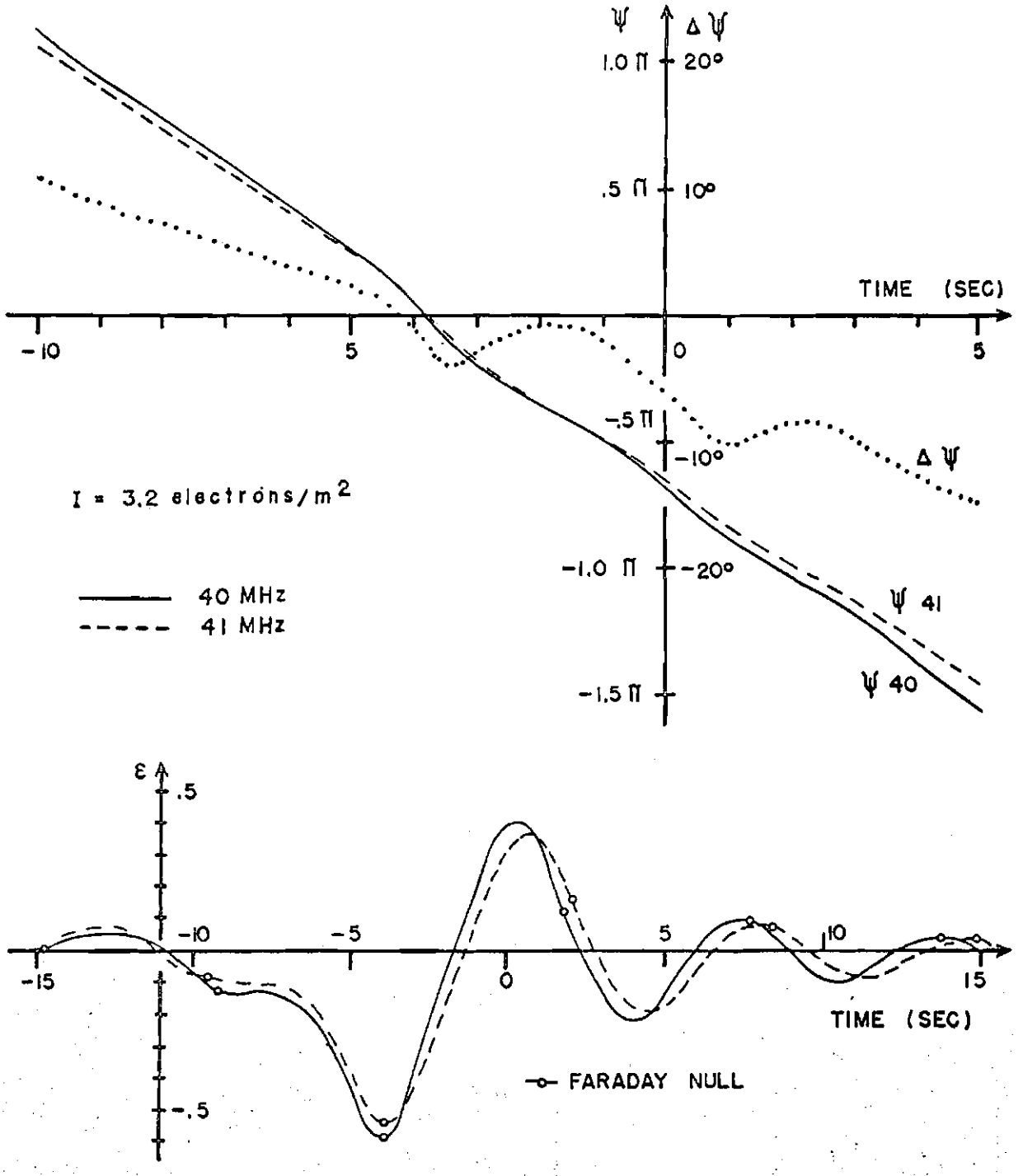

Fig.218 - Plot of ψ, ε for 40 and 41 MHz and the difference $\Delta\psi$ as a function of time.

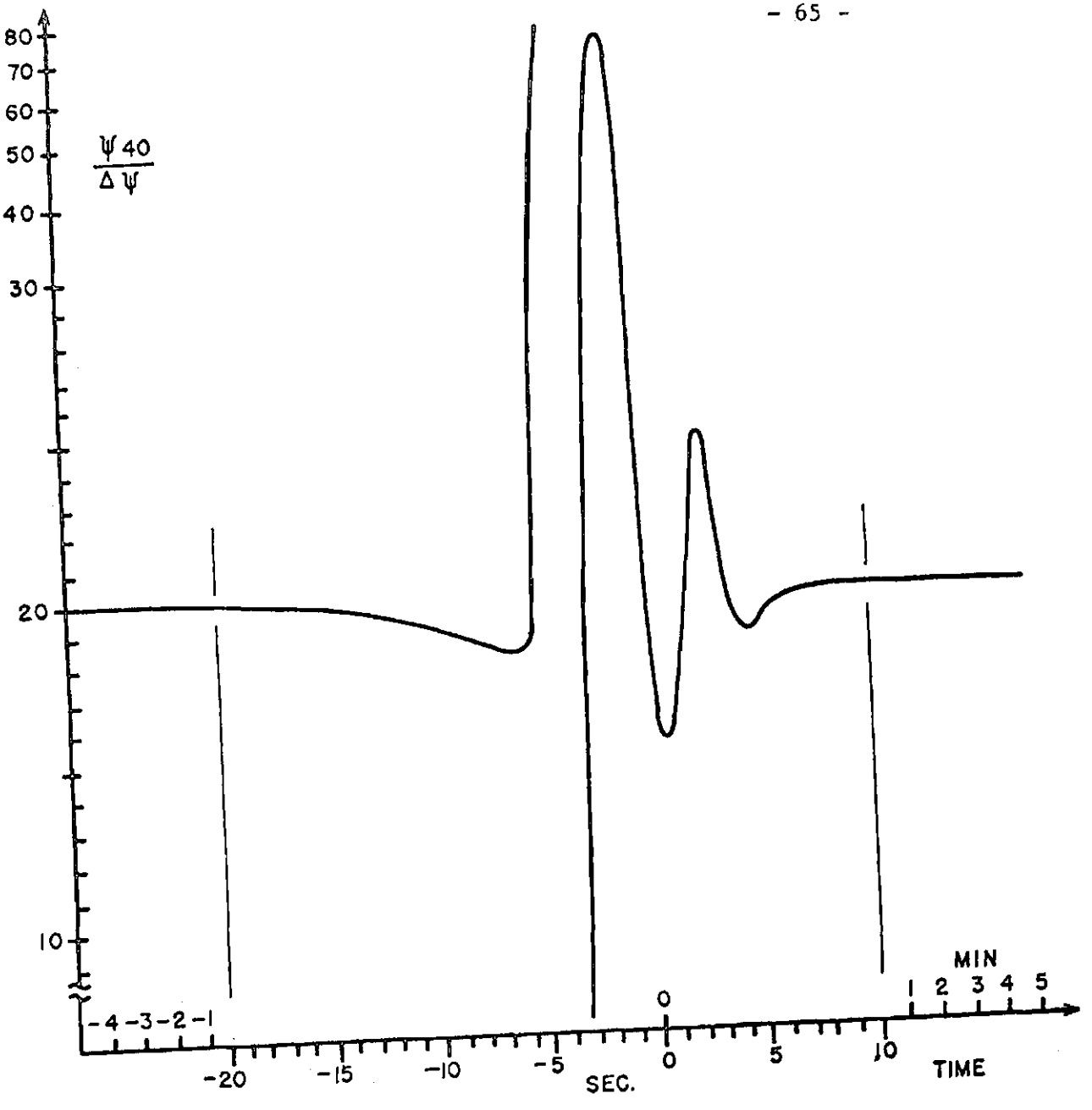

Fig.2.19 - Variation of $\psi_{40}/\Delta\psi$ with time. Both abscissa and ordinate are discontinuous. The electron content for this simulation is 3.2×10^{17} el/m^2

has an almost constant value of 20.05 and has large oscillations near the QT point (See § 4.3.6.2 for its implications).

2.6 - Parameters of the Ionosphere that can be measured near the Quasi-Transverse Region

We make here some approximations to deduce an expression that will enable us to obtain the electron density at the height of a transverse point.

We consider a ray path which contains a transverse point and divide the propagation into three regions

Region I: $h_s \rightarrow h_1$ (longitudinal)
Region II: $h_1 \rightarrow h_2$ (transverse)
Region III: $h_2 \rightarrow 0$ (longitudinal)

In region I and III, applying (2.49) we have

$$\text{Region I} \quad \begin{cases} \psi_1 = \psi_s + \int_{h_1}^{h_s} xy_L dz \\ \lambda_1 = \lambda_s = 0 \end{cases} \tag{2.59}$$

$$\text{Region II} \quad \begin{cases} \psi = \psi_2 + \int_{o}^{h_2} xy_L dz \\ \lambda = \lambda_2 \end{cases} \tag{2.60}$$

In region II applying (2.51) we have)

$$\rho_2 = \rho_1 = \tan\psi_1$$

$$\phi_2 = \phi_1 + 2\Lambda = 2\Lambda$$

and using (2.18) with the above relations we get

$$\tan 2(\psi_2 - \psi_1) = \frac{-2\sin^2 2\Lambda \cdot \tan 2\psi_1}{1 - \tan^2 2\psi_1 . \cos 2\Lambda}$$

$$\tanh 2(\lambda_2 - \lambda_1) = \sin 2\psi_1 \sin 2\Lambda$$

If

$$\Lambda << 1$$

$$\tan 2(\psi_2 - \psi_1) \simeq - 4\Lambda^2 \tan 4\psi_1$$

and if

$4\psi_2 \pmod{\pi} \neq \pm \pi/2$, we obtain

$$\Delta\psi = \psi_2 - \psi_1 \simeq 2\Lambda^2 \tan 4\psi_1 << 1 \qquad (2.61)$$

which enable us to take $\psi_1 \simeq \psi_{QT}$ (tilt angle on the transverse point). Figure 2.9 shows that this approximation is valid near the transverse point.

Also if $\Delta\varepsilon < 0.25$ we have

$$\Delta\varepsilon \simeq \frac{1}{2} \sin 2\Lambda \cdot \sin 2\psi_1 \qquad (2.62)$$

Using (2.59), (2.60), (2.61) and (2.62) we have the total variation of tilt angle and axial ratio given by

$$\psi = \int_{h_1}^{h_s} xy_L dz + \int_{o}^{h_2} xy_L \, dz + \Delta\psi \simeq \int_{o}^{h_s} xy_L dz$$

$$\varepsilon \simeq \frac{1}{2} \sin 2\Lambda \cdot \sin 2\psi \qquad (2.63)$$

Expressing Λ (2.41) into its terms

$$\Lambda = \int_{h_1}^{h_2} xy_L dz \simeq K \overline{y_T^2}\, \Delta h \sec\chi \cdot N_{QT} \qquad (2.64)$$

where

$$K = \frac{e^2}{4\varepsilon_o m\omega c}$$

$\overline{y_T^2}$ is mean square value of y_T over the interval (h_1, h_2)

$\Delta h = h_1 - h_2$ (equivalent transverse thickness)

χ is the ray path zenith angle

N_{QT} is the electron density at the transverse point.

Substituting (2.64) in (2.63) we get

$$\varepsilon \simeq \frac{1}{2} \sin 2\psi_{QT} \cdot \sin(K \overline{y_T^2}\, \Delta h \cdot \sec\chi \cdot N_{QT}) \qquad (2.65)$$

We use the values in the simulation to compute an equivalent transverse thickness Δh. Table 2.3 shows the obtained values for the simulation with electron content equal to 8.1×10^{17} el/m^2 when $|\sin 2\psi_{QT}| \simeq 1$

Table 2.3 - Values of equivalent transverse thickness for a simulation

Time (sec)	$\lvert\varepsilon\rvert$	X_{QT}	Y_T	Δh(km)
-9	0.5	.04849	.01239	166
-5	0.7	.08631	.01289	130
-2	0.96	.11863	.01325	147
-0.5	0.7	.125	.01345	84
-1	0.8	.11	.01365	133

The obtained mean h is 132 km which corresponds to the points in the ray path where $|q_{LT}| = 3$.

Equation (2.65) shows that the axial ratio is given by the product of two sinusoidal terms, one with rapid oscillations ($\sin 2\psi_{QT}$) which is responsible for the sinusoidal aspect of the axial ratio variation, and the other with a phase proportional to the electron density, which for normal values of electron density do not exceed $\pi/2$. So this term only affects the amplitude of the axial ratio oscillations.

The values of ψ_{QT} can be obtained from the points where the axial ratio becomes zero. At these instants we have

$$\psi_{QT} = \int_{h_{QT}}^{h_s} xy_L dz = \frac{n\pi}{2} \qquad n = 0,1,2 \ldots \tag{2.66}$$

Figure 2.20 shows a curve of ψ_{QT} for a simulation as a function of height. The instant of occurrence of a zero value of ε can be associated with the height of the transverse point by knowing the ephemerides and the magnetic field model.

The electron density could be calculated using ψ_{QT} by differentiating with respect to height,

$$x = \frac{1}{\overline{y_L}} \left[\frac{d_{QT}}{dh_{QT}} - \frac{QT}{\overline{y_L}} \frac{\overline{dy_L}}{dh_{QT}} \right]$$

where $\overline{y_L}$ is the mean value over the interval (h_{QT}, h_s).

However, when there is no longer a transverse point in the ray path, the remaining oscillations (2.53) affect very much the results.

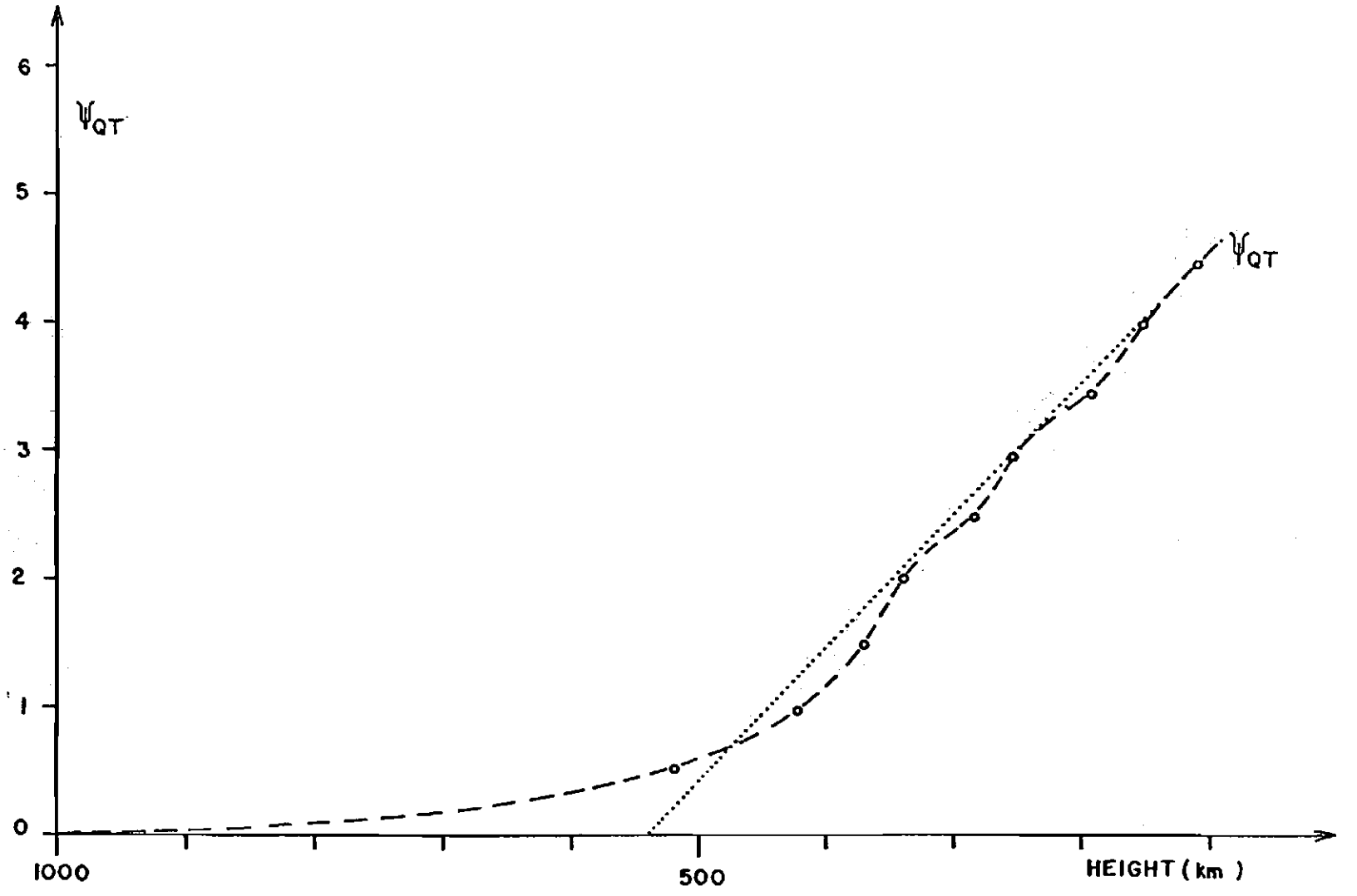

Fig.2.20 - Curve of ψ_{QT} for a simulation as a function of height obtained using the nulls of ϵ simulated at the ground station.

The curve giving ψ_{QT} and ε can be used in (2.65) from which the value of the electron density in the transverse point height can be calculated. The equivalent slab thickness is not known but assuming a value of 132 km, after calculating the N_{QT}, the electron content can be calculated using the computed N_{QT}. This can give a proportionality constant which gives the corrected value of the electron density

$$N(h) = N_{QT} \cdot I / \int_0^{h_s} N_{QT}\, dh$$

where I is the electron content given by the Faraday rotation.

We have no data on axial ratio variation so it is not possible to test the method.

2.7 - Conclusions

We see that for electron content purposes the inclusion of the transverse component of the magnetic field in the polarization description of a wave propagating through a magnetoionic medium gives small differences compared to the description given in §1.7. Near the quasi-transverse regions the tilt angle modifies in respect to QL-approximations, and can even be discontinuous. The QL-approximation does not give any information about the axial ratio of the polarization which is very important near QT-regions. Its measurement can give information of the heigth variation of the electron density.

An attempt was made by Mass (1966) to calculate an expression for the tilt angle on QT region. His expression gives (in our notation)

$$\psi = \frac{c\pi}{2f} \int_0^{h_s} XY_T^2\, dz$$

for the QT region. This expression is obtained substituting $(n^- - n^+)$ for QT-approximation in (1.18). This is not possible to do because the polarization of the waves is not circular, as can be seen in Fig.2.21 which shows the axial ratio of the polarization of the characteristic waves as a function of the transverse-longitudinal ratio q_{TL}.

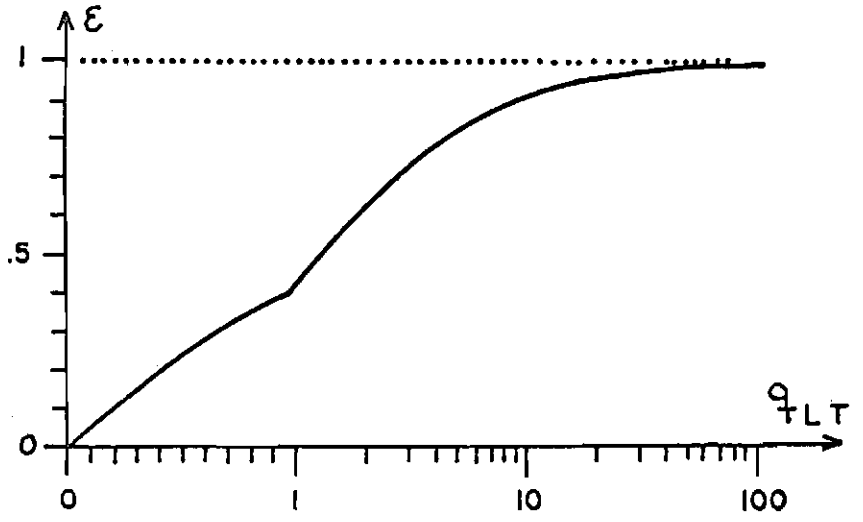

Fig.2.21 - Axial ratio of the polarization of the characteristic waves as a function of the transverse-longitudinal ratio q_{TL}.

CHAPTER 3

DATA ON LOW LATITUDE IONOSPHERIC ELECTRON CONTENT DURING HALF A SOLAR CYCLE

3.1 - Introduction

In this chapter we present some results that were obtained with measurements of the total electron content. The coordinates of our station are as follow:

	Geographic	Geomagnetic
Latitude	23.2°S	12.6°S
Longitude	45.8°W	21.7°E
Dip angle	- 23.7°	

The greater part of the data was obtained using the Faraday rotation method, from the 40 and 41 MHz signals emitted by the BE-B and BE-C beacon satellites. The data used were obtained during the period December 1964 to March 1968. Differential Doppler shift measurements from April and May 1963 have also been used. From this data, annual, seasonal and diurnal variations of total electron content have been derived.

3.2 - Method of Analysis

To compute the electron content we used the method described in §1.7.2 due to Ross (1965) in order to counter-balance the errors due to the high frequency approximation and the non-uniformity of the electron distribution in the ionosphere. For this purpose the close spaced frequency method was used. The modified expression (1.31) was taken for calculations in the computer. We reproduce it here for convenience

$$I_2 = I_1 \left(2 + 20 \frac{\Delta \Omega_m}{\Omega_m}\right) \qquad (3.1)$$

where

I_2 is the second order electron content

I_1 is the electron content calculated ignoring second order effects

Ω_m Faraday rotation for 40 MHz

$\Delta\Omega_m$ difference of Faraday rotation between 40 and 41 MHz

Errors are introduced by the assumption of a horizontally stratified ionosphere, and a fixed value for the mean ionospheric height, the latter causing the value of the field function M to differ from its correct value. It can be shown, however, that a 10 km variation about the assumed value of 350 km for the ionospheric point results in only a 1% change in the computed electron content. The quasi-transverse point was observable on all the records, enabling the total Faraday rotation to be measured unambinguously. In order to correct for errors in the computed path of the satellite the positional data is shifted so as to ensure M = 0 where the Faraday rotation is zero. This corrective procedure was used in order to overcome the discontinuity in computed content that appears close to the Q.T. point.

All data processing was done at our laboratory using either an IBM 650 or a Burroughs' B3500 computer.

3.3 - Experimental Results

A detailed analysis has so far only been made for the 1966 and 1967 data; a full analysis of the data for other years will be presented elsewhere. For this reason the diurnal and latitudinal variations are presented for 1966 and 1967 only. In the other analyses presented in this thesis use was made of particular satellite passes only.

In our laboratory we are also reducing this data by the Doppler and hybrid method but these results are not yet available. When this is done we can better correct the results and analyse some details that we could not analyse with the Faraday method. The discontinuity of the computed electron content near the QT region does not appear with Doppler method. The BE-C Faraday rotations are generally very slow, leading to much error in the electron content, these passes will be better reduced by the other methods. The nighttime content is giving some difficulty that may be eliminated by comparison with the results of the other methods.

The longitudinal variations cannot be seen well with the Faraday method because the variation of the longitudinal component of the magnetic field is very small leading to slow Faraday rotation rates; in this cas it is better to use the Doppler method.

3.3.1 - Diurnal and Latitudinal Variations

Since the time of each pass of the satellite receedes as the day advances, about three month's data are required to construct a diurnal pattern. For this reason the data are grouped in seasons. Combining the information about local time and the dip angle of the earth's magnetic field at the subionospheric point, average electron contents were calculated and used to construct the contour maps of constant total content I shown in Fig.3.1 and 3.2. Contours have not been drawn in these diagrams where the data were few. The contour maps of Fig.3.1 and 3.2 were constructed by visually estimating average diurnal curves drawn on mass plots of each season's data for dip angle intervals of 5^{o}. The data used were obtained from a combined total of 482 satellite passes during 1966, using the BE-B and BE-C satellites, and are for quiet days only (Kp $<$ 5). For 1967 we had 237 satellite passes, and we used only the BE-B satellite.

The day to day variations observed in total content at a given local time and subionospheric point are of the order of $\pm$ 25%. The dispersion

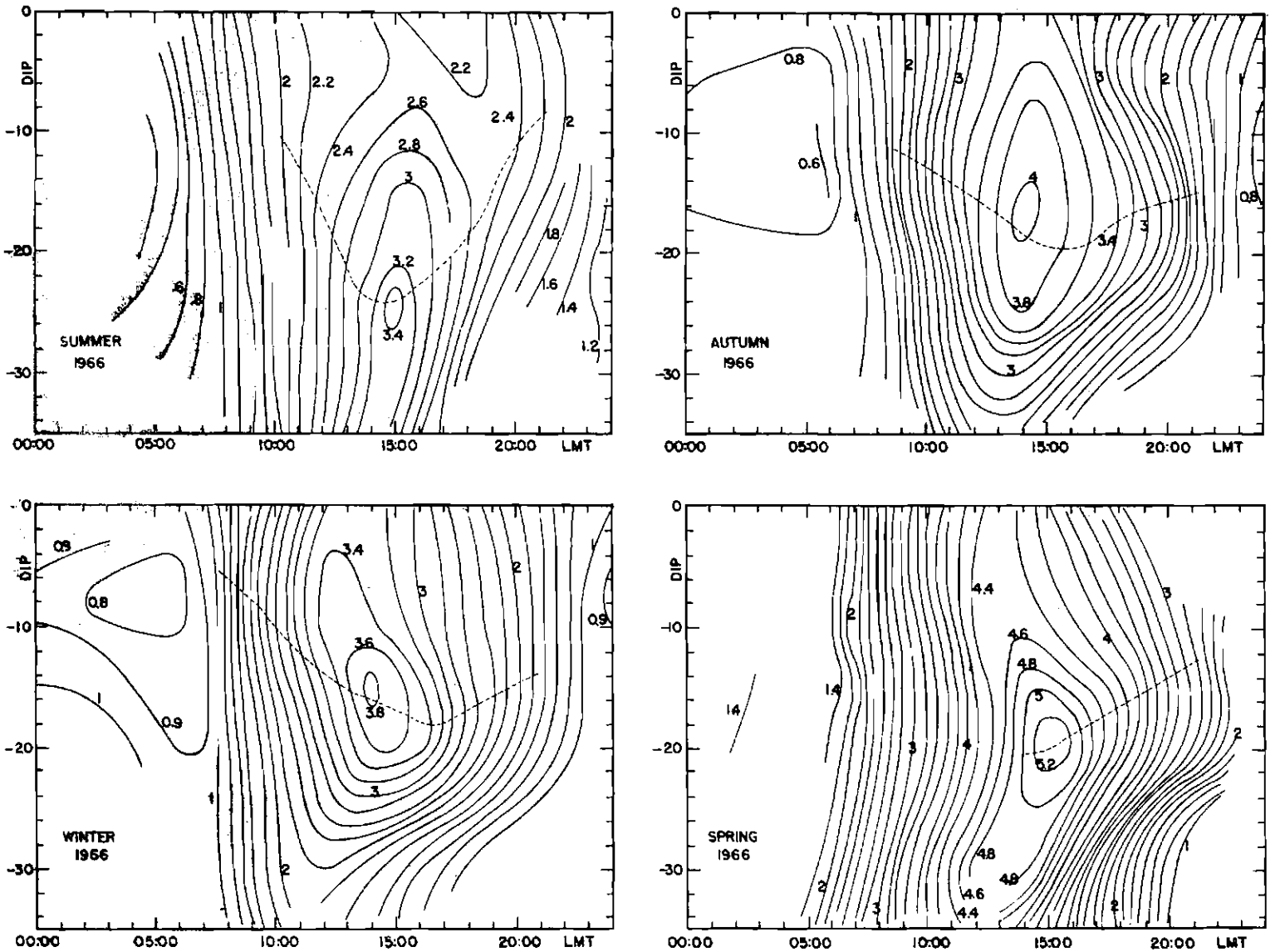

FIG (3.1) CONTOUR MAPS OF TOTAL ELECTRON CONTENT FOR THE FOUR SEASONS OF 1966 (BE−B AND B−C)

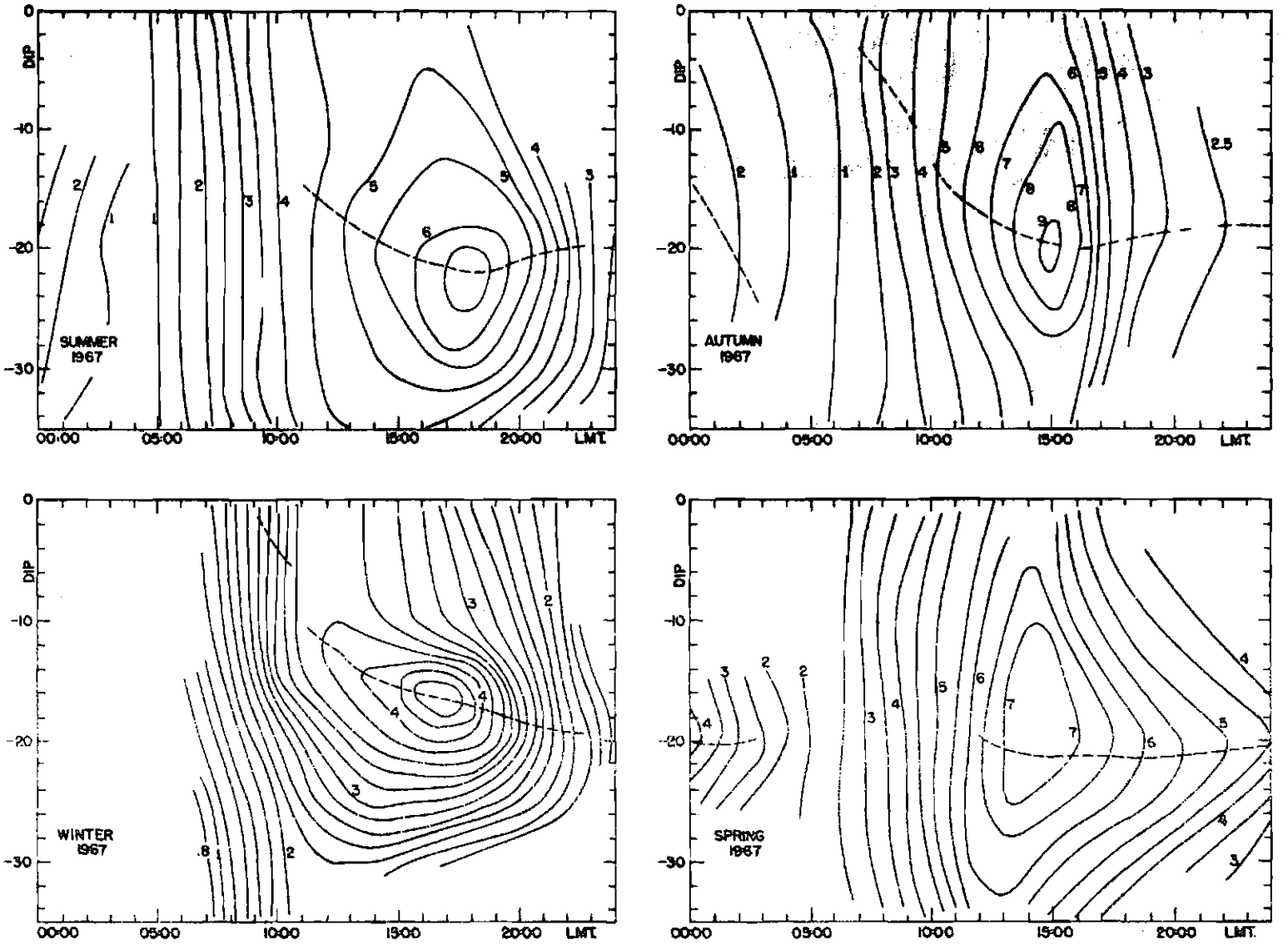

FIG. 3.2. CONTOUR MAPS OF TOTAL ELECTRON CONTENT FOR THE FOUR SEASONS OF 1967 (BE-B).

was measured taking the percentage difference between an actual data point and the mean value for the same local time, divided by the mean value. In table 3.1 we show the r.m.s. deviations for -20^{o} dip angle for the four seasons of 1966 and summer 1967.

Data from BE-B and BE-C agree very well for the same dip angle and local time, not showing any systematic errors. The results for BE-C show a rather greater dispersion than those for BE-B, as can be seen in Table 3.1

Table 3.1 - Day to day variations with respect to the average in total electron content.

	r.m.s. deviation	
Season	BE-B	BE-C
Summer, 1966	15.6 %	18.5 %
Autumn, 1966	20.7 %	24.9 %
Winter, 1966	33.1 %	35.6 %
Spring, 1966	24.5 %	32.8 %
Summer, 1967	9.6 %	15.1 %

and Fig.3.3, because of the low inclination of the orbit of the former satellite, leading to slow Faraday rotation rates at our geographic position. In Fig.3.3 we show a frequency histogram of the dispersion from the mean value for both satellites compared with the mean frequency histogram taking BE-B and BE-C together.

The diurnal ratio of maximum to minimum electron content has an average value of 4.63 taking all the 1966 data together, and 4.74 for 1967. In Table 3.2 we present this ratio for all seasons for 1966 and 1967.

From Table 3.2 this diurnal ratio is greatest in summer and autumn and smallest in winter and spring.

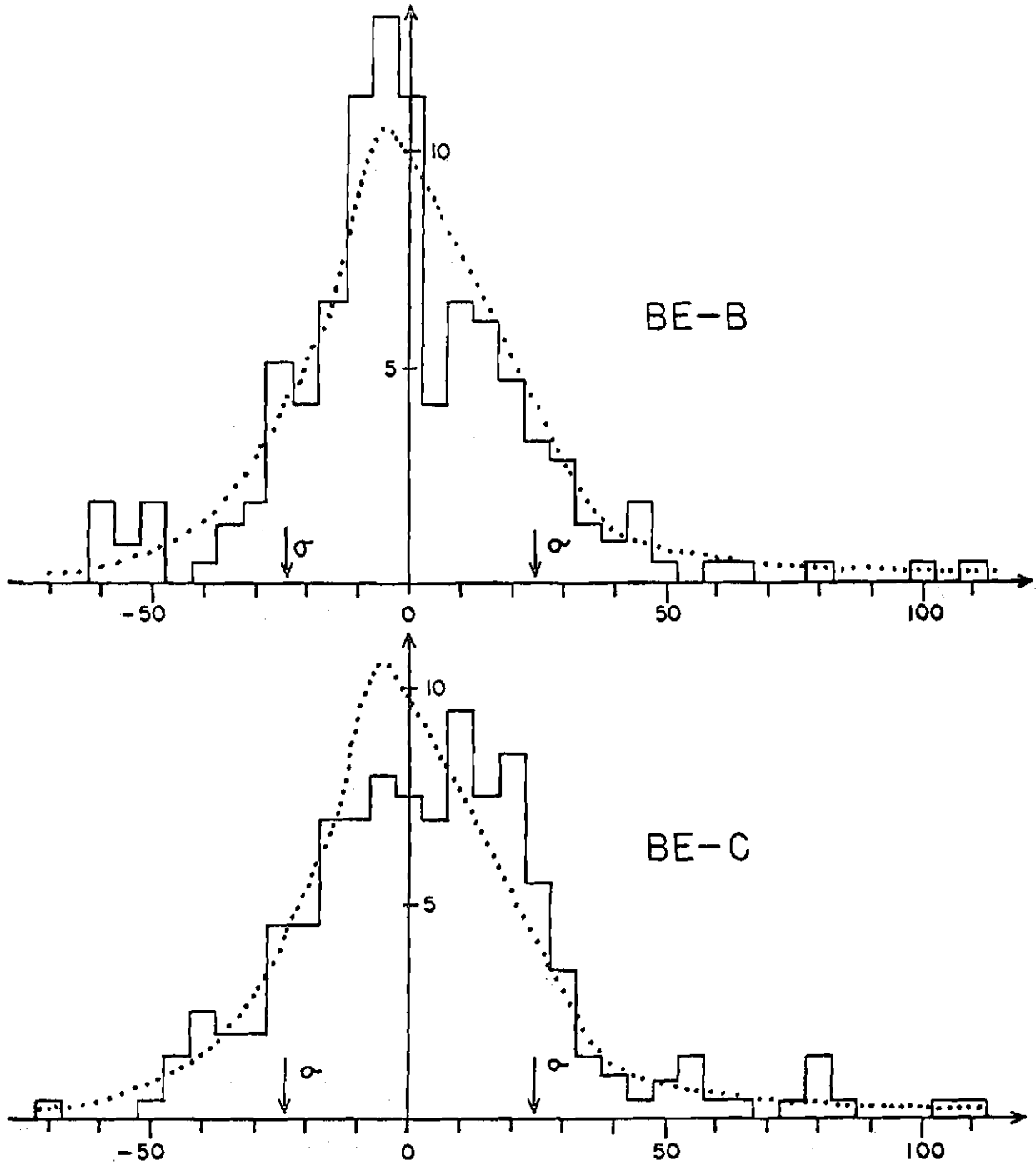

Fig.3.3 - Frequency histogram of the dispersion from the mean value for both satellites compared with the mean frequency distribution taking BE-B and BE-C data together (dotted line).

Table 3.2 - Diurnal ratio of maximum to minimum electron content

	1966	1967
Summer	4.72	5.78
Autumn	5.47	7.35
Winter	4.17	2.27
Spring	4.15	3.55

Our data for nighttime ionization levels are relatively few, but the values that we obtain are unusually high. The mean ratios of maximum to minimum total content of 4.63 and 4.74 are much smaller than those reported by other workers. The Delhi workers for example, obtain values of 8, 13 and 21 for winter, summer and equinox respectively. It is possible that our nighttime values are too high due to errors occurring in the analysis of the Faraday rotation records, and we intend to further investigate this possibility using the Doppler or the hybrid method.

The sunrise and sunset gradients of electron content, normalised by dividing by the diurnal maximum, are nearly constant for all seasons and dip angles. The average sunrise gradient is 1.25 times the average sunset gradient. The nighttime content shows a slow decrease after midnight for all seasons.

In general the post-noon maximum in total content occurs later in summer than in autumn and winter. In Table 3.3 we present the occurrence time and the dip positions of the post-noon maximum.

Tyagi and Somayajulu (1966) have reported measurements made at Delhi, and state that maximum ionization is observed between 1300 and 1500 at all seasons. Skinner (1966), at Zaria, reports a midday 'bite out' following the f_oF^2 results, leading to a second maximum as late as 1600 L.T.

Table 3.3 - Time and position of the post-noon maximum

	1966		1967	
	Time (hours)	Dip	Time (hours)	Dip
Summer	15	-25^{o}	18	-23^{o}
Autumn	14	-16^{o}	15	-20^{o}
Winter	14	-15^{o}	16.5	-17^{o}
Spring	15	-20^{o}	14	-20^{o}

The only other results showing a seasonal effect in the time of maximum ionization appear to be those of Hibberd (1964) who observed a diurnal maximum around 1300 L.T. in winter nad 1500 L.T. in summer. Our result tends to agree with that of Hibberd, working at Pennsylvania State University (40.8^{o}N), in that diurnal maximum occurs later in summer than in winter.

Latitudinal variations of total content at our station are principally associated with the equatorial anomaly, discussed below. During the post-midnight hours when the anomaly is not observed there is little variation with latitude.

Comparing Fig.3.1 with 3.2 we can see that the general aspect of the contour lines is conserved, the greater changes are in the absolute values, resulting from the increased solar activity in 1967, as compared with 1966.

3.3.2 - The Equatorial Anomaly

The equatorial anomaly is clearly visible in the countour maps of Fig. 3.1 and 3.2 the mean position of the maximum of the anomaly is around -20^{o} dip angle, moving south in summer and north in winter. The

extent of this movement of the crest is about $\pm 5^{o}$ of dip angle. In order to show the behavior of the crest in more detail we have plotted in Fig. 3.4 and 3.5 the position of the maximum, in terms of dip angle, as a function of time of day, for the four seasons of 1966 and 1967.

The crest first appears at about 1000 L.T. at a dip angle of -10^{o} and subsequently moves south, reaching its maximum southward point at around 1400 to 1500 L.T., when the total content is also a maximum. During the afternoon and evening hours the crest returns towards the equator, dissappearing at about midnight. The most southerly point reached is approximately -24^{o} dip angle in summer and -17^{o} dip angle in winter.

Comparing Fig. 3.4 with 3.5 we note some differences. During 1967 we have a greater occurrence of the equatorial anomaly during the nighttime and it appears that it tends to move away from the equator.

The mean positions and their maximum deviations from the mean are shown in Table 3.4.

Table 3.4 - Maximum southward excursion of the crest of the equatorial anomaly

	1966	1967
	Dip angle and maximum deviation	Dip angle and maximum deviation
Summer	-24^{o} $\pm 4^{o}$	-24^{o} $\pm 6^{o}$
Autumn	-20^{o} $\pm 7^{o}$	-20^{o} $\pm 9^{o}$
Winter	-18^{o} $\pm 9^{o}$	-16^{o} $\pm 8^{o}$
Spring	-24^{o} $\pm 5^{o}$	-22^{o} $\pm 6^{o}$

The southward excursion is greatest in the summer and least in the winter.

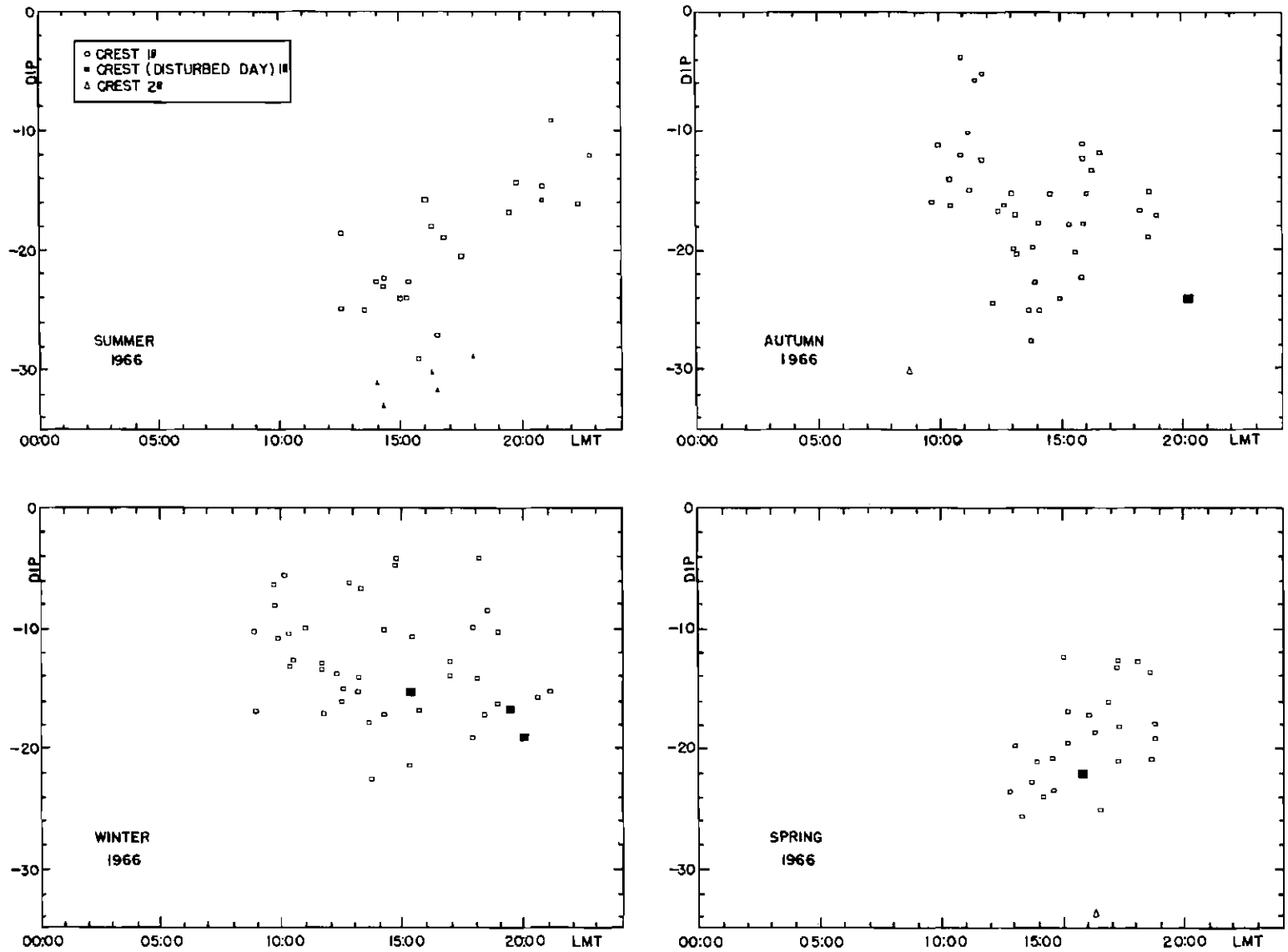

FIG (3.4) DIURNAL VARIATION IN THE POSITION OF THE CREST OF THE EQUATORIAL ANOMALY OF 1966 (BE-B)

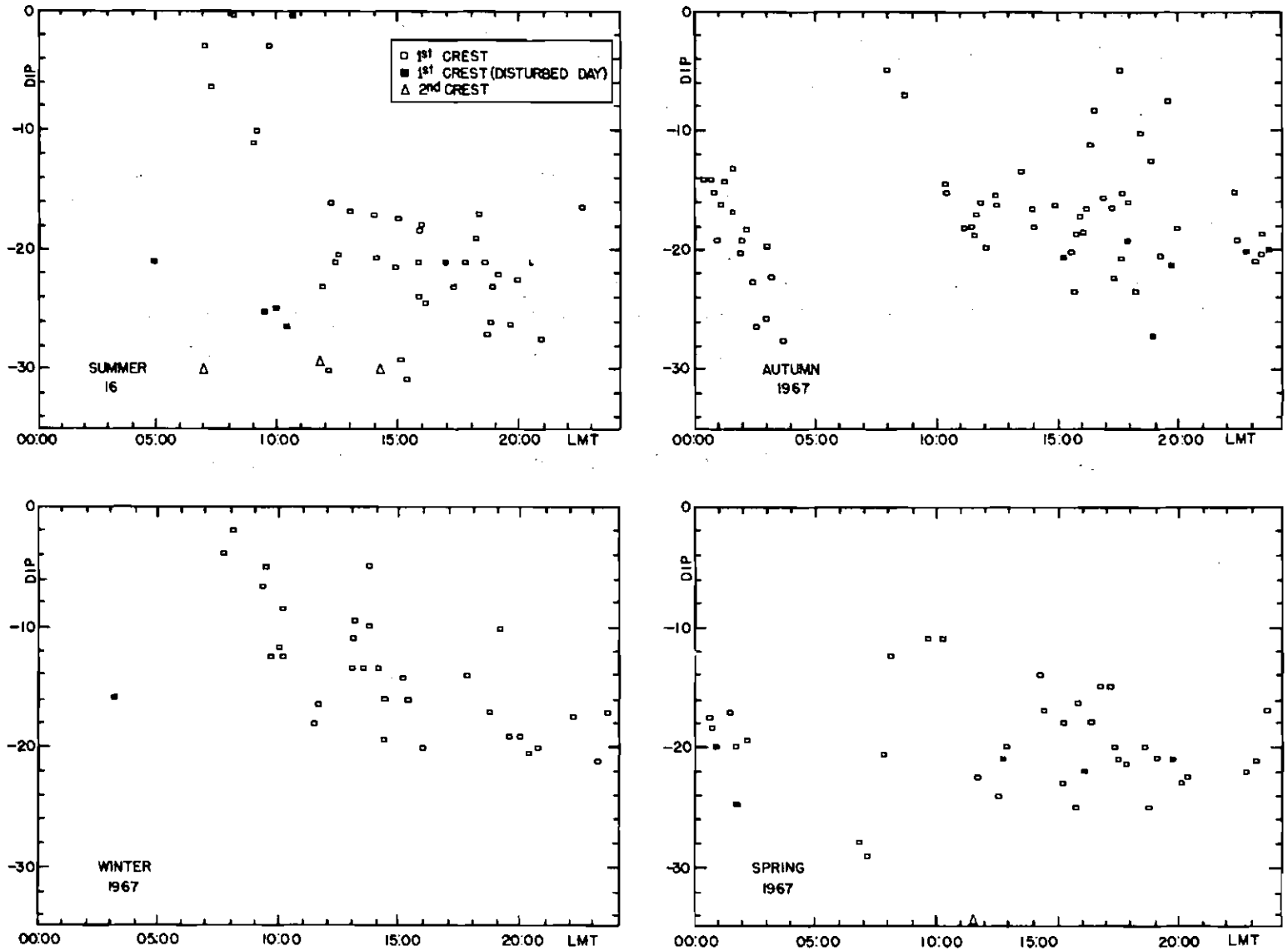

FIG. (3.5) DIURNAL VARIATION IN THE POSITION OF THE CREST OF THE EQUATORIAL ANOMALY OF 1967 (BE-B)

The equatorial anomaly will be assymetric if the same phenomena occurs in the north hemisphere.

3.3.3 - The Brazilian Magnetic Anomaly

Mendonça (1965) has analysed differential Doppler shift measurements taken at São José dos Campos during 1963, and shows enhanced ionization in the region of the Brazilian Magnetic Anomaly at around -35° dip angle. He attributed this ionization as being caused by the trapped radiation from the Starfish Experiment, which would be able to reach F layer heights in the region of the Brazilian Anomaly due to the low magnetic field values. We have analysed our data for 1965, 1966 and 1967 with a view to determining whether or not enhanced ionization continues to exist. Out of a total of 447 records analysed so far, only a few have shown a second maximum to the south of that associated with the equatorial anomaly. In Fig.3.6 we show the percent occurrencies of enhanced ionization per month in satellite passes in which we

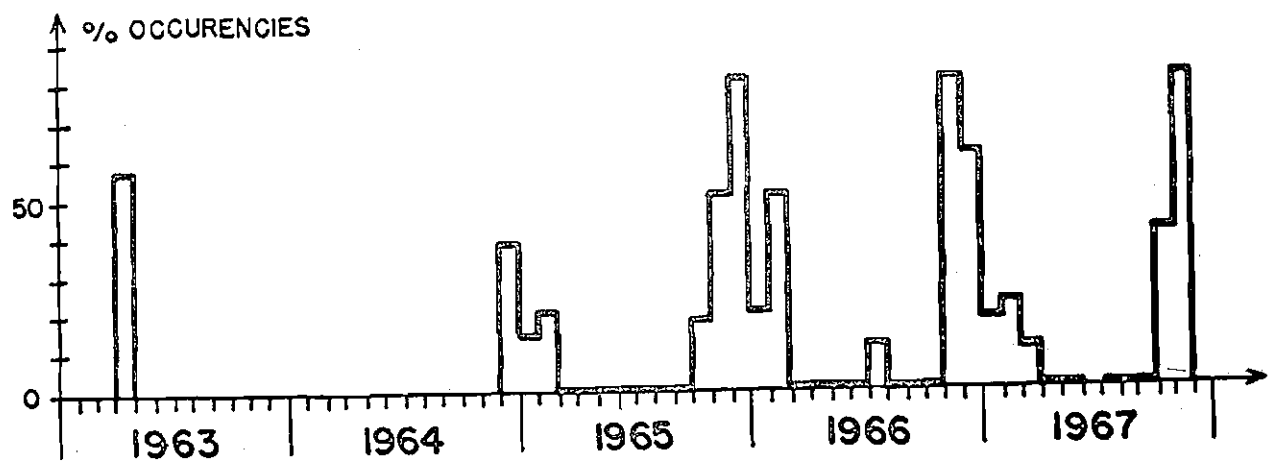

Fig.3.6 - Percent occurrencies of enhanced ionization per month. (N.B.A fains line for the horizontal axis indicates no data).

could observe this phenomena. In 1963 we have only one month of data but in the same month of the subsequent years we have no enhanced ionization occurences . This tends to support the view that the enhanced ionization observed during 1963 was in fact due to the temporary artificial radiation belt produced by the Starfish detonation.

It is of interest to note that the few occasions when we have observed a secondary maximum on our data all occur during the summer. The infrequent observation of a secondary maximum cannot, however, be taken as definitive evidence agains its existence as a normal feature, as its position at -30 to -35 dip angle is at the extreme south of the region which we can examine. The zenith angle subtended at our station by a satellite whose subionospheric points is at -30° dip angle is 60° or greater, making accurate total content measurements using the Faraday rotation method extremely difficult. In Fig.3.7 we present the geographic position of the occurence of the enhanced ionization. It can be seen that it extends between 29° and 34° south latitude.

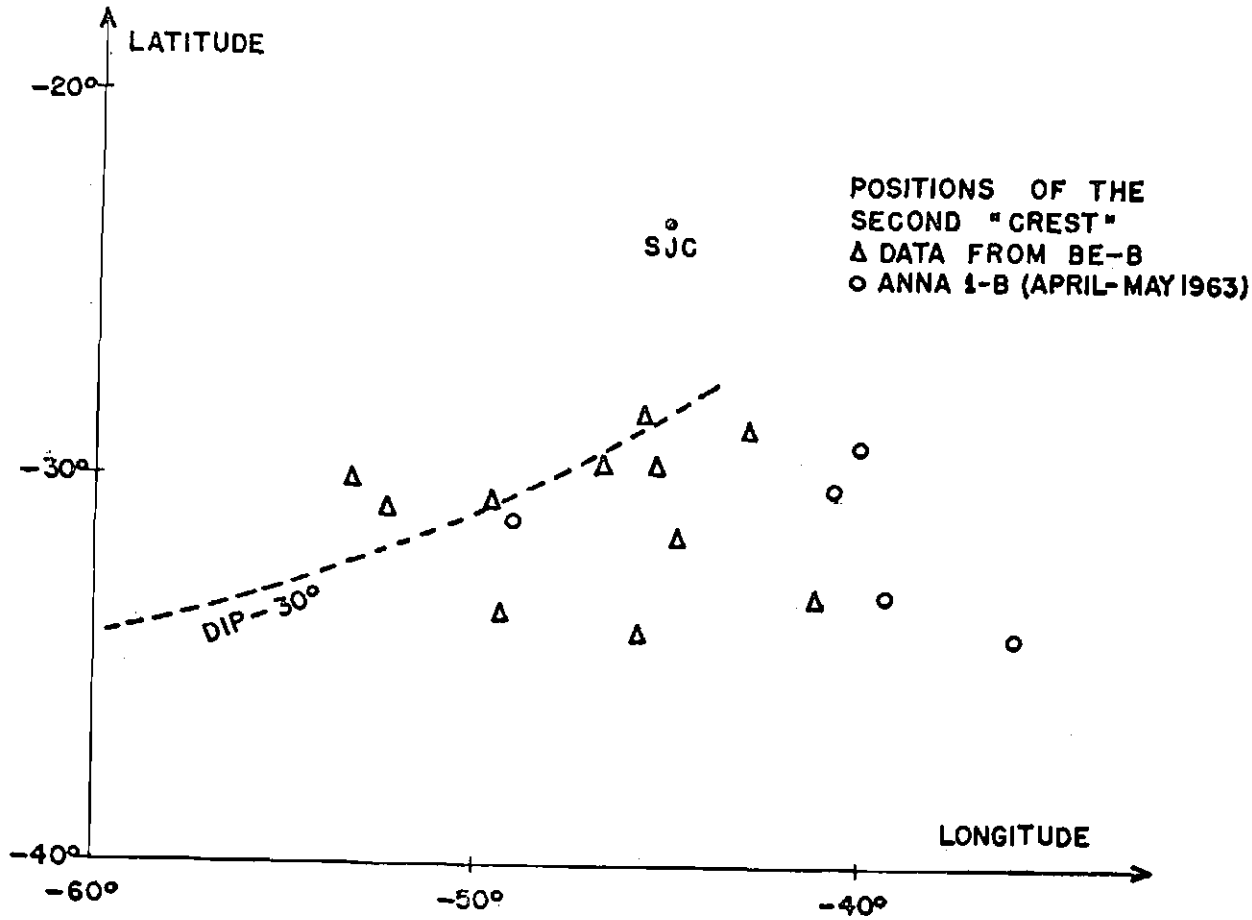

Fig.3.7 - Positions of the second "crest". (Δ) data from BE-B (o) data from Anna 1-B.

3.3.4 - Solar Cycle Variations

In order to determine a relationship between total electron content and solar activity we have analysed data for 1963 to 1968. The mean values of total content I between 14 and 15 hr for dip -20^{o} have been calculated for the four seasons and plotted against the 10cm mean solar flux S_A and the mean Zurich sunspot number $\bar{R}$.

If we express I as a first order function of S_A then we obtain

$$I = I_o \left[1 + a\ (S_A - 80)\right] \times 10^{17} \text{ electrons/m}^2$$

for S_A values greater or equal to 80. Where I_o and a are given in Table 3.5.

Table 3.5 - Values of I_o and a for variation of I with solar flux

Season	I_o	a
Summer	3.7	0.012
Autumn	4.1	0.022
Winter	2.7	0.011
Spring	3.2	0.023

The plot of electron content against solar flux is shown in Fig.3.8

Expressing I in terms of the sunspot number $\bar{R}$ we obtain

$$I = I_o \left[1 + b(\bar{R} - 40)\right] \times 10^{17} \text{ electrons/m}^2$$

for $\bar{R}$ values greater or equal to 40. Where I and b are given in Table 3.6.

In Table 3.6 we also give, for comparison, the values of b obtained by Bhonsle et al (1965) working at Stanford, and Yeh and Flaherty (1966) working in Illinois. It should be noted that the Stanford and Illinois results were obtained during the declining phase of a sunspot cycle, whereas our results are for the increasing phase.

The plot of electron content against sunspot number is shown in Fig.3.9

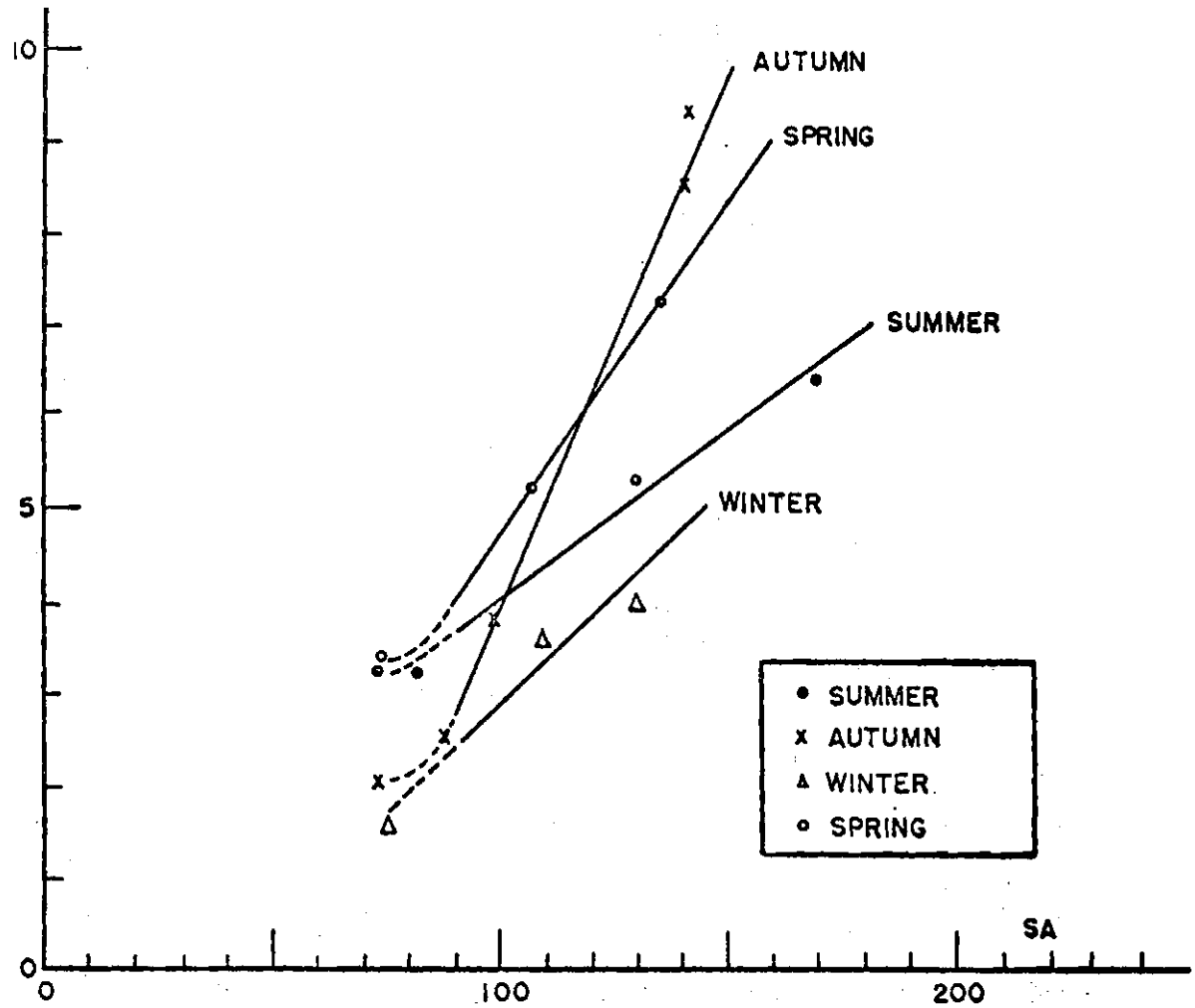

Fig.3.8 - Variation of total electron content with 10.7 cm solar flux. Data for 1965 to 1967, for dip -20°, between 14-15 hr LMT.

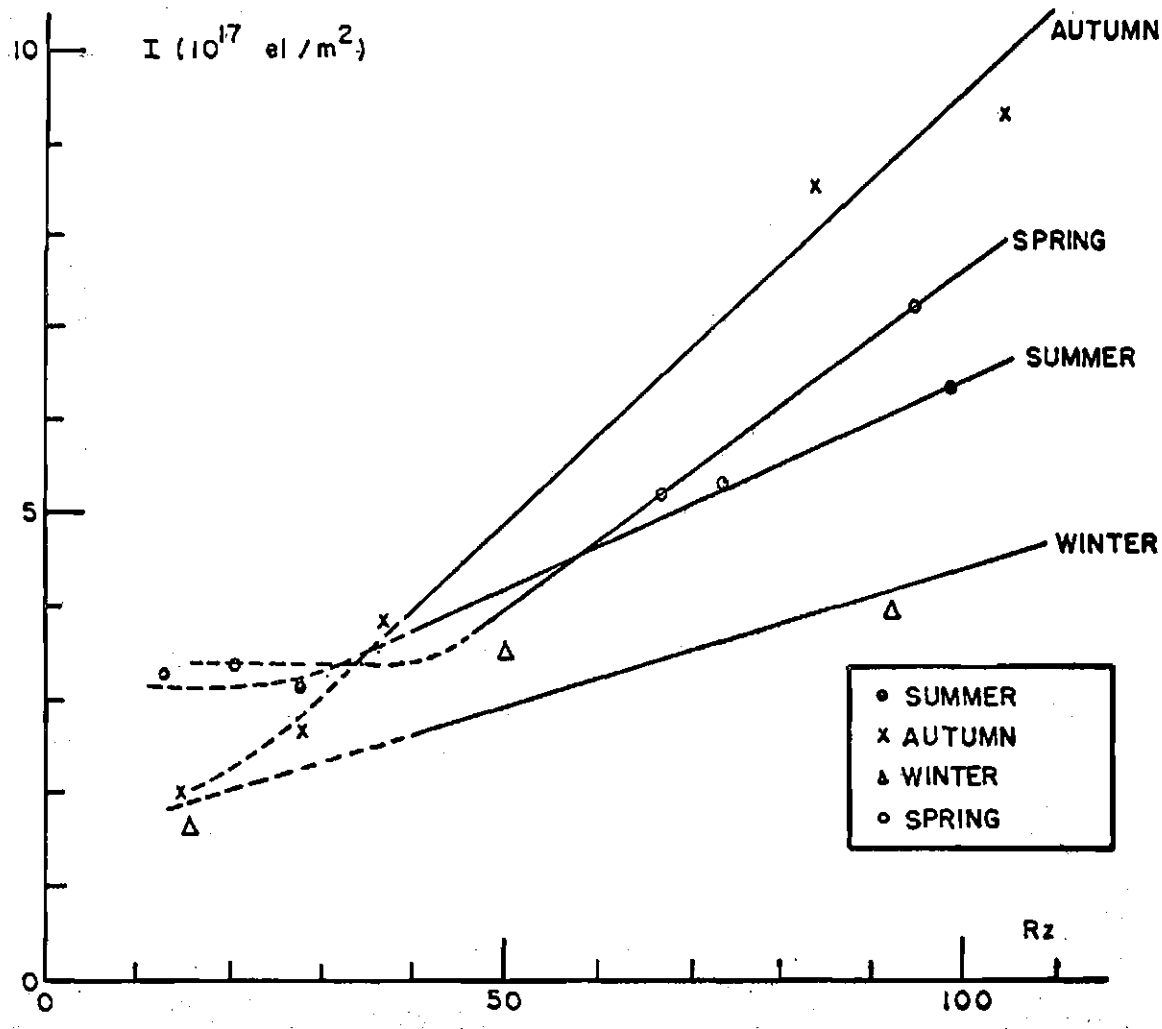

Fig.3.9 - Variation of total electron content with sunspot number. Data from 1965 to 1967, for dip -20°, between 14-15 hr LMT.

Table 3.6 - Values of I_o and b for São José, Stanford and Illinois for sun spot number variation

	S. José		Stanford	Illinois
	I_o	b	b	b
Summer	3.30	0.011	0.011	0.028
Winter	1.65	0.032	0.022	0.032
Equinox	2.70	0.037	0.025	0.024

The plot of electron content against sunspot number is shown in Fig.3.9.

Comparing Fig.3.8 with Fig.3.9 the electron content seems to be bettter correlated with solar flux than with sunspot number.

3.3.5 - Seasonal Variation

From Fig.3.8 and Fig.3.9 we can see that the total content peaks at the equinoxes and reaches minimum values at the solstices. This agrees with the results of other workers (see for example the observations of Tyagi (1966) for 1965, 1965 and 1966).

Our summer values of total content are consistently higher than the winter values, showing an absence of any winter anomaly for solar fluxes less than 150.

It is difficult to make a better seasonal analysis because we have for the same local time and dip angle only a small number of points and for each year they do not occur in the same period of the season. A geostationary satellite, would enable a much better analysis to be made.

3.3.6 - Magnetic Activity Variation

In general the behavior of the equatorial anomaly under quiet magnetic conditions is as expected. The motion of the crest away from the equator in the morning hours, returning towards the equator in the afternoon

and evening hours closely follows the behavior of the f_0F2 anomaly. The most southerly excursion of the maximum is -20 to -25° dip angle, which may be compared with the +30° dip angle reported by the Delhi workers. King et al (1967b) also report the maximum to occur at 30° dip angle, using topside data for their analysis.

Basu and Das Gupta (1968) have reported that under disturbed magnetic conditions the magnitude of the equatorial anomaly decreases and the position of the crest moves towards the equator. We have examined our data for 1965 and 1966 in an attempt to determine the effect of sudden commencements on the equatorial anomaly. With regard to changes in the actual total content we see no consistent effect, other than perhaps a slight increase in the day to day variations observed. The position of the crest appears to move away from the equator immediately after a sudden commencement. Our of 10 cases where a clear maximum was observable both on the day before and the day of a sudden commencement we observed a southward movement in 8 cases and a northward movement in 2 cases. Golton et al (1969) also found that in 4 out of 10 cases the peak moved away from the equator in the northern hemisphere. These results appear to contradict that of Basu and Das Gupta as mentioned above. In Fig.3.10 we show the displacement of the crest from its position on the day proceeding a sudden commencement as a function of storm time.

The ionospheric behavior during a magnetic storm shows a marked dependence upon the geographic latitude, season and local time, indicating that rather more data should be used to arrive at reliable conclusions. Using Alouette 1 data, King et al (1967a) show that the equatorial anomaly seems to disappear completely on a disturbed day, but Mack (1968) indicates that it vanishes only during moderately severe magnetic storms ($Kp > 6$). Our data refers to a non-vanishing equatorial anomaly but some of the results of King et al (1967a) could be used. It is not impossible that errors in the reduction of the data could affect our

results. The fact that the measurements on sucessive days are not exactly on the same local time (the difference is less than 15 min) does not affect very much the results. King et al (1967a) and Mack (1968) refer to an upward movement of the layer (the electron density peak can be 100 km greater during the magnetic storm) which will change the mean ionospheric height, the magnetic field also changes by up to 4%. The electron content has been calculated neglecting such changes, This can affect slightly our results. The upward movement of the mean ionospheric height would also cause a movement away from the equator when observed by a station located farther from the equator than the equatorial anomaly.

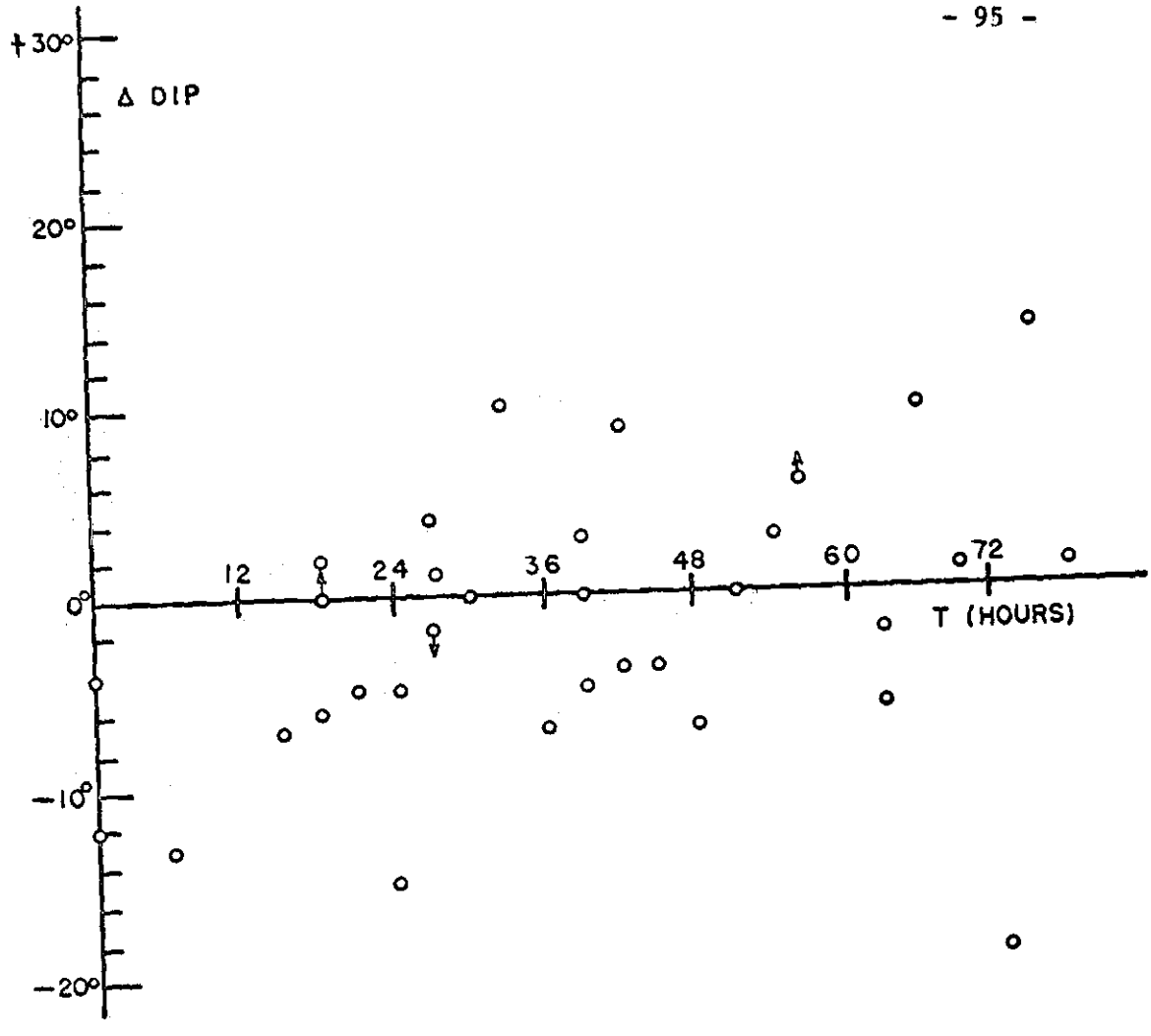

Fig.3.10 - Variations of the positions of the equatorial anomaly crest during magnetic storms, as a function of storm time.

CHAPTER 4

SOME REMARKS ON ELECTRON CONTENT COMPUTATION

4.1 - Introduction

Here we make some comments and references on the way we computed the electron content. The sources of error in this computation are briefly described and some of its aspects are analysed. Some improvement, made in the reduction method, is also presented and some suggestions for further work, are given.

4.2 - Computer Program

Data from 1964 to 1966 were computed with the computer program described by Casali et al (1968) using the IBM650; for the data from 1967 onwards an adaptation was made for the B3500 computer and some more calculations were added: the computation of second order electron content by the Ross equation (1.27) and a second order electron content calculated by a modified formula given in §4.4.1.

The computation of second order electron content by the Ross equation (1.27) uses the parameters β (Distribution Parameter) and G (Geometrical Parameters) that were introduced in § 1.7.2.

Since B_H is the horizontal projection of the magnetic field on the plane of incidence of the ray path, B_z, the vertical component and χ the zenith angle of the ray path; the parameter G defined in equation 1.26 can be calculated by using the expressions

$$B_l = B_z \cos\chi + B_H \sin\chi ,$$

$$B_L = B_z \sin\chi - B_H \cos\chi ;$$

after substituition of the above relations in (1.26) we get

$$G = B_H (1 + \tan^2\chi) \tan\chi / M$$

where M is defined in relation 1.20. For magnetic field computation we use the expressions given in §1.4

For the parameter β we used the value 3.6 reported by S. Basu (1967) for daytime. When ionosonde data for S.J.Campos is available local values can be used.

The subroutine used for solving the Ross equation is given on the next page and here we give the description of the method used.

From Ross equation (1.27) we have

$$I_1 = I_{2R} (1 + \alpha I_{2R}) \tag{4.1}$$

where

$$\alpha = \frac{40.25}{f^2 h_s} \left[\beta + (\beta - 1)\, G\right]$$

f is the signal frequency

h_s is the satellite height;

units are in MKS

Relation (4.1) is quadratic in I_2 and the positive root is given by

$$I_{2R} = \frac{\sqrt{1 + 4\alpha I_{2R}} - 1}{2\alpha}$$

Usually the term $4\alpha\, I_{2R} << 1$, so there is a problem in finding the square root with the computer, because of the truncation. This difficulty was pointed by S.Basu (1967), showing an appreciable divergence between the exact solution and the binomial expansion of (4.2) or an iterated solution for general electron content value. The problem was solved using a digit by digit computation.

```
      SUBROUTINE ICROSS(ICR,I1,DALT,BETA,G)
C     SUBROUTINE TO COMPUTE THE ELECTRON CONTENT
C     WITH ROSS SECOND ORDER CORRECTION
C     INPUT =I1(FIRST ORDER CONTENT)
C     DALT(SATELLITE HEIGHT)
C     G(GEOGRAPHICAL PARAMETER)
C     IVAN J.KANTOR-14/11/68-CNAE
      DOUBLE PRECISION DALT
      REAL I1,ICR
      DATA F1/40.E+6/
      Z(X)=Y-X*(X+A)
      Q=80.5E-3/F1**2
      ALPHA=Q*(BETA+(BETA-1.)*G)/(2.*DALT)
      ICR=I1
      IF(ALPHA.EQ.0.) RETURN
      Y=4.*ALPHA*I1
      IF(1.+Y.LT.0.) RETURN
   10 IF(ABS(Y).LT.1.) GO TO 20
      ICR=DSQRT(1.+Y)-1.
      GO TO 100
   20 S=SIGN(1.,Y)
      A=2.
      X0=S
      DO 30 N=1,99
      X0=X0/10.
      IF(S*Z(X0))30,40,50
   30 CONTINUE
   40 ICR=X0
      GO TO 100
   50 ICR=0.
      DO 90 I=1,8
      X=-X0
   60 X=X+X0
      IF(S*Z(X))80,70,60
   70 ICR=ICR+X
      GO TO 100
   80 X=X-X0
      Y=Z(X)
      A=A+2.*X
      ICR=ICR+X
   90 X0=X0/10.
  100 ICR=ICR/(2.*ALPHA)
      RETURN
      END
```

To solution to be found is of the following type

$$x = \sqrt{1 + y} - 1 \qquad \text{with} \qquad y << 1$$

solving for y we have $y = x\,(x + 2)$. In a general form

$$y = x\,(x + a) \tag{4.3}$$

Supposing that we know a solution x_o correct to the n-th digit, let us calculate the (n + 1) th digit

$$x = x_o + x_1 ;$$

this substituted in (4.3) gives

$$y - x_o\,(x_o + a) = x_1\,\left[x_1 + (2x_o + a)\right]$$

and for $x_1 << 1$ we have

$$x_1 = I\left[\frac{y - x_o\,(x_o + a)}{a + 2x_o}\right]$$

where I (x) represents the largest integer contained in x.

Substituting $y \leftarrow y - x_o\,(x_o + a)$

$$a \leftarrow a + 2x_o$$

we come back to the same type of equation (4.3). So the equation (4.3) can be solved by solving sucessive integer equations of the same type.

Comparing the precision we get in a computer program using floating point numbers we find that, N being the mantissa length:

a) By the method shown above we have (N-1) exact digits.

b) Calculating the square root, n being the order of magnitude of $(4\alpha I_2)$ (v.g. $3.7 \times 10^{-5} \rightarrow n = -5$), we obtain the solution with $(N + n)$ exact digits. It does not give any result when $N + n < 0$.

In Fig.4.1 we present the electron content for a satellite pass calculated by expressions (1.27) I_{2R} and (1.31) I_2.

It can be seen that the electron content computed from Ross equation I_{2R} follows closely the one calculated from (1.31), I_2 diverging less than 15% for zenith angles less than 70°.

4.3 - Error Analysis

4.3.1 - Ionospheric-Point height

The value of the computed electron content is inversally proportional to $\overline{M}$ (1.20), which is determined by calculating M at the ionosphere centroid height. The actual height where M should be computed is not known, and this leads to some error. However, a 10 km variation about the assumed value of 350 km for the ionospheric point results in only a 1% change in the computed electron content. When ionosonde data is available a better value of the ionospheric-point height can be used.

The ionospheric point is also a function of the satellite height. A variation of 100 km in the satellite height leads to a variation of 8km in the ionospheric point, which corresponds to 0.8% change in the computed electron content.

The ionospheric point height is not constant during a satellite pass (Foltz, 1965 and Kuntman, 1966) but this variation is not greater than 50 km for a 10° latitude range.

4.3.2. - Comparison with other Data

Comparison between results using other reduction methods (Garriot and Mendonça, 1963; Almeida and Waldman, 1967 and Rao and Yeh, 1968), receiving simultaneous passes of two satellites (Almeida and Waldman, 1967) and

using widely spaced stations (Taylor and Earnshaw, 1965) shows a good agreement in the results.

4.3.3 - Geometrical Factors

The computation of the electron content is limited to zenith angle $<60^{o}$ because the second order corrections in (1.31) are not effective when the non-linearities are too high.

The orientation of the antenna in respect to the emitted polarization of the satellite signal and the zenith angle which the ray path makes with the antenna can displace the position of the Faraday nulls (Wernik, 1967), that may introduce an error of up to $\pm$ 20% and its influence is especially important at satellite elevations less than 60^{o}.

4.3.4 - Horizontally Stratified Ionosphere

An oblique ray path passing through regions where there is a horizontal gradient of electron density will give a false idea of the electron content in the subionospheric point. The influence is more pronounce during the sunrise and sunset.

4.3.5 - Estimated Error

The estimated absolute accuracy of the results is rather bette than 10% for the daytime records but is perhaps as poor as 30% for some nighttime records when the polarization rotation is extremely low.

4.3.6 - Quasi-Transverse Region

4.3.6.1 - First-Order Discontinuity

In S.J.Campos we observe the QT point on all the satellite records, enabling the total Faraday rotation to be measured unambiguously. The rotation angles are read by counting null points from the zero rotation QT region taken as reference, as shown in Fig. 2.12. In § 2.5.2 we saw that

the distorted Faraday null does not necessarily occur where $\Omega = 0$, and also that it depends on the orientation of the antenna. There is also a scaling error and an error in the time measurements. So that the QT point cannot be precisely determined and so when $\bar{M}$ is evaluated, Ω and $\bar{M}$ do not converge to zero simultaneously, leading a discontinuity in I_1 (1.22). The technique employed to smooth the I_1 versus time curves is based in shifting all the data in position so as to ensure $M = 0$ where we have the QT point. This does not change significantly the values of I_1 far from the QT point and remove the first order discontinuity.

The approximations made in (1.22) do not hold in the quasi-transverse region. In Fig. 2.15 we can see the difference between the simulated tilt angle for QL-approximation (Ω) and the complete solution (ψ). This difference increases when the electron content is higher, and can hardly be greater than a half turn, but gives rise to a distortion in the computed electron content when we use eqn. (1.22).

4.3.6.2 - Second-Order Discontinuity

The discontinuity that appears in the second order electron content is more complicated than that in the first order, because it involves two parameters $\Delta\Omega_m$ and Ω_m. In the simulation of the tilt angle of the polarization we have made many simplifications (§ 2.3 and § 2.5) but even so the ratio $\psi_{40}/\Delta\psi$ (Fig. 2.19) which is used in (1.31) has a large discontinuity during 12 seconds, in this example, near the QT region. This implies that if the first order electron content is smoothed near the QT region, I_2 will be discontinuous near this region.

Even so, when we consider the second order effects (§1.7.2) the parameter G (1.26) is discontinuous near the QT region resulting in a marked discontinuity in I_2.

The scaling errors in measuring $\Delta\Omega_m$ near the QT region also

affect very much the values of I_2 because it is always measured as an integer.

Using texpression (4.4), near the QT region

$$\left| \frac{\Omega_m}{\Delta\Omega_m} \right| \simeq \frac{21.8}{1.05} = 20.8$$

The problem in determining $\Delta\Omega_m$ consists in searching for a coincidence of the Faraday nulls of both frequencies. Considering the periods ($T_1 > T_2$) of the Faraday cycles to be constant, the nulls for both frequencies will occur in respect of the QT point taken as origin

$$t_1 = \pm T_1 m_1$$

$$t_2 = \pm T_2 m_2$$

where $m_1, m_2 = 0, 1, 2 \ldots$

An exact coincidence will occur when

$$\frac{T_1}{T_2} = \frac{m_2}{m_1} = \frac{\alpha_1}{\alpha_2}$$

α_1 and α_2 being integers. So there is an exact coincidence only at the instants

$$t = \pm n T_2 \alpha_1 \qquad n = 0, 1, 2 \ldots$$

The Faraday cycle when we have

$$n = m_2 - m_1 \qquad (n = \frac{1}{2}, 1, \frac{3}{2}, \ldots)$$

is given by

$$m_1 = \frac{n T_2}{T_1 - T_2}$$

Depending on the values of T_1 and T_2, m_1 is not always an integer and because the reduction method only measures integers, m_1 is given by

$$m_1' = I\left[\frac{nT_2}{T_1-T_2} + \frac{1}{2}\right]$$

where $I[x]$ is a function that gives the greater integer contained in x. So the error in m_1 is given by $m_1' \pm 1/2$.

This implies an error in the computed I_2

$$I_2 \pm \Delta I_2 = I_1\left[2.05 + 21.8\,\frac{\Delta\Omega_m}{\Omega_m \pm 1/2}\right];$$

making the reasonable approximations we get

$$\frac{\Delta I_2}{I_1} \simeq \pm \frac{10.9\ \Delta\Omega_m}{\Omega_m^{\,2}}$$

and assuming $I_1 \simeq I_2$ and $\Omega_m \approx 20.8\Delta\Omega_m$

$$\frac{\Delta I_2}{I_2} \simeq \pm \frac{2.5}{\Delta\Omega_m} \quad (\%)$$

In Table 4.1 we present some numerical values of the above expression.

Table 4.1 - Scalling error in the determination of $\Delta\Omega_m$

$\Delta\Omega_m$	$\Delta I_2/I_2$ (%)
0.5	5
1.0	2.5
1.5	1.66
2.0	1.25
2.5	1
5.0	0.5
10.0	0.25

As can be seen from Table 4.1 far from the QT point the scaling error decreases

In order to smooth the second-order discontinuity we tried to make the best least square fit of the data with the second order electron content computed with Ross equation (1.23) but the results were unsatisfactory (See §4.4.2) Perhaps a least square fit of $\Delta\Omega_m$ and a displacement of the data could eliminate the discontinuity, but the results should be compared with the results of other methods (v.g. Doppler) to ensure that for data far from the QT region the results will not be disturbed.

4.4 - Additional Comments on Reduction Method

4.4.1 - Difference Faraday rotation

The expression (1.30) was derived by differentiating (1.27), but if we use the difference of Faraday rotations the final expression will be more correct and its form is similar to the expression (1.30).

The difference of the measured Faraday rotation given by (1.28) for two frequencies f_1 and f_2 is

$$\Delta\Omega_m = \Omega_{m2} - \Omega_{m1} = \Omega_{c1} \ (k^{-2}-1) \left[1 + \frac{\overline{X}_1 C}{2} \ (k^{-2}+1)\right]$$

where $k = f_2/f_1$ and the subscripts refer to the respective frequencies.

Substituting (1.29) in the above expression and rearranging, we get

$$\Omega_{c1} = \Omega_{m1} \left[(1 + k^2) + \frac{\Delta\Omega_m}{\Omega_{m1}} \cdot \frac{k^2}{1-k^{-2}}\right]$$

The second-order I_{2D} will then be given by

$$I_{2D} = I_1 \left[1 + \left(\frac{f_2}{f_1}\right)^2 + \frac{\Delta\Omega_m}{\Omega_{m_1}} \ \frac{(f_2/f_1)^2}{1-(f_1/f_2)^2}\right]$$

For the frequencies transmitted by BE-B and BE-C satellites, $f_1 = 40$ MHz and $f_2 = 41$MHz.

$$I_{2D} = I_1 \left(2{,}05 + 21{,}8 \frac{\Delta\Omega_m}{\Omega_{m_1}}\right) \qquad (4.4)$$

$(N.B. \Delta\Omega_m/\Omega_{m1} < 0)$

Normally the value obtained by (4.4) is 5% lower than that obtained by (1.31), and the difference is greater when the zenith angle of the satellite increases. Figure 4.1 shows the electron content calculated by both methods for a satellite pass. It can be seen that the I_{2D} follows more closely to the electron content calculated using the Ross equation (1.27). The differences between I_2 and I_{2D} is nearly constant.

4.4.2 - Additional Comments on Ross Equation

The equations (4.4) and (1.30) were deduced from eqn. (1.27) making possible the computation of the second order correction term in (1.27) using only the data obtained with the satellite signal. It seemed possible to compute the value of β using the values of Ω_m and $\Delta\Omega_m$. We tried to find the values of β and Ω_0 (displacement between the observed QT point and the point where $\psi = 0$) which give the least square difference between the electron content computed with (1.27) and (1.30). The calculations were made using data near the QT point in order to reduce the second order discontinuity, but it gave absurd values of β.

In Fig.4.2 we present the percent correction

$$C(\%) = 100 \frac{I_2 - I_1}{I_1}$$

for equations 1.27 and 1.30, respectively (C_R and C_2). The value of the parameter G was computed using magnetic field model of § 1.4. It can be seen that for this particular satellite pass the correction terms do not agree; β obtains absurd values in order to reduce the difference between the two curves.

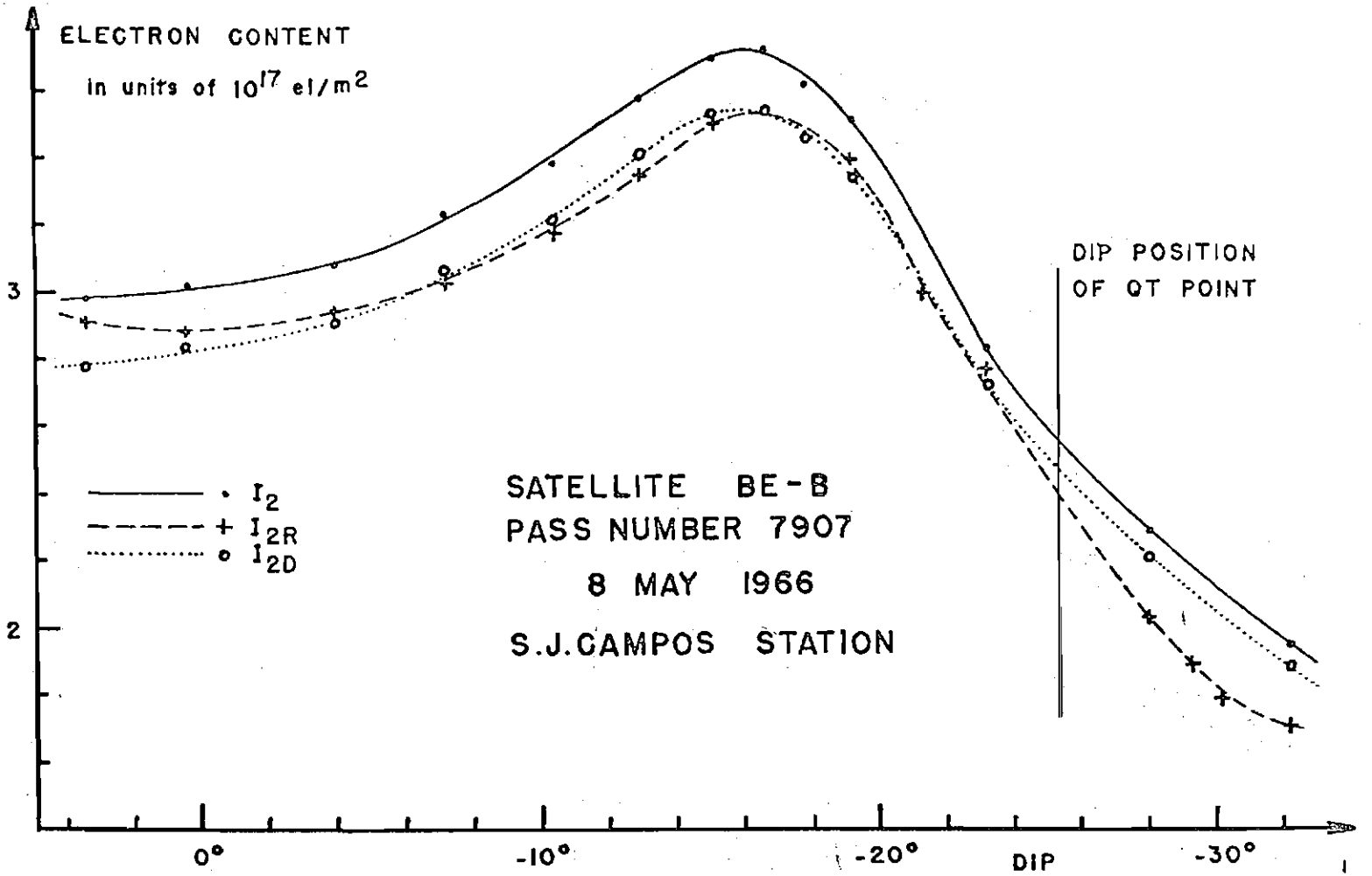

Fig.4.1 - Electron Content variation for a satellite pass calculated by equations 1.27, 1.31 and 4.4

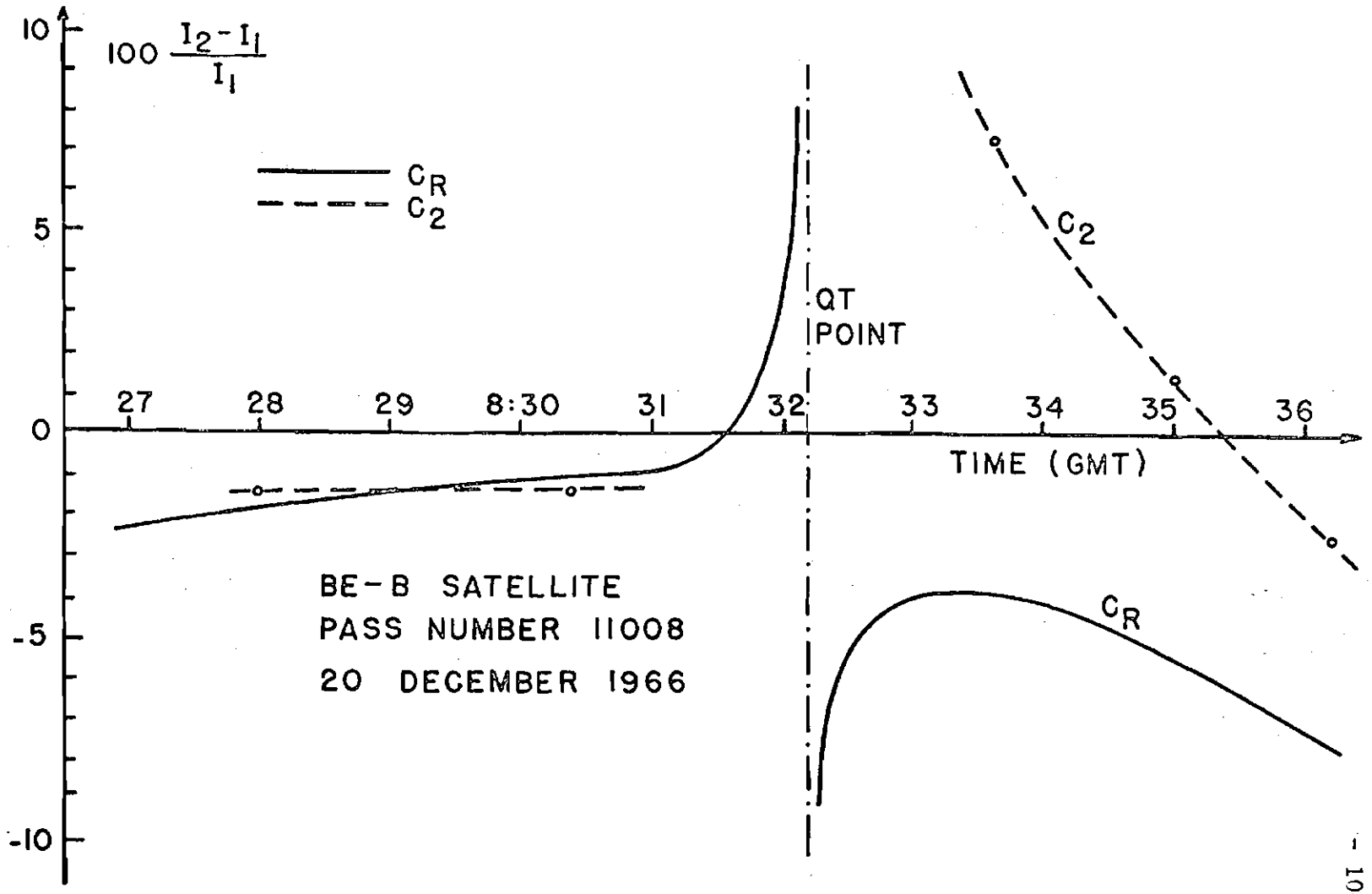

Fig.4.2 - Percent second order corrections C_2 and C_R (see text §4.4.2) for a satellite pass.

APPENDIX A

We give here the derivation of the expression for $k/(R^+ - R^-)$, that is used in (2.33). From (1.13).

$$n^{+2} - n^{-2} = \frac{X}{(1-iZ)-iY_L R^-} - \frac{X}{(1-iZ)-iY_L R^+}$$

$$= \frac{-i\ X\ Y_L (R^+ - R^-)}{(1-iZ-iY_L R^-)(1-iZ-iY_L R^+)} \qquad (A.1)$$

For high frequencies the second term in (1.13) is small. Expanding (1.13) in a binomial series and using the second order term, we have

$$n \simeq 1 - \frac{1}{2} \frac{X}{1-iZ-iY_L R}$$

The sum of the two refractive indices will be given

$$n^+ + n^- \simeq \frac{2(1-iZ)^2 + 2iY_L(1-iZ)(R^+ + R^-) - 2Y_L^2 - 2X(1-iZ)}{(1-iZ-iY_L R^-)\ (1-iZ-iY_L T^+)} \qquad (A.2)$$

Making use of (1.11) and (1.9), neglecting all products of the small quantities X, Y_L, Y_T, Z, the numerator of (A.2) reduces to $2\ (1-iZ-X)$.

So, from (A.1) and (A.2) the difference of the refractive indices becomes

$$n^+ - n^- = \frac{n^{+2} - n^{-2}}{n^+ + n^-} \simeq - \frac{iXY_L\ (R^+ - R^-)}{2\ (1 - X - iZ)}$$

but $k = \omega n/c$ so that we have in the second order approximation

$$\frac{\Delta k}{R^+ - R^-} = \frac{\omega(n^+ - n^-)}{c(R^+ - R^-)} = \frac{-\ iXY_L}{2(1-X-iZ)} \frac{\omega}{c} \qquad (A.3)$$

APPENDIX B

Here we present one of the computer programs used to simulate a wave passing through the ionosphere; the others are modifications of this one.

The computer used is a Burrough's B3500, and the language is the FORTRAN IV.

The simulation uses the equations 2.43, 2.45, 2.46, 2.47 and 2.36. For integrating we divide the ionosphere in slabs of thickness dh=1km and calculate the increments of ψ and ζ up to a height of 100 km, when we have no change of these parameters we calculate ψ in terms of degrees and half turns and the tilt angle ε.

We used the electron density profile model described in §1.3; the magnetic field components were computed separately according to §1.4 and we made a least square polynomial fit for them; these polynonials were used in the program. This was necessary to reduce the time of computation, and implies that all the analysis was made using only one particular orbit. To compute one down-coming wave the computer takes 55 seconds.

A condensed block diagram of the program is presented in Fig.B.1, and in the next page we present the program itself.

We also compute how the received wave would be recorded in our actual system. In Fig.B.2 we present the response of the system that is registered for a given input in the antenna for 40 and 41 MHz. These curves are not necessarily fixed and can be changed by control buttons on the panel; so for simulation we choose a similar response with a mean gain, also shown in Fig.B.2. If E is the input energy, the registered divisions can be represented by a curve of the type

$$S = \frac{10\alpha}{\Delta d} \log kE$$

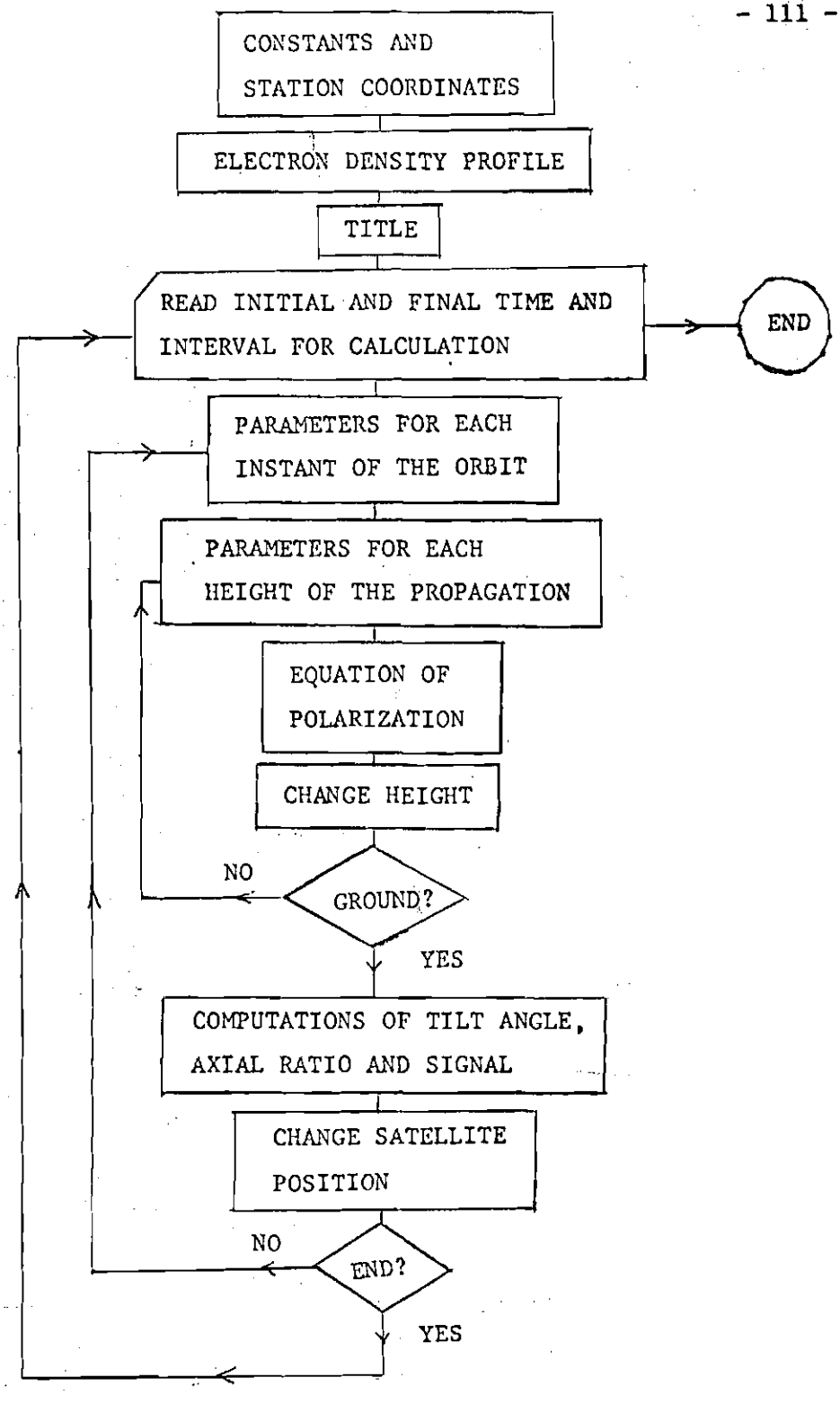

Fig. B.1 - Block diagram of the computer program

```
HOLL
C       SIMULATION OF A WAVE PROPAGATING THROUGH THE IONOSPHERE
C       FOR A POLAR ORBIT
C       KANTOR-5/3/69-CNAE
        REAL LAT,LON,LATO,LONO
        DOUBLE PRECISION PSI,QSI
        ALPHA SPSI,SPOS,SNEG
        DIMENSION XH(1000),DB(4)
        DATA RADGR,GRRAD/57.295779,.017453293/
        DATA LON,HS/-42.501588,1029.5716/
        DATA RT,LATO,LONO/6371.015,-23.220043,-45.88008/
        DATA F,DH/41.E+6,1./
        DATA SPOS,SNEG/1HP,1HN/
        CHAP(Z)=EXP(.5*(1.-Z-EXP(-Z)))
        RATIO(X)=SQRT((1.-X)/(1.+X))
C       BEGINING
        FF=40.E6/F
        VC=1.0471976E-5*F
        LATO=GRRAD*LATO
        LONO=GRRAD*LONO
        SLATO=SIN(LATO)
        CLATO=COS(LATO)
        CLON=COS(LONO-GRRAD*LON)
        DO 10 I=100,1000
        HC=I
        H=75.+.025*(HC-350.)
        Z=(HC-350.)/H
   10   XH(I)=80.5*0.1E+13*CHAP(Z)/(F*F)
C       TITLE
        WRITE(6,150)
  150   FORMAT(10X,9HTIME  LAT,4X,11HLONG' RANGE,4X,3HPSI,6X,
     1  111HRPSI H(M=0),4(6H SINAL),/,7X,7HMM.SSSS/)
    1   READ(5,2,END=99) T,TF,DT
    2   FORMAT(2F5.1,F5.2)
C       ORBIT PARAMETERS
  100   LAT=-26.51178 + 0.055556*T
        DLAT=GRRAD*LAT
        A0= 0.000096*(10.-T)
        A1= -1.E-7*(32.-0.65*T)
        A2=(100.-T)*1.E-11
        COSDS=SLATO*SIN(DLAT)+CLATO*COS(DLAT)*CLON
        D=SQRT(HS*HS+2.*RT*((RT+HS)*(1.-COSDS)))
        SENDS=SQRT(1.-COSDS*COSDS)
        RSENQO=RT*SENDS*(RT+HS)/D
        HQT=0.
        HC=1000.
C       INITIAL PARAMETERS FOR POLARIZATION
        PSI=0.
        QSI=0.
C       HEIGHT PARAMETERS
```

```
 200    SENQC=RSENQD/(RT+HC)
        SQC=1./SQRT(1.-SENQC*SENQC)
        X=XH(IFIX(HC))
        YT=(0.015-45.E-7*HC)*FF
        YL=(A0+HC*(A1+HC*A2))*FF
        IF(YL*YLO.LE.0.) HQT=HC
        YLO=YL
        DZ=DH*SQC
C       EQUATION
        XYL=VC*X/(1.-X)
        XYT=.5*XYL*YT*YT/(1.-X)
        XYL=XYL*YL
        DOMEGA=XYL*DZ
        PSI=PSI+DOMEGA
        QSI =QSI +2.*XYT*SIN(2.*PSI  )*DZ
        PSI=PSI-XYT*COS(2.*PSI)*DZ*SIN(QSI)/COS(QSI)
  250   HC=HC-DH
        IF(HC.GE.100.) GO TO 200
C       FINAL RESULTS FOR EACH INSTANT
        TIMES=AMOD(T,60.)/100.+AINT(T/60.)
        RPSI=SIGN(RATIO(ABS(COS(QSI ))),SNGL(QSI ))
        SPSI=SPOS
        IF(PSI.LT.0.) SPSI=SNEG
        GPSI=  RADGR*PSI
        IPSI=ABS(GPSI)/180.
        GPSI=ABS(AMOD(GPSI,180.))
        ANGL=0.
        DO 500 I=1,4
        R0=RPSI*RPSI
        R0=(1.-R0)/(1.+R0)
        S=.5*(1.+R0*COS(2.*(PSI-ANGL)))
        S=0.72*ALOG10(S/77.5)
        DB(I)=0.
        IF(S.GT.-3.1415927) DB(I)=2.5*(1.+COS(S))
  500   ANGL=ANGL+45.*GRRAD
        WRITE(6,50)TIMES,LAT,LON,D,IPSI,SPSI,GPSI,RPSI,DB
   50   FORMAT(6X,F8.4,2F7.2,F7.0,I4,A1,F4.0,F8.4,6X,4F6.2)
        IF(HQT.NE.0..AND.HQT.LT.999.) WRITE(6,400) HQT
  400   FORMAT(1H+,51X,F6.0)
  300   T=T+DT
        IF(T.LE.TF) GO TO 100
        GO TO 1
   99   STOP
        END

07/07/69     4218 PM      ASR#3  69070  COMPILER
  0 MIN 17 SEC FOR COMPILATION PASS
   95 CARDS AT 317 CARDS PER MINUTE
 13516 DIGITS DATA.  7026 DIGITS CODE.
```

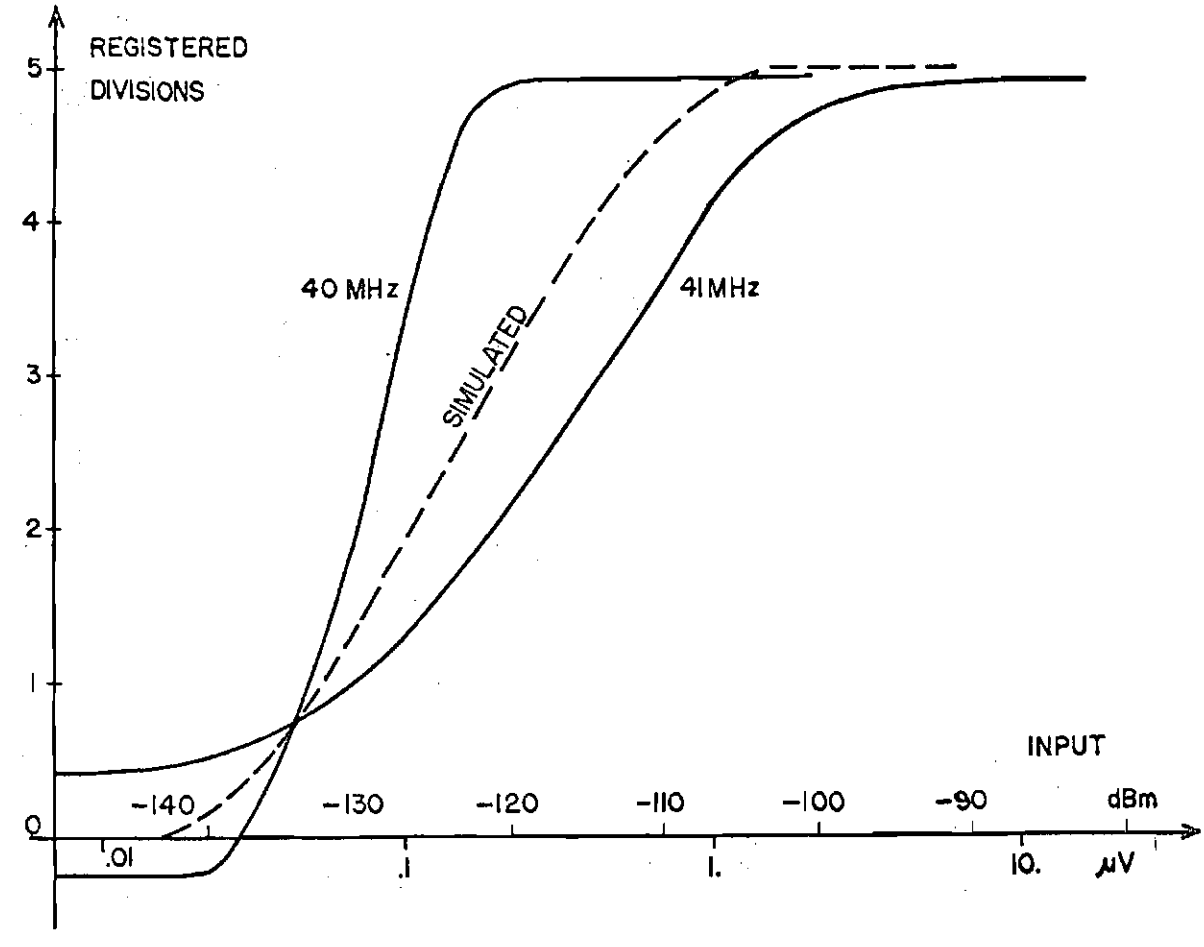

Fig. B.2 - Response of the system for different inputs expressed in terms of divisions on the Sanborn Recording chart, for the two frequency used. The curve designated by "-----" represent the curve used in simulations.

$$\begin{cases} d = \Delta d \cos^2 s & \text{for } 0 > s > -\pi/2 \\ d = 1 & \text{for } s \geq 0 \\ d = 0 & \text{for } \frac{-\pi}{2} > s \end{cases} \qquad (B.1)$$

Where Δd is the maximum amplitude that can be registered; α, k are constants.

We are not interested in the space attenuation, so we only adjust the computed input in order to have a similar maximum value as our actual recordings. So if d_m is the recorded division when E = 0 dB, we have

$$d_m = \Delta d \cos^2 \left(\frac{10\alpha}{\Delta d} \log k\right)$$

which gives k.

The adopted values were $\Delta d = 5$, $d_m \simeq 3$ and $\alpha = 0.18$. Equation B.1 becomes

$$d = 5 \cos^2 (0.36 \log E/77.5) \qquad (B.2)$$

for E between 1 and 1.1×10^{-3}.

The signal received in the antenna (dipole type) can be approximately calculated by the electric field component along the antenna. We assumed that the slabs are normal to the ray path and consider only the normal incidence of the wave.

The received signal will be given by (2.9). The antenna makes an angle θ with the y axis of §2.2.1 measured clockwise, calculating the mean energy received, where $\langle\rangle$ denotes the mean values, we have

$$\langle E^2 \rangle = \frac{1}{2} (E_{ao}^2 + E_{bo}^2) + E_{ao} E_{bo} \cos 2(\psi - \theta)$$

The total energy of the wave is given by

$$< E_T^2 > = E_{ao}^2 + E_{bo}^2$$

Substituting (2.6) in the above relations we have

$$\frac{< E^2 >}{< E_T^2 >} = \frac{1}{2} \left[1 + \frac{1 - \epsilon^2}{1 + \epsilon^2} \cos^2(\psi - \theta) \right] \qquad \text{(B.3)}$$

This ratio ranges from 0 to + 1, and taking $\langle E_T^2 \rangle = 1$ we use it in expression B.2.

ACKNOWLEDGMENTS

I am greatly indebted to Dr. Fernando de Mendonça for his constant interest and many helpful suggestions and to may advisers Dr. D.B. Rai and Dr. B.R.Clemesha. I am also grateful to Mr. Teracine for some valuable information. The present work was funded in-house and utilized equipment on loan from the National Aeronautics and Space Administration (NASA) under a cooperative research program. We are grateful to GSFC/NASA for providing satellite ephemerides. Thanks are also due to all the staff members of CNAE who participated in different phases of this work, and to Miss Conceição Zanardi for typing the thesis.

REFERENCES

Almeida, O.G. and H.Waldman, Total electron content measurements by differential Faraday rotation method at low latitudes. Report LAFE-56, CNAE, 1967

Basu, S., Effect of Refractive Correction on Latitude Variation of Total electron Content. J. Geophys. Res., 72, 5339-5345, Nov. 1, 1967

Basu, S. and A. das Gupta, Latitude Variations of Electron Content in Equatorial Region under Magnetically Quiet and Active Conditions, J. Geophys. Res., 73, 5599-5602, Sep.1, 1968

Bhonsle, R.V., A.V. da Rosa and O.I. Garriott, Measurements of the Total Electron Content and the Equivalent Slab Thickness of the midlatitude ionosphere. Radio Sci., J. Res. NBS, 69D, 929-938, 1965.

Budden, K.G., Radio Waves in the ionosphere. Cambridge University Press, 1961

Cain, Joseph C., S. Hendricks, W.E. Daniels, D.C.Jensen, Computation of the Main Geomagnetic field from Spherical Harmonic Expansion, private communication, October 1964.

Casali, S., O.G.Almeida and H.Waldman, "Cálculo do Conteúdo Eletrônico da Ionosfera usando efeito Faraday". Report LAFE-70, CNAE, 1968.

Foltz, D.N., An Investigation of second-order corrections to first-order ray theory as applied to beacon satellite transmission Studies. Scientific Report nº 225, the Pennsylvania State University, 1965.

Garriot, O.K. and F.de Mendonça, A Comparison of Methods used for obtaining Electron Content from satellite observations, J. Geophys. Res., 68, 4917-4927, 1963.

Golton, E., G.O. Walker and K.H. Ma, Latitudinal Profiles of Electron Content across the Magnetic Equator. Radio Science, in press, 1969.

Hibberd, F.H., A study of the Ionosphere at Mid Latitudes, Based on Total Electron Content. Sci. Rep. nº 213, The Pennsylvania State University, July 10, 1964.

King, J.W., K.C. Reed, E.O. Olatunji and A.J.Legg, The behavior of the topside ionosphere during storm conditions. J. Atmospheric Terrest. Phys., 29, 1355-1363, 1967a.

King, J.W., E.O.Olatunji, D.Eccles and W.S.Newman, The integrated Electron Content in the Equatorial Ionosphere. J.Atmospheric Terrest., 29, 1391-1396, 1967b.

Kuntman, D., A method for the determination of Mean Ionospheric height from Satellite signals. Sci. Report nº 278, The Pennsylvania State University 1966.

Mack, D.G., Changes in the upper ionosphere during severe magnetic storms. Sci. Report nº 325, The Pennsylvania State University, 1968.

Mass, J., The Faraday Fading Rate for nearly Transversal Propagation. Radio Sci., 1, 1137-1140, 1966.

Mendonça, F. de, Ionospheric Electron Content Measurements in Regions of low Magnetic dip and through the Brazilian Magnetic Anomaly. Proc. of the Fifth COSPAR Symp. Florence, 1965.

Mendonça, F. de, J.L.R.Muzzio and F.Walter, Second Order Correction on Electron Content Measurements with Faraday Rotation Technique. Report on Aeronomy, 162-166, SISEA, 1965.

Pagagiannis, M.D., A new method to Measure Electron Collision Frequencies in the Ionosphere by means of the Faraday Rotation process. Sci. Rep. nº 4 AFCRL-66-618, 1966.

Potts, B.C., Ionospheric studies using Polarization Rotation of Satellite Radio Signals. Sci. Rep. nº11, AFCRL-62-155, 1962.

Rao, N.Narayana and K.C.Yeh, Comparison of Faraday and Doppler Methods of Obtaining Ionospheric Electron Content. J. Geophys. Res., 73, 2447-2458, 1968

Ratcliffe, J.A., The Magneto-ionic Theory and its Applications to the Ionosphere. Cambridge University Press, 1962

Ross, W.J., Second-Order Effects in High-Frequency Transionospheric propagation. J. Geophys. Res., 70, 597-612, 1965.

Skinner, N.J. Measurements of Total Electron Content near the Magnetic Equator. Planetary Space Sci., 14, 1123-1129, 1966.

Taylor, G.N. and R.D.S. Earnshaw, Comparison of electron contents computed with satellite Faraday data from widely space stations. J. Atmospheric Terrest. Phys., 27, 525-533, 1965.

Teracine, E.B., Satellite Observations of the Low Latitudes Ionosphere. Sci. Report LAFE-76, CNAE, 1968

Tyagi, T.R. and Y.V. Somayajulu, Some Results of Electron Content Measurements at Delhi from Faraday Fading of S-66 Transmissions. Sci., Rep. nº 26, Nat. Phys. Lab. Delhi-12, India, June 15, 1966.

Wernik, A., Continuous measurements of the Faraday effect using crossed antenna. KGO Report nº 677, December 1967.

Yeh, K.C. and B.J. Flaherty, Ionospheric Electron Content at Temperate L Latitudes during the Declining Phase of the Sunspot Cycle. J. Geophys. Res., 71, 4557-4570, October 1, 1966.